# Permanent Magnet Plunger

# Bi-directional Solenoid Actuator for Direct Alternative Fuel Injector

**Da-Gang He**

A Thesis

in

The Department

of

Mechanical and Industrial Engineering

Presented in Partial Fulfillment of the Requirements

For the Degree of Master of Applied Science (Mechanical Engineering) at

Concordia University

Montreal, Quebec, Canada

November 2005

*Your file Votre référence*
*ISBN: 0-494-14306-1*
*Our file Notre référence*
*ISBN: 0-494-14306-1*

## ABSTRACT

**Permanent Magnet Plunger Bi-directional Solenoid Actuator for Direct Alternative Fuel Injector**

Da-Gang He

As manufacturers of internal combustion engines and transportation vehicles strive to reduce air pollution resulting from by-products of internal combustion, alterative fuels will gain increasing importance. However, to fully exploit the use of these alterative fuels as commercially feasible fuels for gasoline and diesel operated vehicles novel types of fuel injector will be required.

In this thesis, a new type of alternative fuel direct injection injector actuated by a permanent magnet (PM) plunger bi-directional motion actuator has been developed and investigated. The project composes of the development of the novel PM plunger bi-directional motion actuator, with mathematical modeling and physical analysis, including the system nonlinear magnetic characteristics.

The research demonstrated that this new type of PM plunger actuator could implement bi-directional motion when a properly defined bi-directional voltage is applied to the solenoid. The simulation results and experimental results matched well and validated that the mathematical model of the PM plunger bi-directional motion actuator is appropriate, which can be used as an aid for future design purposes. Moreover, the

simulation results show that the injector employing the bi-directional motion actuator can significantly improve the injector closing speed and reduce post-injection.

## ACKNOWLEDGEMENTS

This research project was an excellent opportunity for me to obtain new knowledge and experience in the field of mechatronic system modeling and simulation. I am grateful to all those who have contributed to this thesis.

I wish to extend my most sincere gratitude to my supervisors Dr. Henry Hong and Dr. Chun-Yi Su. This thesis would be impossible without their guidance, support, and encouragement.

I would like to thank both Gilles Huard and Robert Oliver for their technical assistance in building the experimental circuits and experimental setup.

Also, I would like to thank the Natural Sciences and Engineering Research Council of Canada (NSERC) for the funding of this research project.

Last but not least, thanks to my wife, Huiwen Mai, my daughter, Xuesi He, my parents, my uncle and aunt for their continued encouragement and unwavering patience.

# TABLE OF CONTENTS

## CHAPTER 3

## DEVELOPMENT OF A PERMANENT MAGNET PLUNGER BI-DIRECTIONAL SOLENOID ACTUATOR FOR AN ALTERNATIVE FUEL INJECTOR



## CHAPTER 4

## CONCLUSIONS AND RECOMMENDATIONS FOR FUTURE RESEARCH

## LIST OF FIGURES

Page

## LIST OF TABLES

Page

## NOMENCLATURE

| | |
|---|---|
| $a$ | -Experimentally determined parameter for solenoid body material reluctance *(A/Wb)* |
| $b$ | - Experimentally determined parameter for solenoid body material reluctance *(Wb)* |
| $d$ | -Permanent magnet (PM) plunger diameter*(m)* |
| $d_o$ | -Nozzle orifice diameter*(m)* |
| $d_t$ | -Material damping of needle-to-seat interface *(kg/s)* |
| $d_r$ | -Material damping of the injector needle pulling rod *(kg/s)* |
| $d_p$ | -Material damping of needle-to-stopper interface *(kg/s)* |
| $dV$ | -Element of PM volume in the magnetic field *($m^3$)* |
| $dS$ | -Element area which is normal to the magnetic field *($m^2$)* |
| $g$ | -Gravitational acceleration *(9.806 $m/s^2$)* |
| $i$ | -Current through the solenoid circuit *(A)* |
| $i_f$ | -Fictitious current of the solenoid body*(A)* |
| $k_s$ | -Spring stiffness of the pre-load spring *(N/mm)* |
| $k_p$ | -Spring stiffens of needle-to-stop interface *( kN/mm)* |
| $k_t$ | -Spring stiffens of needle-to-seat interface *(kN/mm)* |
| $k_r$ | -Spring stiffness of the elastic rod *(kN/mm)* |
| $l_a(x)$ | -Length of the air-gap between the pole of the PM plunger and the end of the solenoid body tip *(m)* |
| $l_m$ | -PM plunger length *(m)* |
| $l_m'$ | -PM plunger effective length (*m*) |

| | |
|---|---|
| $m,\ m_c$ | -Mass of the PM plunger of the solenoid actuator *(kg)* |
| $m_n$ | -Mass of the injector needle *(kg)* |
| $v$ | -Velocity of the PM plunger motion *(m/s)* |
| $x$ | -Air-gap between the plunger and the solenoid stator core *(m)* |
| $x_c$ | -Displacements of the PM plunger *(m)* |
| $x_n$ | -Displacements of the needle *(m)* |
| $A$ | -Pole end area normal to the magnetic flux $(m^2)$ |
| $A_1$ | -effective area the magnetic flux passes the air-gap between the pole of the PM plunger and the end of the solenoid body tip |
| $A_g$ | -Boss-end end effective area normal to the magnetic flux $(m^2)$ |
| $A_m$ | -Fuel pressure acting on needle effective area $(m^2)$ |
| $B_r$ | -Magnet remanence *(T)* |
| $\mathbf{B_m}$ | -Permanent magnet field flux density at the operating point *(T)* |
| $\mathbf{B_0}$ | -External magnetic field due to all other sources *(T)* |
| $\mathbf{B_{coil}(i,x)}$ | -Magnetic field due to the coil *(T)* |
| $\mathbf{B_{PM}(i,x)}$ | -Magnetic field due to the PM *(T)* |
| $BH_{max}$ | -Magnet maximum energy product $(kJ/m^3)$ |
| $\mathbf{F}$ | -Total force acting on the PM due to the external magnetic field *(N)* |
| $F(i,x)$ | -The sum of PM force and electromagnetism force acting on the PM plunger *(N)* |
| $\mathbf{F_{coil}(i,x)}$ | -Force due to the solenoid coil current *(N)* |
| $\mathbf{F_{PM}(i,x)}$ | -Force due to the PM *(N)* |
| $F_m$ | -Magnetomotive force (mmf) of the PM *(Amp-turn)* |

$F_P$ -Fuel pressure force acting on the injector needle *(N)*

$F_{pl}$ -Pre-load force of the pre-load spring *(N)*

$F_R$ -Needle reaction force with the injector seat or stopper *(N)*

$H_c$ -Permanent magnet coercivity $(kA/m)$

$Hci$ -Permanent magnet intrinsic coercivity $(kA/m)$

$\mathbf{H_m}$ -Permanent magnet field strength at the operating point *(A/m)*

$H_{\max}$ -Needle fully open position *(m)*

$L$ -Stator core length inside the coil *(m)*

$L(\phi)$ -Nonlinear inductance of the solenoid *(H)*

$L_{coil}(i,x)$ -Nonlinear inductance of the solenoid*(H)*

$L_c$ -Solenoid coil length *(m)*

$L_e$ -Leakage and external circuit inductance *(H)*

$\mathbf{M}$ -Magnetization of the material $(kJT^{-1}m^{-3})$

$N$ -Turns of solenoid coil winding

$P$ -Pressure inside the injector above the effective area *(Pa)*

$P_e$ -Pressure below effective needle area *(Pa)*

$R$ -Solenoid system resistance *(Ω)*

$R_c$ -Solenoid radius *(m)*

$V$, $V_s$ -Supply voltage applies to the solenoid *(V)*

$V_\phi$ -Induced voltage of the solenoid coil *(V)*

$\theta$ -Haft angle of the needle conical tip *(degree)*

$\lambda$ -Flux linkage of the solenoid *(Wb)*

$\mu_0$ -Permeability of free space ($4\pi \times 10^{-7} Wb / A \cdot m$)

$\mu_{rec}$ -PM relative recoil permeability

$\mu_m$ -PM permeability ($Wb / A \cdot m$)

$\phi_m$ -Flux in the magnetic circuit due to the PM *(Wb)*

$\Phi(i, x)$ -Magnetic flux crossing the air-gap *(Wb)*

$\mathbf{\Phi_{PM}(i, x)}$ -Magnetic flux due to the PM *(Wb)*

$\mathbf{\Phi_{coil}(i, x)}$ -Magnetic flux due to the coil *(Wb)*

$\Re_a$ -Reluctance of the air-gap between the solenoid body tip and the PM upper pole *(A/Wb)*

$\Re_B$ -Reluctance of the solenoid ferromagnetic body *(A/Wb)*

$\Re_x$ -Reluctance of the air-gap *(A/Wb)*

$\Re_{PM}$ -Reluctance of the PM plunger *(A/Wb)*

$-\nabla \bullet \mathbf{M}$ -Magnetic volume charge density

$\mathbf{n} \bullet \mathbf{M}$ -Magnetic surface charge density

# CHAPTER 1

# INTRODUCTION

## 1.1 General

Petroleum liquid fuels such as gasoline and diesel are, at present, the principal fuels for transportation vehicles powered by internal combustion engines. However, the operation of these engines using petroleum fuel is a major pollution source of hydrocarbons (HC) and nitric oxides ($NO_x$) in the atmosphere. A recent report suggests that forty percent of air pollution can be attributed to vehicles that use either gasoline or diesel as fuel [1]. To reduce air pollution, alternative fuels, such as hydrogen ($H_2$), compressed natural gas (CNG), and dimethyl ether (DME), with low levels of harmful combustion products, will become the fuels of the future for gasoline and diesel engine operated vehicles [2].

At the present time there are two methods applied by the delivery systems of gaseous fuels for the internal combustion in a vehicle. The first method is similar to the gasoline supply system, as gaseous fuels are delivered to the intake manifold of the spark ignition (SI) engine. In the second method that is similar to the diesel supply, the gaseous fuels are directly injected into the cylinders of the compression ignition (CI) engine. Comparing these two methods, because of pumping losses from the intake throttling in SI engines, and because the CI engine has a much higher compression ratio, the thermal efficiency of the CI engine is much greater which leads to lower fuel consumption.

Hence, direct injection of gaseous fuel into the cylinder of the internal combustion engine is regarded as the more advanced and optimal method.

Solenoid operated fuel injectors have been widely exploited in SI engines burning both gasoline and gaseous fuels. However, the solenoid operated fuel injector, employed by SI engines, cannot directly inject gaseous fuels into the CI engine. This is because the operating pressure of the gaseous fuel in a CI direct injection system is ten times higher than that employed in SI engines. In addition, due to the lower fuel injection pressure, SI engine injectors are not built to be fast enough for a direct injection system. This is because in a direct injection system, the fuel injection time is very short and requires the injector to operate precisely at the selected injection point in time to deliver the proper dose of fuel into the CI engine cylinder.

Moreover, alternative gaseous fuels have quite different physical properties. For example, the gaseous fuels have much higher compressibility and lower viscosity. Therefore, a novel type of fuel injector needs to be developed if the alterative fuels mentioned are to be feasible as efficient vehicle fuels for the objective to reduce tailpipe emission pollutants [3].

The research objective of this thesis is to develop a new type of faster responding bi-directional solenoid actuator for the direct injection of alterative fuels into a CI engine combustion chamber. The bi-directional solenoid actuator is modified from a traditional commercial solenoid actuator. The conventional carbon steel plunger is replaced by a

permanent magnet (PM) plunger. When the solenoid current direction is reversed, the magnetic poles of the solenoid are also reversed while the poles of the PM plunger do not change. As a result, the solenoid will either attract (pull) or repel (push) the PM plunger as its magnetic poles are altered. In this way the PM plunger implements the bi-directional motion.

This bi-directional solenoid actuator applied to the vehicle fuel injector can implement motion control in two directions, and for this reason the return spring is not needed. And, the injector equipped with the bi-directional actuator will also be smaller than the conventional injector. Moreover, this new type of bi-directional motion injector can increase the speed of closing of the injector while the opening time is almost the same as the conventional injector. The faster injector response time means that a more precise dose of fuel can be injected into the engine combustion cylinder, which results in an improvement in fuel efficiency. In addition, because the pulling force upon the PM that is used to close the injector needle onto its seat can be controlled and even reversed, needle bouncing can be minimized to reduce the effects of injector post-injection. It is known that this post-injection caused by the needle bouncing is one of the main causes of tailpipe emission pollutants. Therefore, this bi-directional motion control in the injector actuation will also help reduce combustion products that add to air pollution.

A review of the literature has shown that there is currently no fuel injector that is operated by a bi-directional solenoid. Although there are some solenoids that employ a

PM core for actuator bi-directional motion, their mechanical construction and control methods are significantly different from the design proposed in this research [4–8].

The first objective of this research is to develop a mathematical model for the bi-directional motion of the solenoid PM plunger. This model will be used for the computer simulation and analysis of the dynamic responses of the bi-directional solenoid actuator and fuel injector systems. To have an accurate model of the bi-directional actuator, the nonlinear magnetization property of the ferromagnetic material consisting of the solenoid carbon steel housing, is considered. In addition, the inductance of the solenoid is considered as nonlinear. To determine the nonlinear magnetization curve parameters and validate the simulation results of the solenoid actuator, experimental setups were designed and built. Experimental and simulation results of the bi-directional PM plunger are compared and are discussed.

The second objective of this research is to apply the bi-directional PM solenoid actuator to the direct injection of alternative fuels. The PM solenoid actuated alternative fuel injector is developed and its mathematical model is derived. The computer simulation results of the injector's behavior are discussed, and injector needle bouncing, one of the main causes of post-injection is analyzed.

## 1.2 Literature Review

Solenoid operated injectors have been developed and used commercially for many years. They are widely used in spark ignition (SI) engines, mainly for the manifold injection of gasoline or gaseous fuel such as compressed natural gas. In diesel fuel compression ignition (CI) engines, where the injector is normally operated by the fuel pressure, the solenoid actuators are used as control units to enable or disable the high pressure to push open the injector needle for fuel injection [3]. To improve the efficiency of compression ignition engines that burn gaseous fuel, researchers have developed solenoid-operated injectors for direct injection. The functions and structures of the solenoid operated injectors for SI engines, for CI engines, and for gaseous fuel are all different. However the focus of research and development of all of these injectors are the same, namely to accelerate the injector opening and closing response time; to regulate with precision the quantity of fuel injected; and to minimize post injection. The aim of this research project is develop a novel solenoid type bi-directional actuator with a permanent magnet (PM) plunger applied to gaseous fuel injectors. This chapter will review the major developments for bi-directional linear solenoid actuators equipped with a movable permanent magnet, the developments of solenoid-operated injectors for direct injection, solenoid operated injectors for manifold injection, and solenoid controlled diesel fuel injectors.

### 1.2.1 Review of the Bi-directional Linear Solenoid Actuators with a Movable Permanent Magnet

Linear electric actuators are electromagnetic devices, which provide linear motion to drive moving parts. The linear actuators can be driven bi-directionally by electrical energy, such as the linear induction and synchronous permanent magnet (PM) actuators, DC brush linear actuators, and moving coil PM actuators, were introduced more than fifty years ago. However, the solenoid type based on PM moving bi-directional linear actuators, referred to as linear oscilloactuators (LOA), were only introduced over the past two decades [9]. In addition, there is little published research on the topic of solenoid type PM moving bi-directional linear actuators. This section will review the previous research studies of movable PM solenoid type bi-directional linear actuators.

Lequesne [5] introduced the bi-directional solenoid type actuators equipped with a moving PM in 1990. The author presented two configurations, both having two series wound coils that provided energy to drive the PM. The moving parts included the cylindrical PM with axial magnetization mounted on a stem concentric with the actuator. The two configurations differed in the armature design chosen. One armature was a plate-type with two magnets, placed between two coils; the other armature being plunger-shaped with one magnet that was placed inside the coils. The two coils were in series, provided with bi-directional DC current by the drive circuit. As the current direction alternated, so did the magnetic poles of the coils alternate with the current direction; thus, the magnetic force due to the coils would drive the PM with the stem moving in alternate

directions. In this research, a solenoid dynamic model, based on finite element method (FEM), was presented. The author analyzed and compared four different solenoid designs both theoretically and experimentally. The paper demonstrated that rare-earth permanent magnets could be used for solenoid actuators, and that this type of actuator could provide the high speed motion needed for a fast actuator response.

In 1992, Ebihara and Watada [6] developed a moving PM linear oscillatory actuator. This actuator had a single-winding excitation coil in the stator side, and had two axially magnetized PM combined with three inductors together in the moving side. The moving side was placed inside the wound coil. The same poles of two PM faced to the centre inductor. Switching the coil current on and off, the back and forward mover motion was actuated by the magnetic forces produced by the coil current. The Maxwell stress equation and FEM were employed to analyze the static thrust and frequency characteristics of this actuator; however, there were no more information about the mathematic model of the actuator described in the paper.

Abe et al. [10] presented a new type of linear oscillatory actuator (LOA) in 1996. This actuator was modified from the previous LOA design [6]. Unlike the previous linear oscillatory actuator which had two pieces of PM cores in the moving part, this actuator had only one axially magnetized PM core in the middle of the mover. In the same way as the previous LOA, the moving part was placed inside the wound coil. By alternating the current applied to the coil, the actuator can produce either an attractive or repulsive force between the stator and the moving part. This actuator, with an expected stroke of 15mm,

was applied as an on/off delivery valve for a hydrogen pump for an automobile hydrogen fuel system. The valve characteristics of stroke vs. frequency, and flow rate vs. frequency were experimentally studied. No mathematical model and its analysis were provided.

Lin et al. [11] presented a solenoid type moving PM linear actuator for vibration isolation in 2000. The actuator was equipped with an upper and lower coil. The moveable and axial magnetization cylindrical PM with a non-magnetic stem was placed between the two coils. The movable PM was driven by the magnetic force, which was produced by the two current-carrying coils. Reversing the direction of the current in the coils caused the magnetic flux to produce different directional magnetic forces to drive the PM up or down. To analyze the actuator performance, the dynamic mathematic model of this actuator was developed. However, the mathematic model was empirically based on the experimental data. The magnetic force acting on the PM was calculated by using measured magnetic flux density from inside the actuator, which were then curve fitted and approximated as a function of applied current, instead of being derived from a theoretical formula; and also, the magnetic force of attraction between the PM and ferromagnetic material used a curve fitting equation from experimental data. The position feedback control of the actuator was studied in the research.

In addition, other solenoid type actuators with the axially magnetized moving PM have been presented and investigated in past years. In contrast with the actuators mentioned above, these actuators were air coil actuators, which had the movable PM inside or outside the solenoid, but the actuators did not have a ferromagnetic housing

and/or ferromagnetic core. Thus, it was not necessary to consider the effects of the nonlinear characteristics of the ferromagnetic in the actuator. Some of the previous works describing air coil actuators are reviewed in the following.

Groom [7] introduced an air core bi-directional magnetic suspension actuator in 1992. In this actuator, a PM core was placed on the outside axis of the air solenoid. The author developed the equations for the electromagnet force that was produced by the solenoid, acting on the PM core. The equations showed that the force acting on the PM core was a function of coil height, coil inner and outer radii, and position of PM core to solenoid coil.

In 2002, Jung and Baek [8] presented a contact-free moving magnet type of positioner. An axially magnetized movable PM was on the solenoid longitudinal axis. In the paper, the authors analyzed the magnetic field of the air-core solenoid with an on axis permanent magnet, presented the force characteristic of the air-core solenoid and permanent magnet, and proposed the mathematical model of the air-core solenoid positioner.

### 1.2.2 Review of the Development of Solenoid Operated Injector for Gaseous Fuel Direct Injection in Diesel Engines

The idea of using solenoid operated injectors for the direct injection of gaseous fuel into an internal combustion cylinder was first proposed by T. Krepec et al. [12] at

Concordia University in 1984. Following this idea, a solenoid-operated injection system was designed and developed for hydrogen fuel direct injection in diesel engines [13] in 1987. This injection system included the solenoid-operated injector, electronic control unit (ECU), and the metering valve on the fuel rail. This injector was based on the principle that when the solenoid was actuated, the needle was lifted to open the injector. Thus, the fuel directly injected into the cylinder of the diesel engine. When the solenoid was switched off, the injector was closed by the tension of a return spring. Meanwhile, throttling the flow to the injector with the metering valve controlled the injection time and gas rate.

In 1989, Krepec et al. [14] continued the development of a solenoid-operated injector for natural gas direct injection. The structure of this injector is shown in Figure

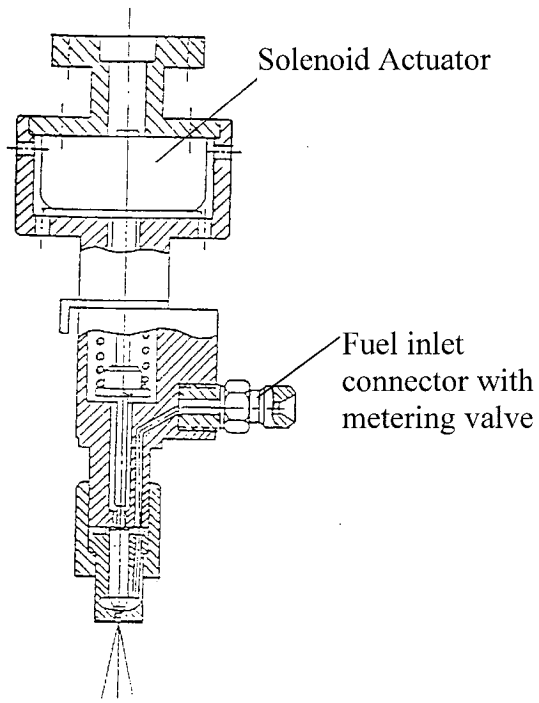


**Figure 1.1 First generation of solenoid operated gaseous fuel injector [11]**

1.1. This injector was based on the conventional diesel injector, with a solenoid actuator on the top of the injector. The solenoid magnetic force lifted the needle to open the injector. The electronic control unit (ECU) sent a signal at the proper time to switch on and off the solenoid. With the solenoid on, the magnetic force assisted the pushing gas pressure acting on the needle to lift the needle and open the injector; and when the solenoid was de-energized, the magnetic force was withdrawn and a return spring forced the needle to close the injector. Moreover, the injector was connected with a metering valve, which was controlled by a stepper motor. Doubly controlled by the solenoid pulse width and metering valve, the required amount of fuel was delivered to the engine cylinder.

Green and Wallace [15] developed two kinds of solenoid-actuated injector for gaseous fuels in 1989. One injector was designed for directly injecting high-pressure hydrogen into the cylinder of four-stroke CI diesel engines; another was designed for injecting compressed natural gas to the intake ports of two stroke diesel engines. The aim of these designs was to achieve fast actuation for quick opening and closing. The two injectors had an almost identical construction, but the actuator for hydrogen was longer and was installed in the cylinder head, while the natural gas actuator was shorter and was used for port injection. Because the magnetic force of any solenoid is proportional to the face area, the multipole solenoid design was chosen as actuators for these injectors since these structures have more face area than the conventional solenoid while the armature are the same. Therefore, the multipole solenoid operated injectors have faster actuation when compared to a conventional solenoid. When the solenoid is activated the injector

opens, and a spring is employed to ensure the injector closing while the solenoid power is off. To achieve faster actuation, a special capacitive discharge solenoid driver circuit was developed, where the capacitor was charged to 100VDC. When the capacitor discharged, this high voltage provides a boost current to open the injector quickly. At the same time the circuit provided a rapid current cut-off function when the injector was closed. As a result, both injectors achieved injection durations as short as 1.5 ms.

Hong et al. [16] developed and optimized the second-generation of the solenoid-operated gaseous fuel injector for high pressure direct injection in 1992. Instead of the large solenoid as was used in the first generation injector [14], a smaller commercial high performance solenoid, Lisk L5, was used. Its smaller size allowed it to be directly installed in existing diesel engines. The injector was a pressure balanced design and thus the needle fit in the nozzle body did not require close tolerances. This provided increased free movement of the needle to avoid needle seizure. As well, because of the pressure balanced design, a smaller compressed and preloaded spring force was required to return the injector needle to its closed position. A special switching circuit was designed to help the needle open faster at higher operating pressure. A multi-objective optimization procedure was employed to select design parameters to improve the injector dynamic performance.

To ensure that the solenoid force is controllable and to meet the stringent timing requirements for the opening and closing of the second-generation gaseous fuel injector, Hong et al. [17] presented a simple but effective switching circuit and solenoid model in

1994. The special switching circuit was to meet the objective for rapid opening and closing of the solenoid injector. The solenoid model considered the nonlinear ferromagnetic material reluctance and eddy current losses, as well as presenting the magnetization curves and dynamic hysteresis loops that described the behavior of the solenoid as a function of various input voltages. A multi-objective optimization method was applied to select the optimal parameters for the complex nonlinear injection system to improve the injector dynamic performance. The study showed that the solenoid mathematical model matched the experimental results well. The injection system performance was improved after optimizing the design parameters that included; supply voltage, capacitance value of voltage-reducing capacitor in the solenoid drive circuit, spring preload value, and spring stiffness of the injector system. The results showed that when the system was optimized the response of the injector was faster, and that the opening and closing time of the injector of 1.0ms could be achieved.

Kekedjian et al. [18] developed the third generation of solenoid operated gaseous fuel injector design from the second-generation injector in 1994. The goal of this study was to overcome the inadequate solenoid force to open the injector at higher gas pressures, to overcome the slower and less repeatable dynamic response of the solenoid operated injector, and to overcome the solenoid overheating problems which could reduce the injector performance. The main features and advantages of this new generation of injector design were:

1. A new type of driving circuit was designed to boost the solenoid force, with a 12V power supply to generate 100V across the solenoid coil;
2. A more powerful but shorter solenoid, Lisk L7, adapted to guarantee the injector opening faster and to obtain the larger needle stroke;
3. The incoming gaseous fuel flowing around the solenoid absorbed excess heat and so reduced overheating;
4. The injector needle rod connecting the needle and the solenoid core was constructed from an elastic material that reduced needle bouncing.

The study showed that the injector opening required less than 0.7 ms to achieve maximum flow from the nozzle.

Following the previous works, Hong et al. [19] further studied the fuel delivery characteristics of the solenoid operated gaseous fuel direct injection injectors in 1996. The authors focused on modifying the injector design to better adapt the gas discharge characteristic to meet the requirements of a high-speed diesel engine. The study concluded that varying the voltage pulse width and/or the metering valve opening at the inlet to the injector could change the injected gas dose. The shape of the gas discharge rate characteristic could be changed to suit the high-speed diesel engine with a throttling pintle nozzle or a double-spring configuration.

Torab [20] proposed research of the alternative fuels solenoid-operated injector for CI engines in 1999. The author adapted the third generation solenoid operated gaseous fuel injectors for use with dimethyl ether (DME) fuel in diesel engines. In his research work, injectors were installed with a common rail; a long elastic rod was employed in the injector to reduce the impact force between the nozzle and its seat; a commercial solenoid Lisk 7, was used to operate the injector; and a new PWM driving circuit was developed to increase the speed of solenoid opening and to reduce energy consumption. Moreover, the study showed that for the low viscosity alterative fuel injector, it was possible to reduce needle bouncing and the impact force between the needle and its seat through the use of an elastic needle pulling rod. As a result, the post-injection that is directly related to increased emission pollutants was reduced, and the wear between the needle and its seat is reduced.

### 1.2.3. Review of Indirect Injection Gaseous Fuel Injector and Solenoid Controlled Fuel Injector in Recent Years

As mentioned in the previous section, the use of a solenoid as a controlling device or acting as a mechanism within a system has been exploited in fuel injectors for many years. However, significant advances have been made in this decade as more new technologies and new research methods were applied to the study of fuel injectors. Increasingly, the advantages of injectors actuated by solenoids became apparent. There is no doubt that the achievements in this period represented significant progress in this field.

In this section, the review of recent developments and technologies for indirect injection using gaseous fuel injectors related to the use of solenoids will be presented.

In 1990, Yuan and Chen [21] published an algorithm for the analysis of the solenoid operated fuel injector systems in dynamic simulation. This algorithm was proposed to solve the coupled electric, magnetic, and mechanical problems involved in the solenoid fuel injector dynamics. The nonlinearity of the electronic circuit and the fluid-flow effects were incorporated in the lumped equations of the armature. The nonlinear property of the magnetic material of the solenoid, the eddy current, and the motion and rebound of the armature were included in the system performance analysis. The Finite Element Method (FEM) was applied to calculate the magnetic field and the magnetic force. The voltage and current of the circuit and magnetic field were solved in an iterative algorithm for each time step. Compared with the previous study, which had neglected the eddy current, and the nonlinear material effect, the results showed this algorithm achieved significant improvements.

Sturman et al. [22] developed a magnetic-latching solenoid injector for fuels such as compressed nature gas (CNG) and liquefied natural gas (LNG) in 1995. A digital gas injector employing a magnetic latching solenoid was designed. Rather than working to eliminate residual magnetism, the force produced by the residual magnetism of the solenoid was used to latch the injector open. In this way this injector saved energy and reduced heat dissipation. The armature was a flat plate connected with the injector needle. When the solenoid was energized, the armature lifted, and the gap between the solenoid

pole and the armature closed. As the armature lifted, the injector opened. When the gap was eliminated, a continuous magnetic flux path was set up between the pole and the armature, and the resultant magnetic force held up the armature to ensure that the injector opened. Once the solenoid was latched, because of the residual magnetism of the solenoid injector, the injector remained in the open position even when the coil was de-energized. To close the injector, a reverse current pulse was applied to the solenoid to cancel the residual magnetism. When the residual magnetism inside the actuator was cancelled, the spring force acting on the armature overcame the magnetic force to push the armature down and the injector closed. Moreover, the injector incorporated a pressure-balanced valve that resulted in the injector opening and closing uniformly in response times that were independent of pressure. The demonstrations showed that for methane at 100psig, the injector opening and closing response times were 1.1 ms and 0.8 ms; for both opening and closing, the current applied to the solenoid was of short duration for only 375 μs.

Also in 1995, Barkhimer and Wong [23] introduced a pulse-width-modulated (PWM) sonic flow injector for gaseous fuels. The injector was a normally closed two-way solenoid operated valve. It included the valve body, which held the solenoid armature, ball poppet, a spring, which pushed the ball poppet to close the valve, and valve seat. While the solenoid was de-energized, the spring forced the ball poppet on its seat to stop gas flow out. When the solenoid was energized, the magnetic force acting on the solenoid core overcame the spring force to push the ball poppet down off its seat. As a result the gas passed through the valve seat and out the injector port. The solenoid was a

low resistance coil designed for rapid response, employing the PWM. The solenoid injector initial opening current was 4 amperes, and during the energized mode this current was reduced to, and held at 1 ampere. The response time of this solenoid injector was less than 3 ms for opening at gas supply pressures of up to 2070kPa, and 3 ms for closing at supply pressure at 690kPa.

At the same year, to address the problem of poor response of the natural gas carburetion system in vehicles, Bates et al. [24] developed an ultra rapid gaseous fuel injector to supply the larger volume flow rates required for a gaseous fuel without additional penalties in response time. In this injector, a disc was used instead of the needle that is typically used in a fuel injector, and the disk acted as a valve. As the solenoid was energized the disk lifted up, and opened the injector. The metering orifice was larger than in a typical injector. Compared with the typical gasoline injector, this new injector exhibited higher opening forces and shorter disc travel distance in large part due to the reduced mass of the moving parts. Therefore, the response times were faster than the typical injector. The conclusions of this research were that the response of the injector to varying excitation periods was linear and that made the injector ideal for multipoint natural gas injection. The test showed that this fuel injection system offered significant potentials to reduce emission gases.

To solve the problem of injection rate control (IRC) of a common rail injector, Ganser[25] introduced a double-stop solenoid operated electro-hydraulically control injector in 1998. In this injector, there were two different springs applied to the solenoid

movable parts, and a solenoid driver supplied two current levels to the solenoid coil. When the first level electric pulse was provided to the solenoid, the solenoid was energized, and the magnetic force opened the solenoid valve. When the force of attraction overcame the first spring force, the solenoid valve opened. At this current level, the magnetic force was not strong enough to overcome the second spring force. Therefore, a movable lift stopper that connected with the second spring would stop the solenoid valve. As a result, the discharge orifice was not completely open, and a lower injection rate was obtained at this pilot stage. When the pilot stage was just finished, the higher current level electric pulse was applied to the solenoid and the magnetic force increased. When this force pulled on the valve and overcame the second spring force, the solenoid valve was lifted higher. As the solenoid valve reached to the final stop position, the injector was fully opened. Therefore, a greater quantity of fuel was injected. The author showed that this two-step injection rate control injector could achieve the injection rate control in a common rail injection system, which had an operating pressures range of about 500-1500bar.

Ando et al. [26] developed a simulation method to determine the dynamic characteristics of a fuel injector in 2001. The authors presented a method for modeling and simulation of the dynamic characteristics of a solenoid actuator-based fuel injector. Eddy currents, magnetic saturation, and magnetic after-effect (defined as the rate of magnetization change after the magnetic field applied to a magnetic material is switched suddenly to a new value) were taken into account in the simulation modeling. Furthermore, this method took into account the magnetic after- effect in the 1-D and

lumped magneto-mechanical coupling mode. The authors confirmed that the injector open time and bouncing time delay was caused by magnetic after-effect.

In 2002, Coppo et al. [27] investigated the common rail type diesel injector for passenger cars by numerical analysis and by experimentation. The authors developed a mathematical model of a commercial type common-rail injector. The equivalent hydraulic scheme of the injector, the dynamic model of moving mechanical components and the electromagnetic model of the solenoid control valve were realized and discussed. In this paper, the electromagnetic model of the solenoid actuator was based on the magnetic equivalent circuit method, and it was used to calculate the reluctances of the solenoid actuator. The saturation phenomenon of the ferromagnetic material was taken into account. However, the magnetization curve was simplified as two stages. Before saturation it was presented as $B = \mu H$ ; while in the saturation stage, the magnetic flux was expressed as a flat line. Also, the material hysteresis and non-linearities were neglected. This model was used to identify the key parameters governing the injector performance.

Passarini and Pinotti [28] proposed a new model for a solenoid operated fuel injector analysis and design in 2003. Unlike most previous studies that solved the fuel injector electromagnetic model using the FEM method, which required numerous calculations, the authors used the surface integral method (SIM) to calculate the magnetic force directly. Moreover, while calculating the magnetic reluctance in the fuel injector

magnetic circuit, the air gap magnetic fringe, the iron and magnetic hysteresis were also considered. The conclusions of this new approach in modeling a fuel injector were:

1. Compared with the FEM and the previous model, it was shown to be more realistic and predicted with good accuracy the various aspects of the injector response, especially the effects of the armature rebounds;
2. The model accounted for many physical effects in injector armature motion, such as the eddy current, material magnetic saturation, and hysteresis.

This model showed more accuracy compared to previous models.

Also in 2003, Passarini and Nakajima [29] investigated the effects of armature mass on the fuel injector dynamic response. The authors modeled the electromagnetic fuel injector mechanical system using a traditional basic linear mass-spring-damper (MKsB) system. This linear MKsB model had the advantage that it allowed the use of Laplace transforms to easily analyze the systems. The results showed that this linear MKsB model was quite suitable in analyzing the physical problem, even though the electromagnetic fuel injector was a complex system. If the moving mass and the return spring characteristics were chosen properly, the dissipation of power would be effective in improving the injector fuel injection linearity at shorter pulses, as a result, the injector operation time was relatively reduced.

The literature review shows that the solenoid type PM moving bi-directional linear actuator was developed in the past fifteen years, and the published research papers in this field are few. Moreover, there is no published paper employing a bi-directional actuated actuator applied to vehicular fuel injectors.

In the literature review, the development of solenoid operated gaseous direct injection injector has been surveyed as well as the research works of other injection systems employing solenoid operated injectors in recent years.

The review showed that the electronic control units could directly and economically control solenoid actuators. When solenoids are employed in injection for CI engines, it is easy to control the fuel quantity, fuel injection timing and injection rate shape. However, the solenoid exhibits hysteresis, and saturation phenomenon that not only affect the accuracy of fuel injection quantity and injection rate, but also lead to incorrect timing of the fuel injection. This prevents the engine achieving its desired performance and increases emissions and fuel consumption. Therefore, the research and development in the field of fuel injection is focused on making the fuel injector respond faster and more accurately to increase the engine efficiency and to lower emissions. To solve these problems, the previous research work includes solenoid actuator design and modification, fuel injection systems optimization, injection rate shaping control, solenoid actuator current drive design, and modeling and simulation of the fuel injector as accurately as possible. The goal of this technology is to accelerate the injector response to

deliver accurate amounts of fuel into an internal combustion engine at the correct time to meet the desired performances of the engine.

### 1.3 Research Objective and Thesis Outline

The main objective of this research is to develop a new type of fast responding bi-directional solenoid actuator for applications to the direct injection of vehicular alternative fuels. Faster response and bi-directional control of the fuel injector means that a more precise dose of fuel can be injected into the combustion chamber; and this leads to improved fuel economy and reduced tailpipe emission pollutants.

A review of the literature has shown that the structure and mode of control of the bi-directional solenoid actuator as proposed in this research is novel and is vastly different from any existing bi-directional solenoid actuators. The literature review has also shown that there is no existence of any fuel injector, which is operated by a bi-directional solenoid actuator.

The initial approach of this research is to design the PM plunger bi-directional solenoid actuator and to analyze and select the PM construction material. The bi-directional solenoid actuator is modified from an existing off-the-shelf commercial solenoid actuator, with a PM plunger replacing the carbon steel plunger that is typically used. Neodymium iron boron (NdFeB) has been chosen as the permanent magnet material for the actuator plunger based on its characteristics of having the highest available magnetic energy, very high remanence and coercivity, and its excellent

magnetic characteristics. Especially, because the permeability of NdFeB is close to that of air, the solenoid force produced is only a function of the applied voltage and is independent of the air gap. This leads to a simpler system mathematical model and possibly simpler control strategies.

The next step is to develop the dynamic mathematical model of the bi-directional solenoid actuator. To have a high-level prediction of the solenoid dynamic performance, the nonlinear magnetic property and nonlinear inductance of the solenoid actuator are considered in the mathematical model. To reveal these characteristics, parameters relating to the solenoid properties are required. These parameters can be determined from the force acting on the PM plunger while varying the applied voltage to the solenoid, and by measuring the corresponding current through the solenoid. Therefore, the experimental setup to measure the solenoid transient current and corresponding force of the PM plunger is developed. Also, to record the experimental data, a computer data acquisition system has been set up. Since the total force acting on the PM plunger is the sum of the electromagnetic force due to the current and the attractive force due to the PM plunger on the steel core, therefore, an experimental set up to measure only the attractive force due to PM without the applied current is required to be built so as to validate the theoretical predications.

With a developed dynamic mathematical model of the bi-directional solenoid, therefore its transient response behaviors can be predicted by simulation. The dynamic mathematical model of the solenoid actuator is expressed by a second-order nonlinear

differential equation. A fourth-order Runge-Kutta integration method written in a C++ program is used to solve the system dynamics. The simulation results are then used to validate the actuator design and to analyze the actuator behaviors.

Finally, a design for an injector operated by a PM plunger bi-directional actuated solenoid actuator for alternative fuel direct injection is proposed. The literature review revealed that there is no bi-directional actuator currently employed in existing fuel injectors. The design of this new type of injector represents a modification of previous works. The mathematical model of the injector is developed based on the actuator model. As explained above, simulation results of the injector transient response behaviors are obtained from computer calculations. The simulation can help analyze the injector design, and define parameters which affect the injector response. The force of impact between the needle and the injector seat causes wear and needle bouncing, which will be further discussed. Also, simulation will allow the comparison of the novel design with injectors operated by traditional solenoid actuators.

The structure of this thesis is as follows. Chapter 1 reviews the published literature associated with the PM plunger bi-directional solenoid actuator and the development of solenoid operated fuel injectors, including alterative fuels and oil fuels, in recent years are reviewed; also, it describes the research objective and the thesis outline. Chapter 2 covers the research and development of the PM plunger bi-directional solenoid actuator. This chapter includes modeling the PM plunger bi-directional actuated solenoid actuator, the experimental setups to measure the dynamic currents and the corresponding

forces of solenoid actuation, computer simulation and validation, and analysis. Chapter 3 treats the application of the PM plunger bi-directional actuated solenoid actuator in an alternative fuel injector. The injector mathematical model is built and the simulation results, injector's parameters, and injector performance are discussed. Finally, Chapter 4 offers the conclusion and recommendations for future research in this domain.

# CHAPTER 2

# DEVELOPMENT AND MODELING OF A PERMANENT MAGNET PLUNGER BI-DIRECTIONAL SOLENOID LINEAR ACTUATOR

## 2.1 Introduction

The simplicity of its construction combined with a relatively low cost of production, leads to linear solenoid electromagnetic actuators being used extensively in many different applications. In most transportation vehicles, solenoid electromagnetic linear actuators are main components in fuel injectors.

In general, the operational requirements from the injection system are extremely demanding. The duration of the fuel injection is very short and must be very precise. Therefore, for the solenoid-operated injector, the solenoid actuator must respond fast to be able to regulate with a high degree of precision, the timing of the injector opening and closing and the dosage of fuel.

A new type of actuator that is intended to be applied to improve the injection performance of injectors is described in this chapter. This new actuator was modified from a conventional solenoid actuator, and can be actuated in bi-directional motion when the direction of the drive current is changed. The mathematical model of this new type of solenoid actuator has also been elaborated where the nonlinear effects of the magnetic properties of the solenoid are taken into account. Furthermore, an experimental setup has

been designed and built and was used to acquire the necessary data for determining the parameters of the mathematic model. The mathematical model of the actuator was computer simulated and the results were compared to experiments performed on the actuator. The two results demonstrated a high degree of correlation.

## 2.2 The Moveable Permanent Magnet (PM) Plunger Bi-directional Linear Solenoid Actuator

A conventional solenoid actuator consists of the static parts, namely, the solenoid coil, and the steel body frame (or housing) with the carbon steel static core or stator. The dynamic part is the carbon steel plunger or armature. When the current is applied to the solenoid coil, it produces a magnetic field and the electromagnetic energy is stored in the field. The resulting magnetic field set up between the static core and the movable plunger produces a magnetic force to attract the plunger towards the static core.

Normally, the plunger of the traditional solenoid actuator is fabricated from a ferromagnetic material such as carbon steel. In this type of solenoid actuator, the magnetic force produced by the current, can pull only, even if the direction of the current in the coil is reversed. Therefore, a spring is needed to help move the plunger off the static iron core in this type of actuator. In other words, for the traditional solenoid actuator, the current applied to the solenoid cannot produce a bi-directional plunger motion. The disadvantage of using this type of solenoid actuator in a system design is that

it needs a larger space for the spring that is used to move the plunger back to its original position. As well, the position of the steel plunger with a return spring is less controllable.

As mentioned in Chapter 1, electromagnetic bi-directional drive linear actuators have been in use for more than fifty years. However, applying a permanent magnet (PM) as a moving plunger for the solenoid type linear bi-directional actuator has been developed in the past twenty years. In this research, a new type of movable PM plunger bi-directional solenoid linear actuator is proposed; this new type of actuator is different from the PM plunger bi-directional motion actuators that have been shown in the literature review. The structure of the new type bi-directional actuator is similar to the typical solenoid actuator. It has a wound coil, carbon steel housing/frame and stator iron core, but a moveable PM plunger replaces the traditional carbon steel plunger.

The schematic diagram of this solenoid is shown in Figure 2.1. It was modified from an existing commercial linear solenoid actuator, Lisk Model L7 Solenoid, made by the G.W. Lisk Company [30]. The difference between the original solenoid actuator and the modified solenoid actuator described in this research is that the carbon steel cylindrical plunger is replaced by a PM cylindrical plunger having the same dimensions and with the direction of magnetization along its longitudinal axis. The cylindrical PM plunger has the diameter $d$ and the length $l_m$; the solenoid coil length is $L_c$; the static iron core length inside the coil is $L$; and the air-gap between the core and the moving plunger is $x$.

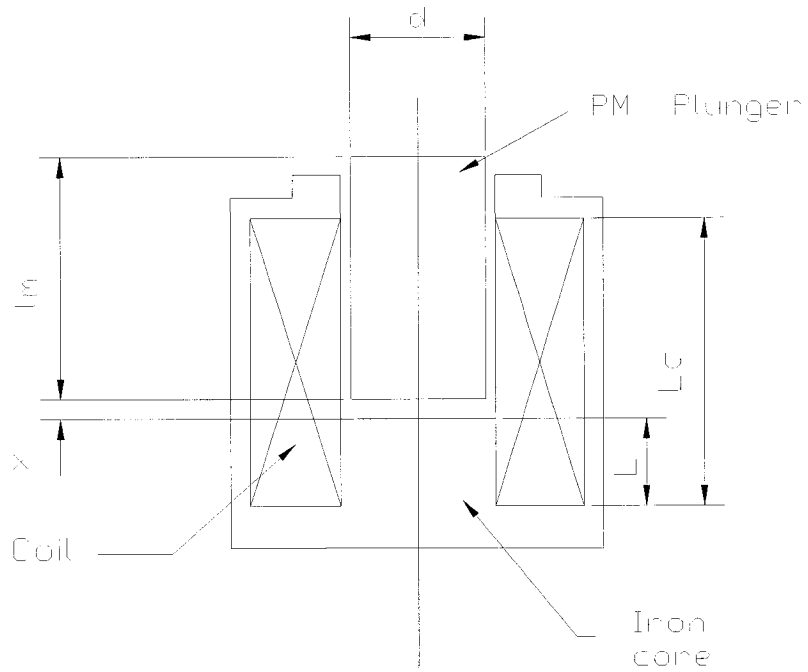


**Figure 2.1 Solenoid type bi-directional actuator with a movable PM plunger**

When the solenoid is not energized, the PM plunger (assuming that its south pole faces the solenoid static iron core pole) will attract the solenoid iron core pole due to the magnetic field of the PM. When the solenoid is activated with current flowing in the direction such that the magnetic field due to the coil enters the iron core, therefore the iron core will become a south pole. This south pole then produces a force to repel the south pole of the PM plunger. When this force exceeds the PM force of attraction, it will push the plunger away from the iron core. Conversely, when the solenoid current is changed to flow in the opposite direction, the solenoid iron core pole reverses to a north pole, and the resulting magnetic force pulls the PM plunger towards the iron core. Therefore, by alternating the solenoid current direction, the PM plunger bi-directional motion can be achieved.

## 2.3 The Properties of Neodymium Iron Boron (NdFeB) Permanent Magnet (PM)

To understand the permanent magnet (PM) moveable plunger solenoid actuator, it is necessary to know the properties of the PM as used in the solenoid.

Normally, the magnetic material properties are characterized by the B-H curve, where B is magnetic induction, and H is the magnetic field strength. The second quadrant of the B-H curve, as shown in Figure 2.2, is commonly referred to as the Demagnetization Curve, which describes the conditions under which permanent magnets are used in practice. The three most important characteristics of the B-H curve are the points at which it intersects the $B$ and $H$ axes (at $B_r$, the residual induction, and $H_c$, the coercive force, respectively), and the point at which the product of B and H are at a maximum ($BH_{max}$ - the maximum energy product). $B_r$ represents the maximum flux the magnet is able to produce under closed circuit conditions. $H_c$ represents the point at which the magnet becomes demagnetized under the influence of an externally applied magnetic field. $BH_{max}$ represents the point at which the product of $B$ and $H$, and the energy density of the magnetic field into the air gap surrounding the magnet, is at a maximum. The higher this product, the smaller need be the volume of the magnet.

The PM material used for the solenoid actuator plunger in this research is Neodymium Iron Boron (NdFeB). NdFeB magnets are a third generation permanent magnet that became commercially available in the mid 1980's and has become increasingly popular since its inception. The advantages of NdFeB magnets are [31, 32, 33]:

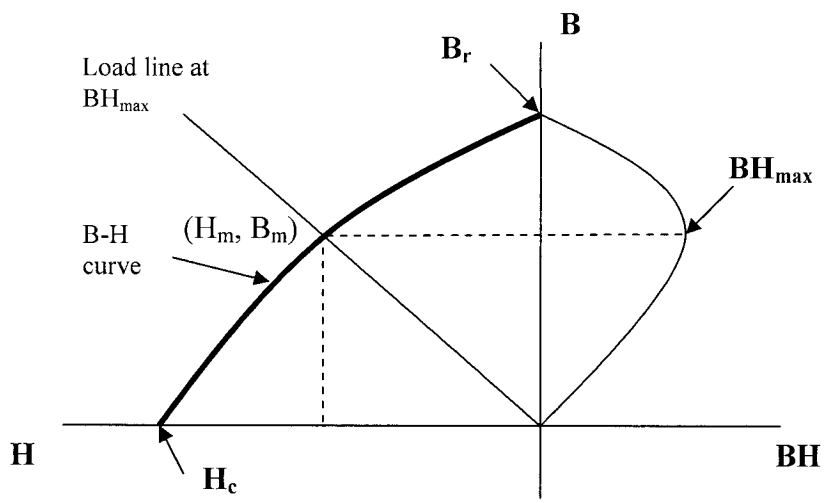


**Figure 2.2 Magnetic material B-H curve sketch**

1. They provide the highest available magnetic energies of any material. They are the most powerful commercialized permanent magnets available today, with maximum energy product ranging from 26 MGOe to 52 MGOe.

2. They have a combination of very high remanence *Br* and coercivity *Hc* in a wide range of magnetic grades.

3. They have linear demagnetization characteristics throughout the entire second quadrant in its magnetic characteristics curve. The

recoil line of the NdFeB in the operating region is a straight-line with a slope equal to 1.05 $\mu_0$ to 1.06$\mu_0$, which is almost the same as the slope of its demagnetization line; thus, it is convenient to consider the B-H curve as linear in the operating region.

4. With its excellent magnetic characteristics, abundance of its raw material, and relatively low cost, NdFeB offers flexibility in designing new or replacing traditional magnet materials.

5. The irreversible loss and moderately high reversible temperature coefficient of remanence *Br* and intrinsic coercivity *Hci*, allows its use in maximum temperatures to 200 °C for high coercivity grades.

The demagnetization curves for different grades of NdFeB, are shown by the straight lines in Figure 2.3 [31]. The curves, on the left of the figure, are the corresponding "intrinsic magnetization characteristics", and are not discussed in this thesis. The interested reader may refer to reference [32] for more detail.

In this research, the PM material NdFeB is made by the Dexter Magnetic Technologies Company, USA. The high PM material grade ND45 has been selected as the solenoid plunger in this research for its higher magnetic grade and ability to contain a high amount of energy.

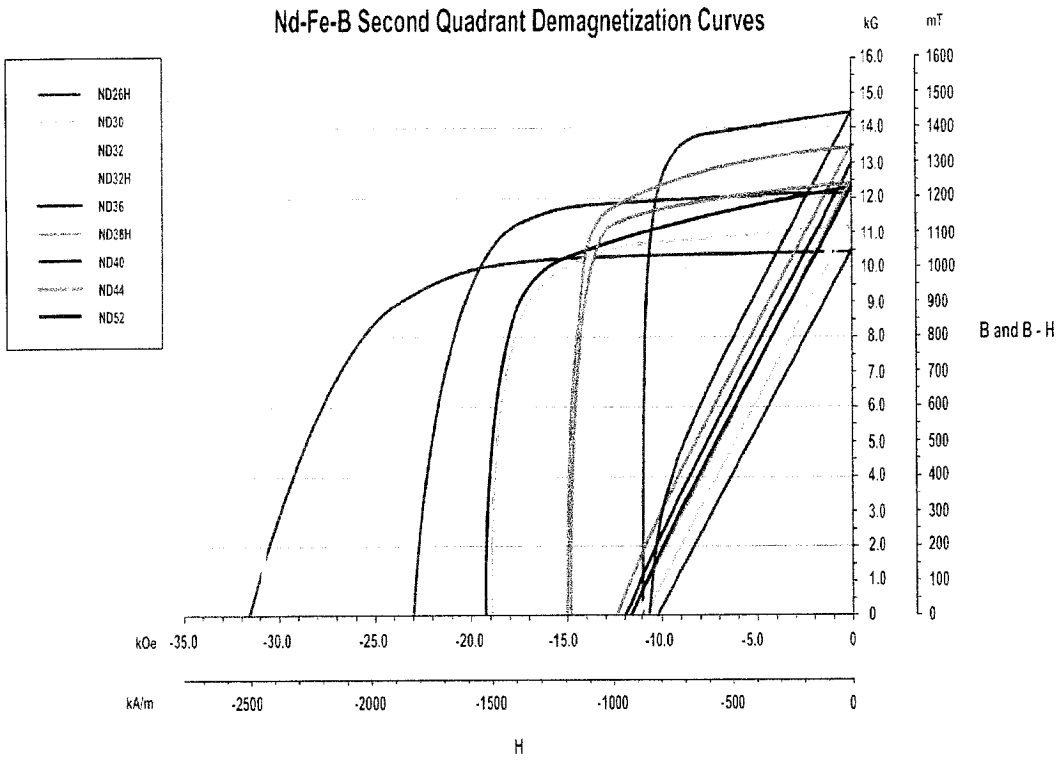


**Figure 2.3 NdFeB demagnetization curves [31]**

The relevant parameters with respect to grade ND45 NdFeB PM are [34]:

Maximum energy product $BH_{\max} = 358kJ/m^3$ ;

Permanent remanence $B_r = 1.35T$;

Coercivity $H_c = 1011kA/m$;

Maximum Operating Temperature 100 °C.

For the PM material, the magnetic operating point ($B_m$, $H_m$) is given by [32]:

$$\mathbf{B_m} = \mu_0(\mu_{rec}\mathbf{H_m} + \mathbf{M}) \tag{2.1}$$

where, $\mathbf{B_m}$ and $\mathbf{H_m}$ are the field flux density and the field strength of the PM at the operating point; $\mu_0$ is the permeability of the air; $\mu_{rec}$ is the PM relative recoil permeability; and $\mathbf{M}$ is the magnetization of the material

For the NdFeB PM, as mentioned previously, the demagnetization lines are linear in the operating range and thus $M$ is a constant for a uniformly magnetized magnet [32, 33]. The PM with this feature may be called an Ideal Magnet.

Defining the PM permeability $\mu_m$ as:

$$\mu_m = \mu_0 \mu_{rec} \tag{2.2}$$

then, Equation (2.2) can be rewritten as:

$$\mathbf{B_m} = \mu_m \mathbf{H_m} + \mu_0 \mathbf{M} \tag{2.3}$$

Note that for PM material NdFeB, its permeability $\mu_m$ and the air permeability $\mu_0$ are expressed as: [33, 35]:

$$\mu_m = 1.05\mu_0 \tag{2.4}$$

Because $\mu_m$ is normally very close to $\mu_0$, the permeability of this permanent magnet is regarded as an air [35, 36]. Thus, it can be approximated as:

$$\mu_m \approx \mu_0 \tag{2.5}$$

Therefore, equation (2.3) becomes:

$$\mathbf{B_m} = \mu_0 \mathbf{H_m} + \mu_0 \mathbf{M} \tag{2.6}$$

In this research, the PM plunger is cylindrical with magnetization along its longitudinal axis. To simplify the mathematical manipulation, a cylindrically shaped PM with longitudinal axis magnetization can be considered as uniformly magnetized. For a uniformly magnetized magnet, the magnetization **M** is a constant inside the magnet [32]. Therefore, when an applied magnetic field makes the PM strength $H_m = 0$ , the remanence $B_r$ of the PM can be obtained from equation (2.6):

$$B_r = \mu_0 M \tag{2.7}$$

Or the value of ideal PM magnetization $M$ is:

$$M = \frac{B_r}{\mu_0} \tag{2.8}$$

Also, when $B_m = 0$, the coercivity $H_c$ of the PM is known as:

$$H_c = M \tag{2.9}$$

## 2.4 Modeling of the Bi-directional Solenoid Linear Actuator with Movable Permanent Magnet Core

### 2.4.1 The Dynamics Equations of the Solenoid Actuator

Ignoring the effect of eddy current losses and the hysteresis of the solenoid, the equivalent circuit of the solenoid can be expressed as shown in Figure 2.4. It consists of the solenoid coil resistance $R$, the nonlinear inductance $L(\phi)$ due to the coil and the

material, and the external circuit inductance $L_e$ which is the leakage inductance caused by the flux leakage; $V$ is the supply voltage applies to the solenoid; $i$ is the current through the solenoid circuit.

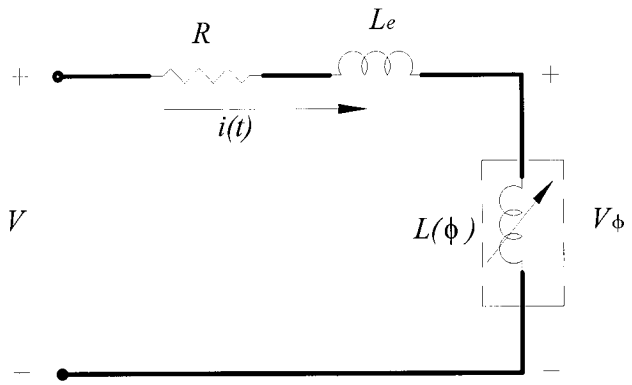


**Figure 2.4 Equivalent circuit of the solenoid**

From the equivalent circuit given in Figure 2.4, the voltage equation of the solenoid can be expressed as:

$$V = iR + L_e \frac{di}{dt} + V_\phi . \tag{2.10}$$

where $V_\phi$ is the induced voltage of the solenoid coil. From Faraday's law, $V_\phi$ can be expressed as:

$$V_\phi = \frac{d\lambda}{dt} \tag{2.11}$$

where $\lambda$ is the flux linkage of the solenoid, a variable that is dependent on the current $i$ through the coil, and the air-gap $x$ between the plunger and the stator core. For $N$ turns of coil winding, a solenoid coil with the magnetic flux $\Phi(i,x)$ crossing the air-gap $x$, the flux linkage can be expressed as:

$$\lambda = N\Phi(i,x) \tag{2.12}$$

Thus for the variables $i$ and $x$, the partial derivative form of the flux linkage is:

$$\frac{d\lambda}{dt} = \frac{d[N\Phi(i,x)]}{dt} = N\frac{\partial\Phi(i,x)}{\partial i}\frac{di}{dt} + N\frac{\partial\Phi(i,x)}{\partial x}\frac{dx}{dt} \tag{2.13}$$

Substituting equation (2.13) into equation (2.11), it becomes:

$$V_\phi = N\frac{\partial\Phi(i,x)}{\partial i}\frac{di}{dt} + N\frac{\partial\Phi(i,x)}{\partial x}\frac{dx}{dt} \tag{2.14}$$

Then equation (2.10) can be rewritten as:

$$\begin{aligned} V &= iR + (L_e + N\frac{\partial\Phi(i,x)}{\partial i})\frac{di}{dt} + N\frac{\partial\Phi(i,x)}{\partial x}\frac{dx}{dt} \\ &= iR + (L_e + L_{coil}(i,x))\frac{di}{dt} + N\frac{\partial\Phi(i,x)}{\partial x}\frac{dx}{dt} \end{aligned} \tag{2.15}$$

$L_{coil}(i,x)$ is the nonlinear inductance of the solenoid, which is a function of the current $i$ and air-gap length $x$. Equation (2.15) comprises of three terms: the voltage drop due to the coil resistance; the inductive voltage caused by the change of the current; and the electromotive force due to the plunger motion.

For the solenoid actuator as shown in Figure 2.1, ignoring the friction between the plunger and the solenoid inner shell, based on Newton's Second law, the dynamic motion equation of the PM plunger is:

$$m\frac{dv}{dt} = F(i,x) - mg \tag{2.16}$$

where $F(i,x)$ is the total force acting on the PM plunger, which includes two forces, namely the force between the PM and the iron core, and the force due to electromagnetism produced by the solenoid coil; $m$ is the mass of the PM plunger; $v$ is the velocity of the plunger motion; and $g$ is the gravitational acceleration.

When the PM plunger moves through a displacement $x$, the velocity $v$ of the plunger can be expressed as:

$$v = \frac{dx}{dt} \tag{2.17}$$

Therefore, the solenoid actuator dynamic mathematical model can be expressed as:

$$\begin{cases} V = iR + (L_e + L_{coil}(i,x))\dfrac{di}{dt} + N\dfrac{\partial\Phi(i,x)}{\partial x}\dfrac{dx}{dt} \\ m\dfrac{dv}{dt} = F(i,x) - mg \\ v = \dfrac{dx}{dt} \end{cases} \tag{2.18}$$

When the characteristics of magnetic flux $\Phi(i,x)$, the nonlinear inductance $L_{coil}(i,x)$ and the total force $F(i,x)$ acting on the plunger are known, then system equation (2.18) can be solved for the variables of current $i$ and air-gap $x$ with respect to time $t$. $\Phi(i,x)$, $L_{coil}(i,x)$ and $F(i,x)$ in the solenoid actuator system as discussed in the next section.

### 2.4.2 The Flux $\Phi(i,x)$ in the Solenoid

When a PM is in an external magnetic field, the total field can be treated separately as an external magnetic field and the PM magnet field. When current is applied to the PM plunger solenoid actuator under investigation there will be two magnetic sources in the actuator. One is the PM magnet field, and another is the solenoid electromagnet field due to the activating current. Here, the electromagnetic field is the external field. In this case the magnetic field and the flux that are in the air-gap $x$ can be expressed, respectively, as [37, 11]:

$$\mathbf{B(i,x)} = \mathbf{B}_{\mathbf{coil}}\mathbf{(i,x)} + \mathbf{B}_{\mathbf{PM}}\mathbf{(i,x)} \tag{2.19}$$

$$\Phi(i,x) = \Phi_{coil}(i,x) + \Phi_{PM}(i,x) \tag{2.20}$$

where $\mathbf{B}_{coil}(i,x)$ and $\mathbf{B}_{PM}(i,x)$ is the magnetic field due to the coil and the PM respectively; $\Phi_{coil}(i,x)$ and $\Phi_{PM}(i,x)$ is the magnetic flux due to the coil and the PM respectively. Equations (2.19) and (2.20) show that the total fluxes inside the solenoid is contributed by two sources, the flux due to the coil and that due to the PM.

As there are two field sources in the solenoid, then, the total magnetic force acting on the PM plunger is [37,11]

$$\mathbf{F}(i,x) = \mathbf{F}_{coil}(i,x) + \mathbf{F}_{PM}(i,x) \tag{2.21}$$

where $\mathbf{F}_{coil}(i,x)$ and $\mathbf{F}_{PM}(i,x)$ is the force due to the coil and the PM respectively.

### 2.4.3 The Flux Due to the PM plunger $\Phi_{PM}(i,x)$

As mentioned in section 2.3, the direction of magnetization of the PM plunger is parallel to the cylindrical longitudinal axis. In addition it is considered that the magnetic field inside the cylindrical PM is uniform in its magnetization direction.

For the solenoid actuator when there is no current activating the solenoid, the only magnetic source will be from the PM plunger. Ignoring the magnetic fringes in the

magnetic circuit, the ideal magnetic path and the equivalent magnetic circuit of the solenoid actuator are shown in Figure 2.5 and Figure 2.6, respectively.

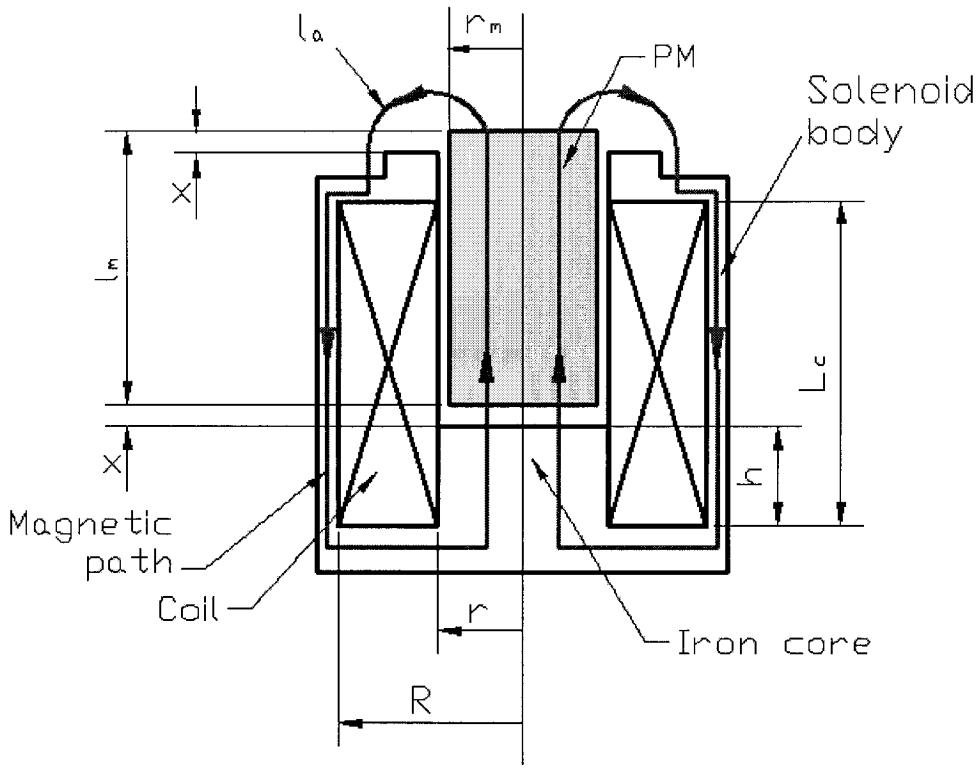


**Figure 2.5 Solenoid actuator magnetic path due to PM**

In the magnetic circuit Figure 2.6, $\Re_x$ is the reluctance of the air-gap between the iron core pole and PM plunger pole; $\Re_a$ is the reluctance of the air-gap between the solenoid body tip and the PM upper pole. $\Re_{PM}$ is the reluctance of the PM plunger; $\Re_B$ is the reluctance of the solenoid iron body; and $F_m$ is the magnetomotive force (mmf) of the PM, respectively.

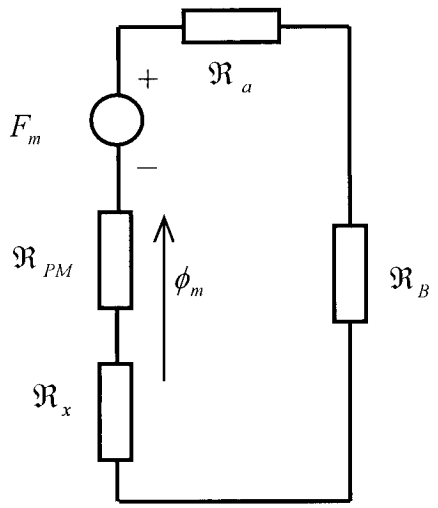


**Figure 2.6 Solenoid actuator equivalent circuit due to permanent magnetic plunger**

From the equivalent circuit, the mmf of the PM is given by:

$$F_m = \phi_m(\Re_{PM} + \Re_x + \Re_B + \Re_a) \tag{2.22}$$

where $\phi_m$ is the flux in the magnetic circuit due to the PM. When a PM has a length $l_m$ and its magnetization direction along its length, the mmf of the PM can be expressed as [33]:

$$F_m = H_c l_m \tag{2.23}$$

From equation (2.8) and (2.9), the mmf of the magnet can be rewritten as:

$$F_m = \frac{B_r}{\mu_0} l_m \tag{2.24}$$

Hence, the magnetic flux $\phi_m$ due to the permanent magnet in the magnetic circuit is obtained from equation (2.22):

$$\phi_m = \frac{F_m}{\Re_{PM} + \Re_x + \Re_B + \Re_a} \tag{2.25}$$

Note that high material permeability can result in low reluctance. Compared with the air and the steel body of the solenoid, the reluctance of the solenoid body is much smaller than that of air; thus, the reluctance of the solenoid body $\Re_B$ normally can be neglected in the magnetic circuit. As a result, equation (2.25) normally is regarded as:

$$\phi_m = \frac{F_m}{\Re_{PM} + \Re_x + \Re_a} \tag{2.26}$$

In equation (2.26), $\Re_x$, $\Re_{PM}$ and $\Re_a$ are given as [33]:

$$\Re_x = \frac{x}{\mu_0 A} \tag{2.27}$$

$$\Re_{PM} = \frac{l_m}{\mu_m A} \tag{2.28}$$

$$\Re_a = \frac{l_a(x)}{\mu_0 A_1} \tag{2.29}$$

where $x$ is the air-gap between the moving PM and the static iron core, $A$ is the pole end effective area or the cylindrical PM end effective area, which is normal to the magnetic flux path; $l_a(x)$ is the length of the air-gap between the pole of the PM plunger and the end of the solenoid body tip. From Figure 2.5, it can be seen that this air-gap is a function of $x$. To simplify the calculation, $l_a(x)$ will be determined by experimental method, and will be discussed in section 2.6. $A_1$ is the effective area that the magnetic flux passes the air-gap between the extruding pole of the PM plunger and the end of the solenoid body tip. Because magnetic flux is continuous, to simplify the calculation, $A_1$ is regarded equal to the pole end and the boss end effective areas $A$, or $A_1$=$A$.

Because of equation 2.5, $\mu_m \approx \mu_0$, then, equation (2.26) can be rewritten as:

$$\phi_m = \phi_m(x) = \Phi_{PM}(i,x) = \frac{B_r l_m A}{x + l_a(x) + l_m} \tag{2.30}$$

Equation (2.30) shows that the flux in the solenoid due to the PM is a function of the air-gap $x$ when its structure is determined. As the air-gap is increased, the flux due to the PM is reduced because of the increase in reluctance.

### 2.4.4 The Flux Due to the Coil $\Phi_{coil}(i,x)$

When the solenoid is activated by the current, in the ideal state, the solenoid flux path due to the coil is as shown in Figure 2.7. It can be seen that there are four parts of reluctances in the magnetic path: the air-gap reluctance $\Re_x$ between the iron core pole and PM plunger pole; the air-gap reluctance $\Re_g$ between the boss end and the plunger; the reluctance of the PM plunger $\Re_{PM}$, where as discussed as in equation (2.5), $\mu_m \approx \mu_0$; and the reluctance of the solenoid body $\Re_B$.

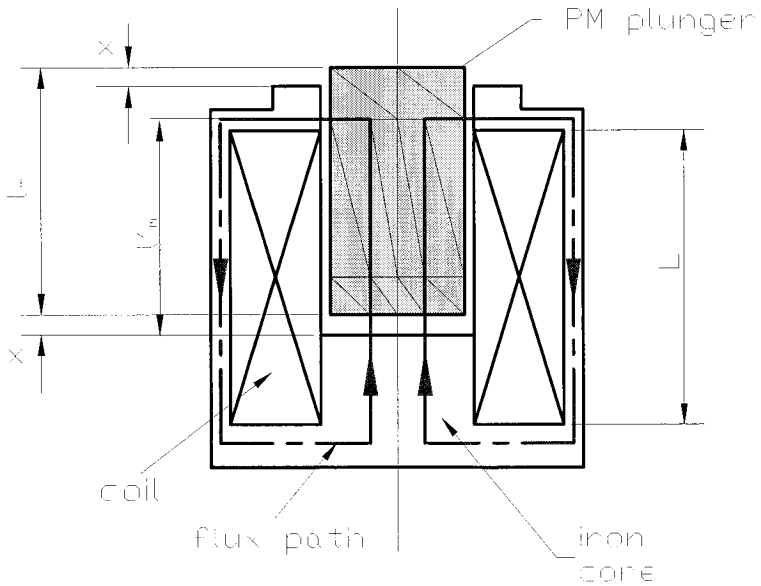


**Figure 2.7 Solenoid actuator magnetic flux path due to current**

The magnetomotive force (mmf) equation of the magnetic circuit due to the applied current is expressed as:

$$Ni = \phi_{coil}\left(\Re_x + \Re_g + \Re_{PM} + \Re_B\right) \tag{2.31}$$

where $N$ is the solenoid coil winding turns; $i$ is the coil current; $\phi_{coil}$ is the magnetic flux through the cross-sectional area of the solenoid due to the activating current.

Also, $\Re_x$ is given as equation (2.27); $\Re_g$ and $\Re_{PM}$ are given as:

$$\Re_g = \frac{l_g}{\mu_0 A_g} \tag{2.32}$$

$$\Re_{PM} = \frac{l_m' - x}{\mu_0 A} \quad \text{since } \mu_m \approx \mu_0 \tag{2.33}$$

where $l_m'$ is the effective length of the PM plunger while the air-gap $x$ is zero.

For the ferromagnetic materials, such as steel or iron, when they are inside a mutative current generated magnetic field, their permeability is not constant due to their material properties. As the flux through the iron core varies, its permeability will change with the flux. Moreover, this variance is a nonlinear function of the flux. Therefore, the reluctance of the core $\Re_B$ is a nonlinear function of the magnitude of its magnetic fluxes. Note that in this solenoid, the current produces these magnetic fluxes; consequently, $\Re_B$ is a nonlinear function of the current applied to the solenoid.

The mathematical model of the iron core nonlinear reluctance $\Re_B$ can be expressed by Froelich's equation [17, 38]:

$$\Re_B = \frac{a}{b - \phi_{coil}} \tag{2.34}$$

where the parameters $a$ and $b$ are related to the property of the material and the construction of the solenoid actuator. They may be determined by experiment, as discussed in the following section 2.6.

Substituting equation (2.27), (2.32), (2.33), and (2.34) into equation (2.31), then it becomes:

$$Ni = \phi_{coil}(\Re + \frac{a}{b - \phi_{coil}}) \tag{2.35}$$

where $\Re$ is the sum of the reluctance of the boss-end air-gap $\Re_g$, the reluctance of the air-gap $\Re_x$ and the reluctance of the PM $\Re_{PM}$, and it is:

$$\Re = \frac{l_g}{\mu_0 A_g} + \frac{l_m^{'}}{\mu_0 A} \tag{2.36}$$

Equation (2.36) shows that the sum of the reluctances $\Re$ is not a function of the PM plunger traveling air-gap $x$. It is only a function of the solenoid actuator's structure: the fixed air-gap between the solenoid boss-end and the plunger and its area; and, the length of the PM and the cross-sectional area of the PM plunger. The fact that the

reluctance $\Re$ does not depend on the PM plunger travel $x$ can be clearly seen by observing equations (2.27) and (2.33). The second term on the right hand side of equation (2.36) is the sum of these two reluctances, and because $\mu_m \approx \mu_0$ . Therefore, from equation (2.35), it can be seen that that when the parameters, $a$ and $b$, of the solenoid actuator are determined, the magnetic flux $\phi_{coil}$ due to current $i$ can be solved.

### 2.4.5 The Inductance of the Solenoid $L_{coil}(i,x)$

When a solenoid coil with $N$ turns is activated by the current $i$ it will produce the magnetic flux $\phi$ . Then, the inductance of this solenoid is defined as:

$$L = N\frac{d\phi}{di} \tag{2.37}$$

Differentiating both sides of equation (2.35) and rearranging the terms, the following equation can be obtained:

$$d\phi_{coil}(i,x) = \frac{N}{\Re + \dfrac{ab}{(b-\phi_{coil})^2}}di \tag{2.38}$$

Then, the inductance of the solenoid coil $L_{coil}(i,x)$ is obtained as:

$$L_{coil}(i,x) = N\frac{d\phi_{coil}(i,x)}{di}$$
$$= \frac{N^2}{\Re + \frac{ab}{(b-\phi_{coil})^2}} \tag{2.39}$$

As discussed in Section 2.4.4, the reluctance $\Re$ is known as a constant. However, the flux due to the coil current is a nonlinear function of the current; also, it is related to the solenoid material and structure; therefore, the inductance of the solenoid actuator in equation (2.39) is a nonlinear function.

## 2.5 The Force Acting on the Plunger

In section 2.4.2, it was proposed that the magnetic force acting on the plunger consists of two parts: the attractive force due to the PM and the electromagnetic force due to the current flowing through the coil. The total force acting on the PM plunger is the sum of these two forces. In this section, these two forces will be discussed and analyzed.

### 2.5.1 The Force Due to PM $F_{PM}(i,x)$

For the solenoid actuator shown in Figure 2.1, when the current does not activate the solenoid, the magnetic field of the PM exists in the air-gap between the PM plunger pole and the iron core pole. This magnetic field produces a force to attract the iron core

and the PM to each other. This magnetic attractive force can be calculated by the following equation[32]:

$$F_{PM}(i,x) = \frac{\phi_m^2(i,x)}{2\mu_0 A} \tag{2.40}$$

Substituting equation (2.30) into equation (2.40), one has:

$$\begin{aligned} F_{PM}(i,x) &= F_{PM}(x) \\ &= k\frac{A}{2\mu_0}\left(\frac{B_r l_m}{x + l_a(x) + l_m}\right)^2 \end{aligned} \tag{2.41}$$

It should be noted that a loss factor $k$ has been introduced in equation (2.41). In theory, the magnetic circuit is regarded as ideal, where the magnetic fringe and leakage were ignored; therefore, errors will arise between the theoretically predicted results and the experimental results. To account for these effects and make the theory closer to the real data, a loss factor $k$ can be added to the ideal model. The method that is applied to determine the loss factor $k$ will be discussed in section 2.6.

### 2.5.2 The Force Due to the Coil $\mathbf{F_{coil}(i,x)}$

When a PM is in a continuous external magnetic field, the field produces a force that acts on the PM. The total force **F** acting on the PM due to the external magnetic field is given by [39]:

$$\mathbf{F} = \int(-\nabla \bullet \mathbf{M})\mathbf{B}_0 dV + \int \mathbf{n} \bullet \mathbf{M}\mathbf{B}_0 dS \tag{2.42}$$

where $\mathbf{B_0}$ is the external magnetic field due to all other sources and does not include the effect of the source due to PM itself; $dV$ is the element of PM volume in the field, and $dS$ the area element which is normal to the field; $\mathbf{M}$ is the magnetization of the PM. $-\nabla \bullet \mathbf{M}$ and $\mathbf{n} \bullet \mathbf{M}$ are defined as magnetic volume charge density and magnetic surface charge density.

In this research, the PM is cylindrical and is considered to have uniform magnetization $\mathbf{M}$ along the cylindrical axis. Furthermore, for the problem at hand, it may be noted that the external field $\mathbf{B_0}$ is only the coil field $\mathbf{B_{coil}}$ that is produced by the activating current, which is along the longitudinal axis of the cylindrical PM. Because the uniform magnetization $\mathbf{M}$ is in the direction of the axis; the magnitude of the magnetization is $M$; in addition, the uniform magnetization $\mathbf{M}$ has no divergence; therefore, the magnetic surface charge densities and volume charge densities are [40], respectively:

$$\mathbf{n} \bullet \mathbf{M} = M \tag{2.43}$$

$$-\nabla \bullet \mathbf{M} = 0 \tag{2.44}$$

Then, the force acting on the PM plunger $F_{coil}$ due to the coil can be calculated from equation (2.42) as [41]:

$$F_{coil}(i,x) = \int_A MB_{coil}(i,x)dA$$
$$= MA\left[B_{coil}(i,x)\big|_{x1} - B_{coil}(i,x)\big|_{x2}\right] \tag{2.45}$$

where $B_{coil}(i,x)\big|_{x1}$ and $B_{coil}(i,x)\big|_{x2}$ are the magnetic fields due to the coil at the two pole ends of the PM plunger.

For a solenoid coil having $N$ turns of length $L_c$ and of radius $R_c$, and by choosing the solenoid center point on the longitudinal axis as the reference point 0, therefore the magnitude of magnetic field along the axis with distance $x$ from the reference point is given by [40]:

$$B(x) = \frac{\mu_0 Ni}{2L_c}\left[\frac{L_c/2 - x}{\sqrt{R_c^{\,2} + (L_c/2 - x)^2}} + \frac{L_c/2 + x}{\sqrt{R_c^{\,2} + (L_c/2 + x)^2}}\right] \tag{2.46}$$

From equation (2.46), the shape of the magnetic field of the solenoid along the longitudinal axis is as shown in Figure 2.8. It can be seen that inside the solenoid the magnitudes of the magnetic field have almost the same value. And at the two ends of the solenoid, the magnetic field is much less than inside the solenoid. As the distance increases, the magnitude of the magnetic field trends to zero.

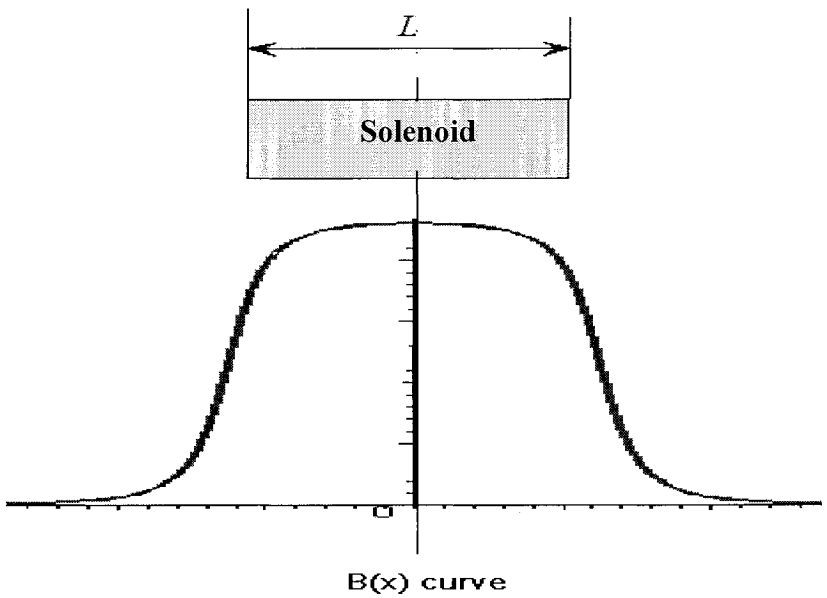


**Figure 2.8 The shape of the magnitude of the solenoid magnetic field along the longitudinal axis**

The proposal in this research is to use this type of novel solenoid actuator with the PM as the moving plunger for automobile fuel injectors. Normally, the traveling stroke of the injector needle is around 0.5mm to 0.7mm [3, 38]. It is assume that the PM plunger actuator has the maximum traveling distance of 0.8mm. Compared with the solenoid coil length $L$, this traveling distance is very small. When a solenoid actuator has the structure as shown in Figure 2.7, it can be seen that only one pole of the PM plunger is inside the solenoid and that this pole is very close to the center of the solenoid. To simplify calculations, it is assumed that the field $B_{coil}(i,x)\big|_{x1}$ of the pole end inside the solenoid is equal to the field $B_{coil}(i,x)$ at the solenoid center. From Figure 2.8 it is known that the field magnitudes in the center region of the solenoid are almost the same. Also from Figure 2.7, it can be seen that the other pole end of the PM plunger is outside of the

solenoid, and this distance is approximately $L/2$. Therefore, it can be assumed that this pole end of the PM plunger is far from the solenoid end. From Figure 2.8 which shows the shape of the solenoid magnetic field, it can be seen that the field $B_{coil}(i,x)\big|_{x2}$ at this position is almost zero. Thus, equation (2.45) can be simplified as:

$$\begin{aligned} F_{coil}(i,x) &= MAB_{coil}(i,x)\big|_{x1} \\ &= MAB_{coil}(i,x) \\ &= M\phi_{coil}(i,x) \end{aligned} \tag{2.47}$$

Equation (2.47) shows that the force which acts on the PM plunger is a function of the magnetic field or flux strength due to the coil. As discussed above, the magnitude of the magnetic field inside the solenoid, especially in the region around the center part, can be considered the same. This means that for a small stroke PM plunger solenoid actuator, the field or flux acting, on the PM plunger pole end inside the solenoid can be regarded as the same. The field or flux inside the solenoid is determined only by the current $i$ applied to the solenoid coil.

## 2.6 Experimental Setup and Discussion

Two experimental setups were built. One experimental setup measures the forces due to the PM acting on the solenoid stator iron core for different air-gaps. This experimental setup determines how the forces differ between the theoretical predications and the observed data. Another experimental setup is applied to measure the bi-

directional PM plunger solenoid actuator transient forces and currents. This experimental setup is applied to determine the magnetic characteristics due to applications of different voltages.

### 2.6.1 Experimental Setup to Measure the PM Force Acting on the Plunger at Different Air-gaps and Experimental Results

As discussed in section 2.5.1, since the magnetic circuit was considered as ideal, errors will occur between the theoretical predictions and observed data; it is necessary to determine the loss factor $k$ in equation (2.41). The method that determines $k$ involves measuring the real force due to the PM at different air-gap settings. By comparing the experimental results with the ideal theoretical values, the loss factor $k$ can be determined.

The experimental setup to measure the force between the PM plunger and the solenoid stator iron core is illustrated in Figure 2.9. The setup includes an adjustable threaded rod which connects the solenoid housing/body together. The threaded rod can move in and out through the threaded hole in the frame plate; a non-ferromagnetic brass pin is connected with the PM plunger; a plane-head pin is on the other side of the frame, and its plane-head can fully contact the piezo load cell transducer surface. This load cell is on the frame plate; the two pins are connected by a connector and the PM plunger position is fixed. By turning the threaded rod in or out, the solenoid housing will move with the rod and as a result, varying air-gaps between the PM plunger and the iron core can be established and be measured by knowing the length of the threaded rod in/out

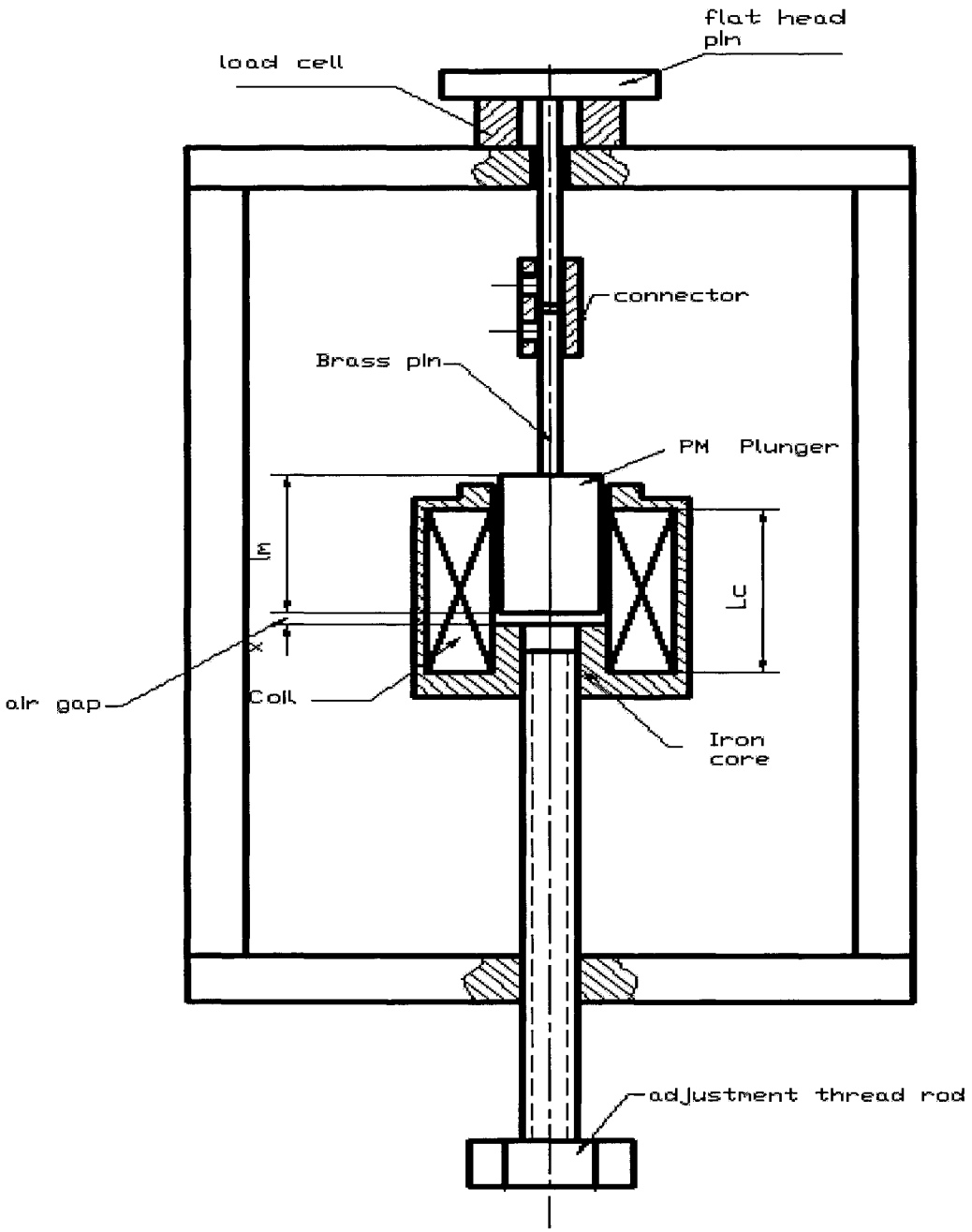


**Figure 2. 9 Experimental fixture to measure the PM force**

movement. Meanwhile, the force of attraction between the PM plunger and the iron core is transferred to the plane-head pin, and this force presses the piezo load cell. As a result, the force of attraction between the PM plunger and the iron core for different air-gaps can be measured.

Figure 2.10 shows the experimental results of the force acting on the PM plunger due to the PM. The results show that when the air-gap between the stator iron core and the PM plunger is near zero, the force acting on the PM plunger or the force of attraction between both reaches to the maximum value of 21.49 N. As the air-gap distance $x$ is increased, the force acting on the plunger decreases.

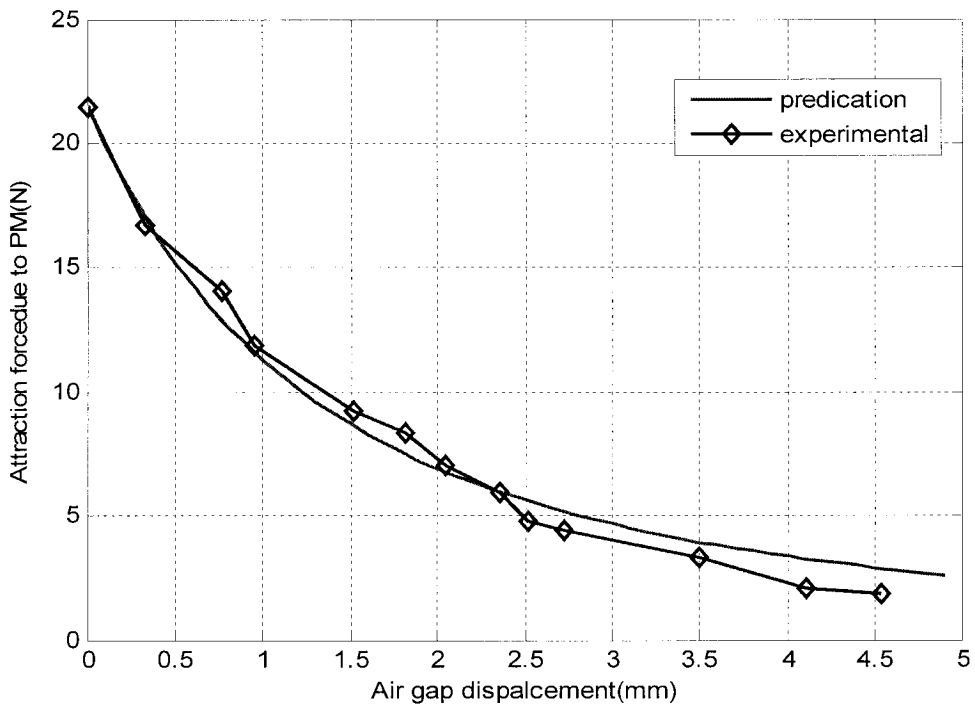


**Figure 2.10 Force acting on the PM due to PM -- Experimental result vs. predication result**

In equation (2.41), select the air-gap length $l_a(x)$ as:

$$l_a(x) = 3.2x \tag{2.48}$$

Also the loss factor $k$ is chosen as:

$$k = 0.81 \tag{2.49}$$

For the PM plunger solenoid actuator in this research, as $k$ is determined, the predicated magnetic force acting on the plunger due to PM can be obtained from equation (2.41). Figure 2.10 shows the experimental results and predicated results of the magnetic force acting on the PM plunger due to PM. It can be seen in Figure 2.10 that when the air-gap distance $l_a(x)$ and the loss factor $k$ in equation (2.41) are properly selected, the experimental and predicated results of the magnetic force of the PM match well.

Therefore, let $l_a(x) = 3.2x$ and $k = 0.81$ in equation (2.41), then the mathematic model of the magnetic force due to PM is expressed as:

$$F_{PM}(x) = 0.81\frac{A}{2\mu_0}\left(\frac{B_r l_m}{4.2x + l_m}\right)^2 \tag{2.50}$$

### 2.6.2 Experimental Setup to Measure the Solenoid Actuator Transient Forces and Currents

As discussed in the previous Section 2.4.4 and 2.4.5, to obtain the nonlinear magnetic characteristics $\phi_{coil}(i,x)$ and the nonlinear inductance $L_{coil}(i,x)$ of the solenoid actuator, the parameters $a$ and $b$ due to the magnetic material and the solenoid structure in equation (2.35) and (2.39) need to be determined. The previous work showed that these two parameters, $a$ and $b$, can be determined by experiment [38].

The method used to determine $a$ and $b$ consists of applying different voltages to the solenoid actuator at various air-gaps $x$, and measuring the corresponding transient currents $i$ and the forces $F_{coil}(i,x)$ due to the current. Then, the fluxes due to the current in the coil $\phi_{coil}(i,x)$ at a fixed air-gap can be evaluated by equation (2.47). Applying the known current and flux results to equation (2.35), the parameters $a$ and $b$ can be evaluated.

The experimental setup is shown in Figure 2.11. The setup consists of the fixture to hold the solenoid actuator, the piezo load cell transducer for measuring the force due to the coil current, and the threaded rod which is for fixing the solenoid and the load cell. The solenoid actuator is held in a brass holder and a cap nut to ensure the solenoid actuator cannot move freely. A small hole is drilled through the solenoid iron core in such a way that a brass pin can be placed through the solenoid bottom. Therefore, the different air-gaps $x$ between the PM plunger and the stator iron core are obtained by

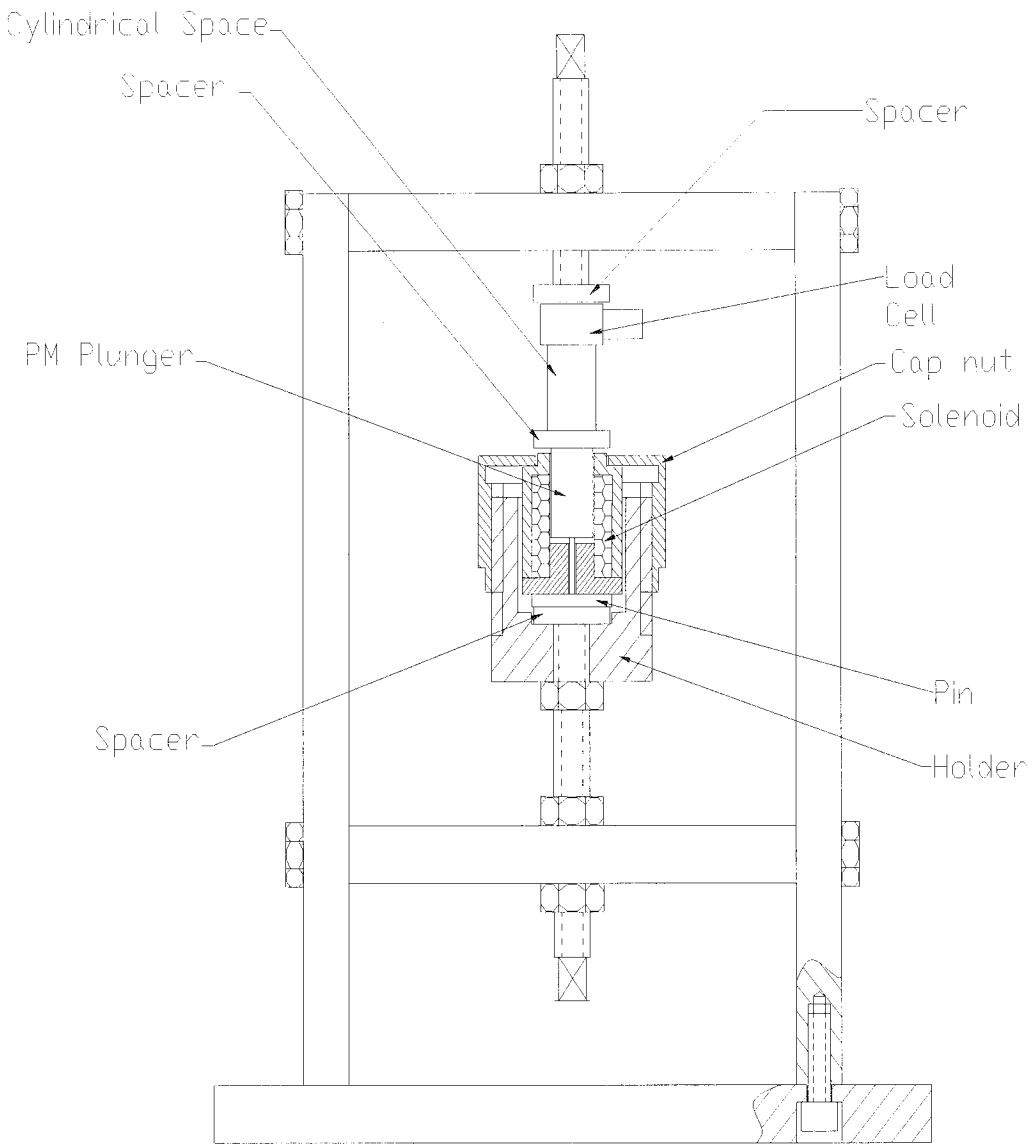


**Figure 2.11 Experimental setup for measuring the magnetic force due to coil**

changing the pin lengths.

Considering that the force transducer is made of a magnetic material, a cylindrical brass spacer is added between the PM and the transducer to avoid the magnetic flux from affecting the transducer. To fix the PM plunger and transducer position, a pre-load is applied by a threaded rod on the fixture top. When the solenoid is activated it produces a magnetic force that acts on the PM plunger. Since the plunger is fixed, the force will be transmitted to the load cell transducer, and thus data of the magnetic force due to the coil is obtained. The piezo transducer not only can be compressed but it also can be extended if it is first compressed by a pre-load. This means the piezo transducer can measure the push force when it is compressed and can measure the pull force when it is extended. Therefore, when the pre-load is set properly, and by altering the solenoid coil current direction, both the magnetic pushing force and pulling force due to the coil can be obtained.

The switching circuit used to activate the solenoid actuator is shown in Figure 2.12. An N-channel power MOSFET is used as a switch to control the current through the solenoid. A square voltage signal applied to the gate of the MOSFET is used to turn the transistor on and off. The step source voltage $V_s$ is applied to the solenoid coil. When the control signal is at high voltage, the MOSFET is on, and the current will pass through the solenoid coil $L$; contrarily, when the control signal at low voltage, the MOSEFT is off; and as a result the solenoid current is cut off. Therefore, the transient magnetic force due to current is measured with the load cell transducer; meanwhile, the corresponding

current through the solenoid coil is obtained with a clamp-on current meter. To measure the reverse force due to the coil, requires only that the solenoid current direction is reversed. As the current direction of the solenoid changes, a reverse direction magnetic force due to the coil is produced. Therefore, magnetic forces in both directions, acting on the plunger due to the coil can be measured. The fly-back diode $D$ in the circuit provides a path for the current to decay when the MOFEST is off. The capacitor in the circuit is provided to avoid the solenoid voltage $V_s$ to drop when the circuit is ON.

In the experiment, five different fixed air-gap positions for the PM plunger are applied for measurement of the force and current of the solenoid actuator. These air-gaps are 0.236 mm, 0.254 mm, 0.386 mm, 0.508 mm, and 0.686mm. At each air-gap, there are

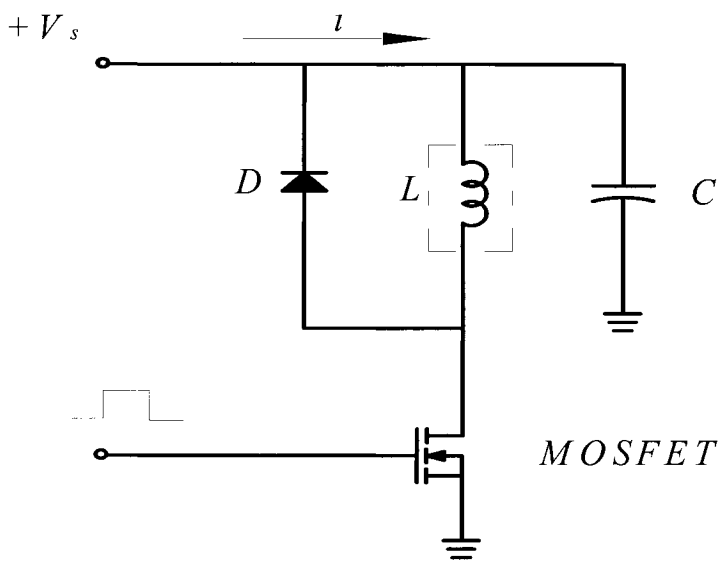


**Figure 2.12 Switch circuit to active the solenoid actuator**

four different voltages applied for the solenoid: 6V, 12V, 24V and 36V. The test results are presented in Figure 2.13 to Figure 2.32, that show the transient currents of the

solenoid coil and their corresponding transient pushing and pulling forces acting on the PM plunger at different fixed air-gaps and different applied voltages.

Normally, the transient current through the solenoid with respect to time follows an exponential curve. As the current reaches a maximum, it will achieve a steady state and keep as a constant. However, the test results show that as the solenoid supply voltage increases, the current through the solenoid drops from the maximum value, and it cannot remain at a steady state. This phenomenon is due to the output impedance of the power supply that causes the current to drop. In addition the power output of the power supply is not sufficient for the solenoid and thus also causes the current to drop.

The figures also show that at low supply voltages, the experimental pushing and pulling forces have very little fluctuation while the forces are near their steady-state; as the supply voltage is higher, the force fluctuation phenomenon are more distinct. This could be because of two reasons. The first is because of the compliance (or elasticity) of the experimental setup, especially from that of the rods holding the load cell and the solenoid together. There is not enough force to affect the experimental structure at low forces, but as the force increases the experimental setup is not stiff enough and its compliance could be acting like a spring. Secondly, because the contact surface between the load cell transducer and the spacers are not ideal flat surface contacts, therefore, force fluctuations could occur due to contact bouncing as when a mechanical switch is closed.

The figures presented show that when the air-gaps are changed, the transient values and shapes of the current at the same supply voltage do not vary with the air-gap. This is because the current through the solenoid is related to the resistance and inductance of the solenoid. The resistance is not a function of the air-gap, and from the equations (2.35) and (2.39) it is known that the solenoid inductance is a function of the solenoid actuator material property and construction, and independent of the air-gap. Therefore, the shape and value of the solenoid currents do not alter while the air-gap is changed. In addition, the current graphs show that as the applied voltage is increased, the current rises more steeply and rapidly to the steady-state value. The difference in shape of the current time response is due to the varying inductance, as is shown in equation (2.39), which is a function of magnetic flux magnitude. Because the magnetic flux and the applied voltage or current is a nonlinear function, the solenoid inductance will also vary nonlinearly.

While changing the current direction of the solenoid, the corresponding transient pushing forces or pulling forces were measured. Comparing with the pushing force and pulling force at a given air-gap, which has the same applied voltage, it can be seen from the experimental results that they have the same magnitude and transients, but the force direction is reversed. These results show that changing the solenoid current direction can alter the PM plunger direction of motion. These results verify the theory in Section 2.5.2, showing that the flux magnitude due to coil current inside the solenoid can be regarded as the same. Consequently from equation (2.35), it is seen that the flux is a function of the coil current, and is not related to the air-gap.

## 2.7 Determination of Magnetic Characteristics

As discussed in the previous section, to determine the magnetic characteristics of the solenoid actuator, the parameters $a$ and $b$ in equation (2.35) must be determined. This section shows the methodology to determine these two parameters.

From equation (2.35), (2.47), and the experimental results it can be shown that the magnetic flux inside the solenoid due to the coil is not a function of air-gap $x$; therefore, the flux is only a function of the current through the solenoid, expressed as:

$$\phi_{coil}(i,x) = \phi_{coil}(i) \tag{2.51}$$

and equation (2.35) can be rewritten as:

$$Ni = \phi_{coil}(i)\Re + \frac{a}{b - \phi_{coil}(i)}\phi_{coil}(i) \tag{2.52}$$

Obviously, the total mmf of the solenoid in equation (2.52) consists of two parts: the mmf due to the PM and air-gap, $\phi_{coil}(i)\Re$, and the mmf due to the solenoid ferromagnetic material body, $\frac{a}{b - \phi_{coil}(i)}\phi_{coil}(i)$.

Defining the mmf due to solenoid ferromagnetic material body as:

$$Ni_f = \frac{a}{b - \phi_{coil}(i)} \phi_{coil}(i) \tag{2.53}$$

where $N$, as in equation (2.52) represents the solenoid coil number of winding turns; $i_f$ is the fictitious current of the solenoid body. Substituting equation (2.53) into (2.52), and solving for the fictitious current:

$$i_f = i - \frac{\phi_{coil}(i)\Re}{N} \tag{2.54}$$

Substituting equation (2.47) into (2.54), the fictitious current is:

$$i_f = i - \frac{F_{coil}(i)\Re}{NM} \tag{2.55}$$

Rewriting equation (2.53), the magnetic flux is expressed as:

$$\phi_{coil}(i) = \frac{bi_f}{a/N + i_f} \tag{2.56}$$

Equation (2.55) shows that when the solenoid current $i$ and its corresponding magnetic force $F_{coil}(i)$ acting on the PM plunger are known, the corresponding fictitious current $i_f$ can be determined. In addition, knowing the magnetic force $F_{coil}(i)$, the magnet flux $\phi_{coil}(i)$ due to coil can be derived from equation (2.47). When the magnet flux

$\phi_{coil}(i)$ and the corresponding fictitious current $i_f$ are known, and using equation (2.56), the magnetic characteristic parameters $a$ and $b$ can be evaluated.

In the previous section the experimental setup for measuring the solenoid currents and the magnetic forces due to the coil has been assembled and the test results have been recorded. As discussed, the solenoid actuator in question is a short stroke solenoid actuator, and varying the PM plunger air-gap does not affect the magnetic force due to the coil while the supply voltage is constant. Therefore, the steady-state data of the currents and corresponding forces at four different voltage supply values obtained from the experiments are used to evaluate the magnetic characteristic parameters $a$ and $b$.

The experimental results of the solenoid currents and corresponding forces at four different supply voltages were shown in Figure 2.13 to Figure 2.32. The data of steady–state currents and forces obtained from these experiments are listed in Table 2.1.

Using the data from Table 2.1 and substituting the current and force values into equations (2.55) and (2.56), and using a Matlab curve fitting function, the parameters $a$ and $b$ can be determined.

**Table 2.1 Experimental Results**

| Source Voltage $V_s$ (V) | 0 | 6 | 12 | 24 | 36 |
|---|---|---|---|---|---|
| Current $i$ (A) | 0 | 10.5 | 19.65 | 41.10 | 63.25 |
| Force $F_{coil}$ (N) | 0 | 7.3 | 13.85 | 26.3 | 37.4 |

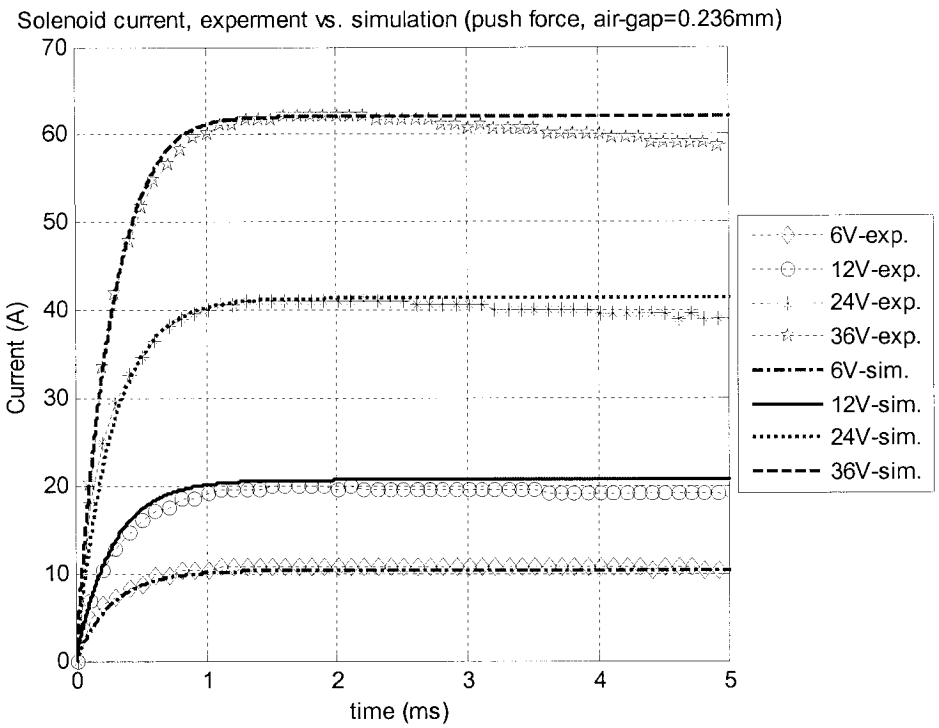


**Figure 2.13 Current experimental vs. simulation results (pushing force, air-gap=0.236mm)**

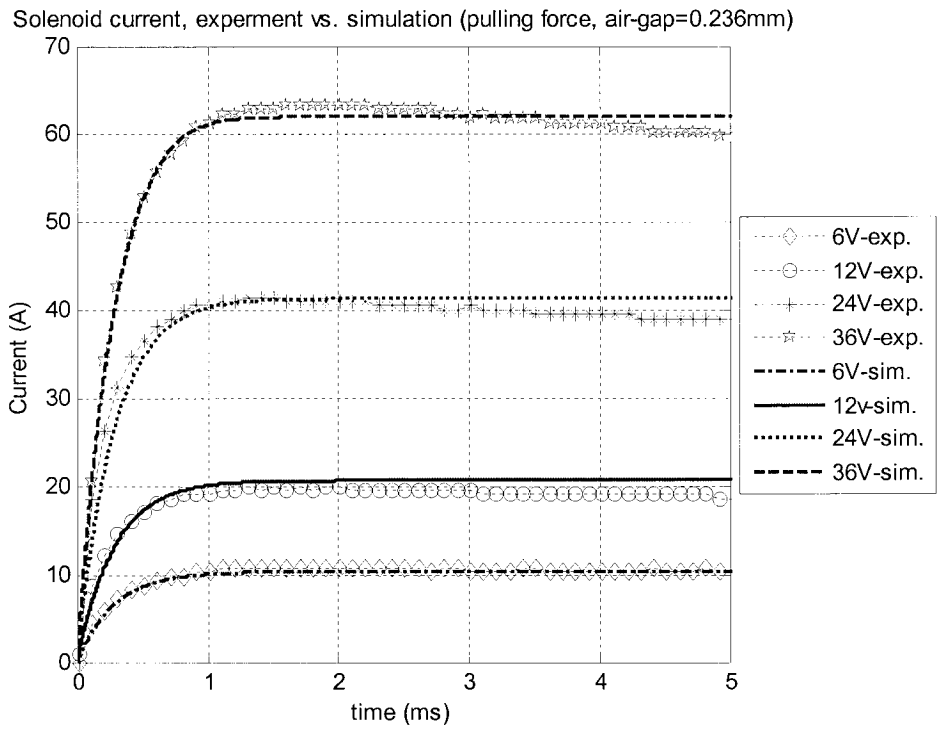


**Figure 2.14 Current experimental vs. simulation results (pulling force, air-gap=0.236mm)**

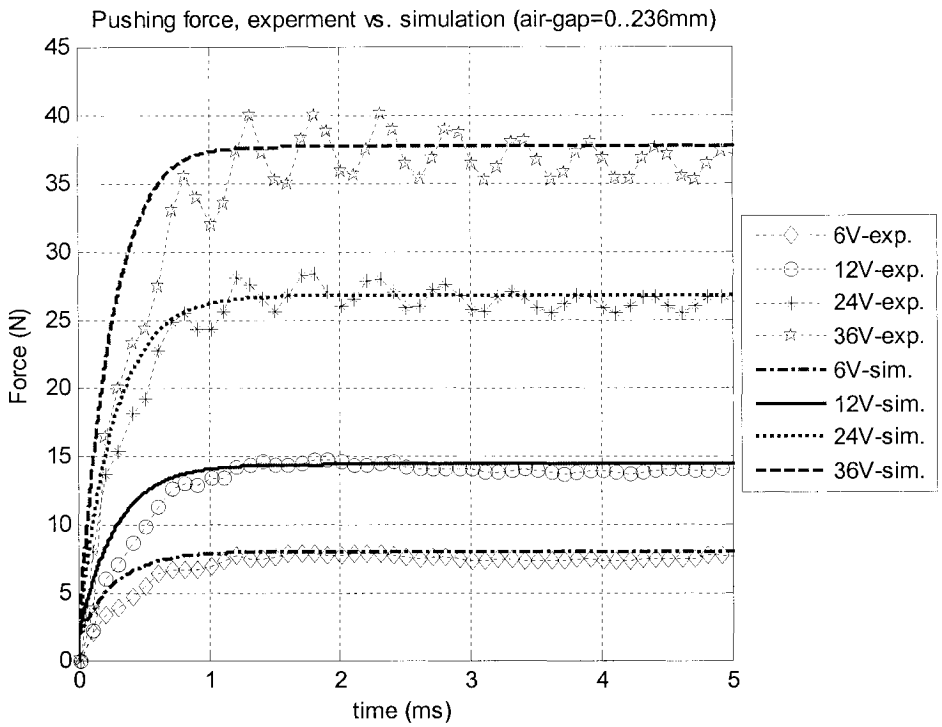


**Figure 2.15 Pushing force experimental vs. simulation results (air-gap=0.236mm)**

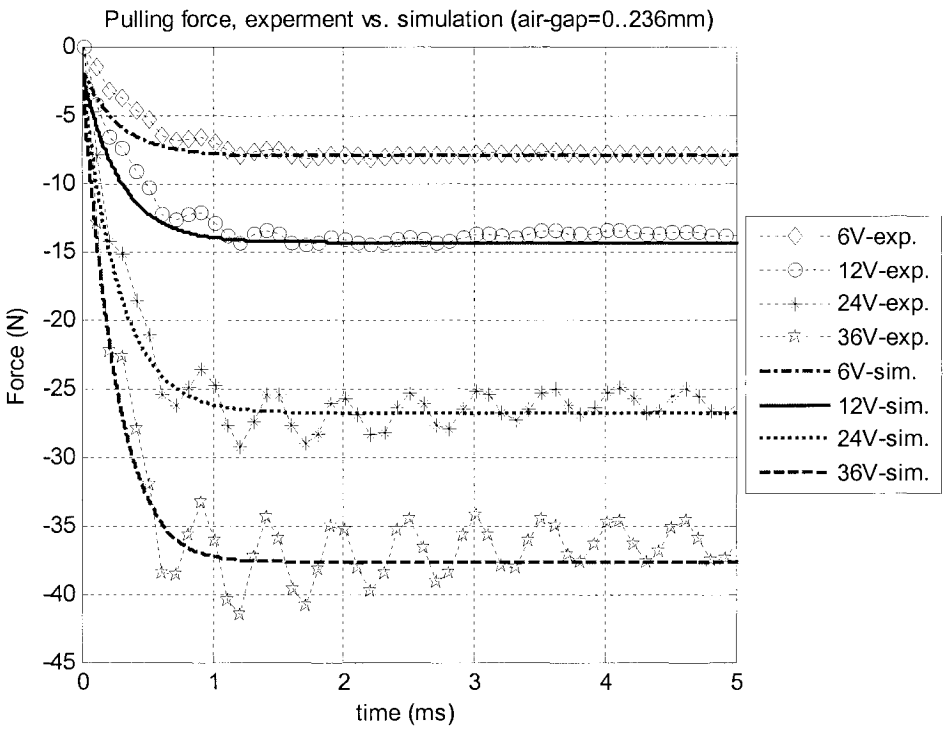


**Figure 2.16 Pulling force experimental vs. simulation results (air-gap=0.236mm)**

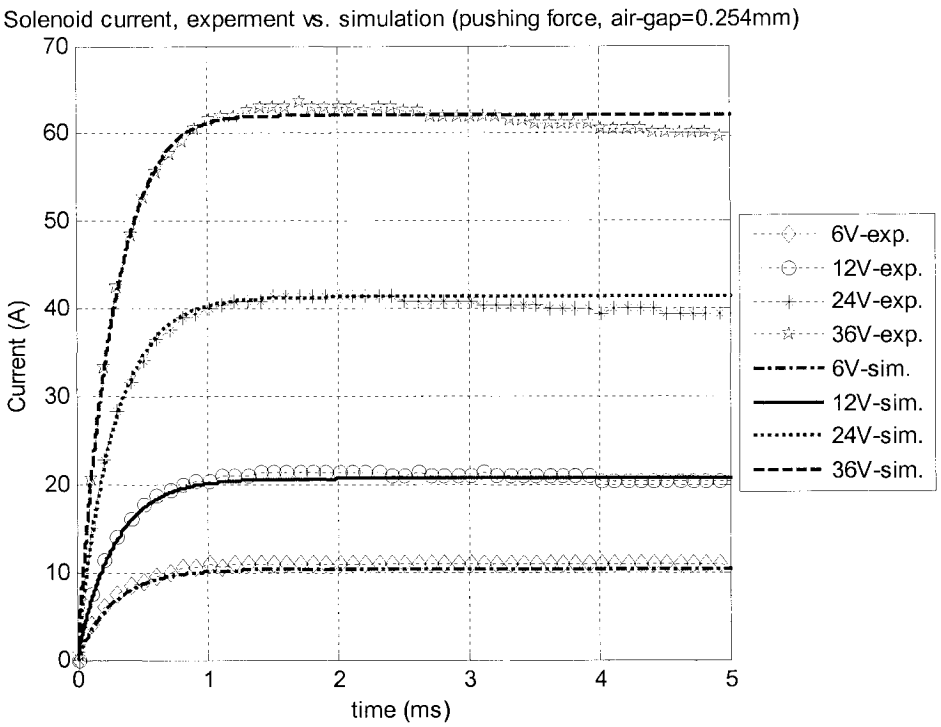


**Figure 2.17 Current experimental vs. simulation results (pushing force, air-gap=0.254mm)**

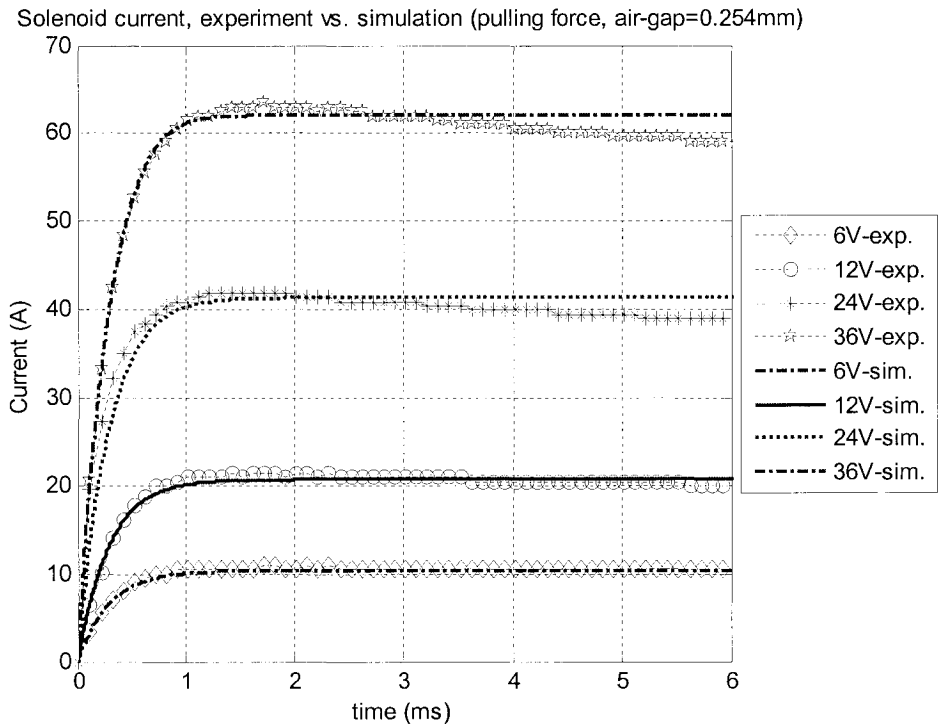


**Figure 2.18 Current experimental vs. simulation results (pulling force, air-gap=0.254mm)**

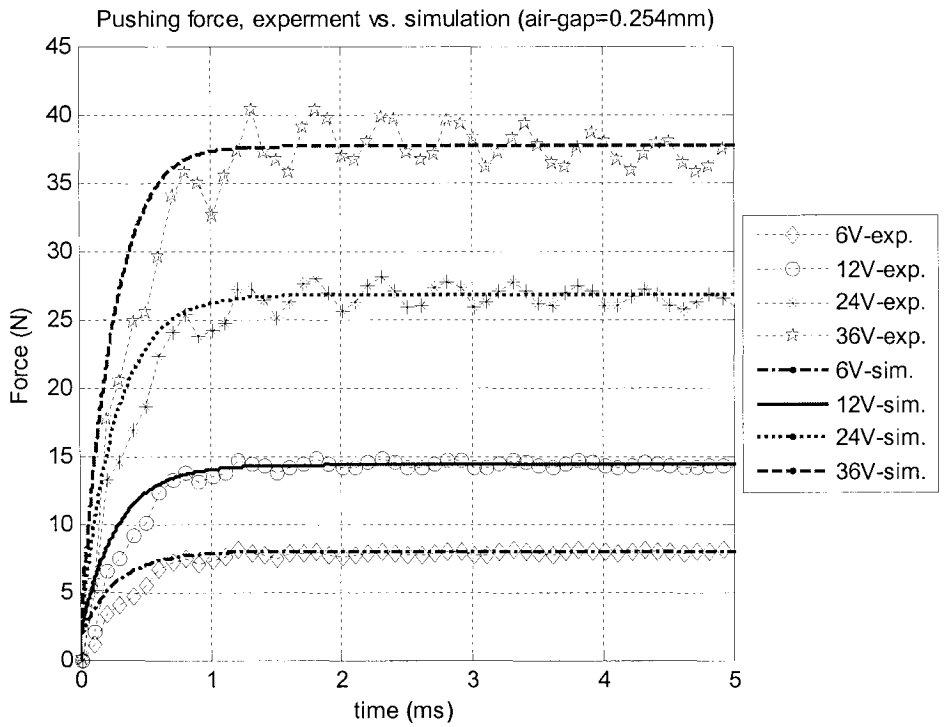


**Figure 2.19 Pushing force experimental vs. simulation results (air-gap=0.254mm)**

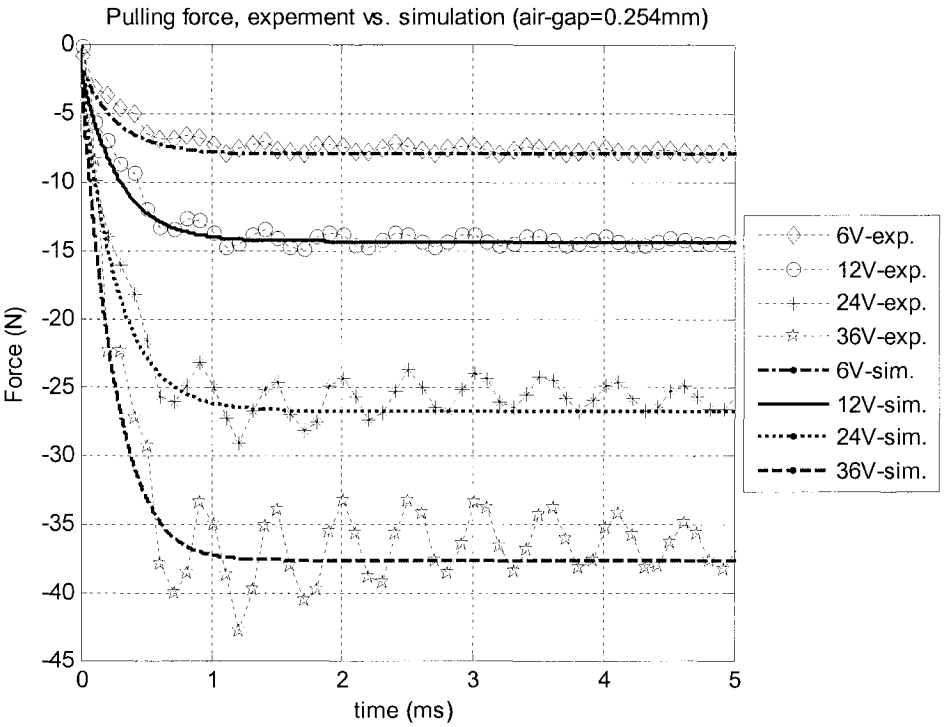


**Figure 2.20 Pulling force experimental vs. simulation results (air-gap=0.254mm)**

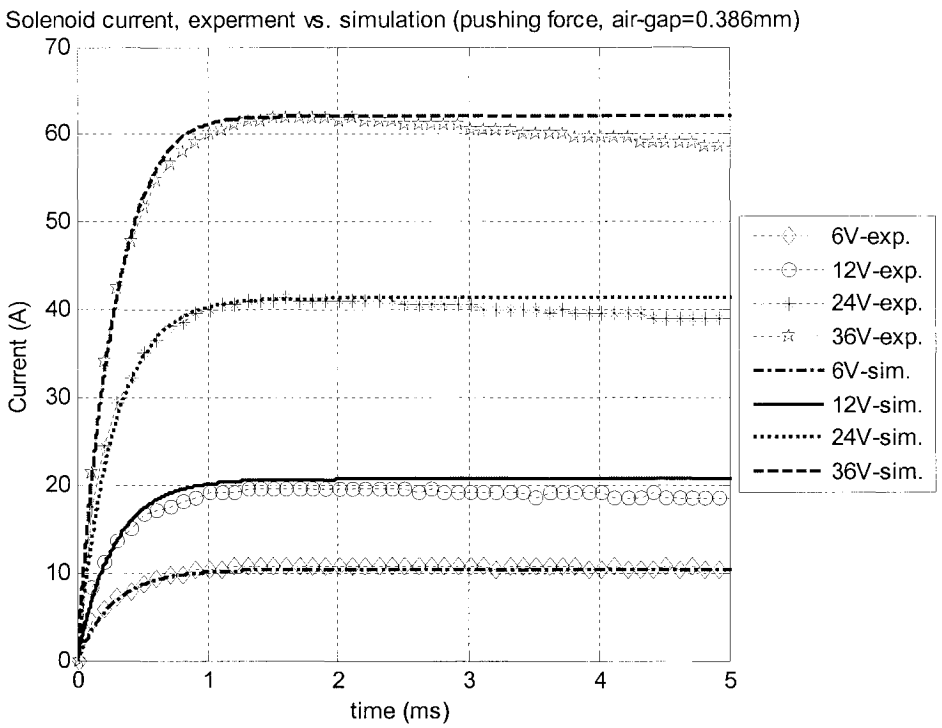


**Figure 2.21 Current experimental vs. simulation results (pushing force, air-gap=0.386mm)**

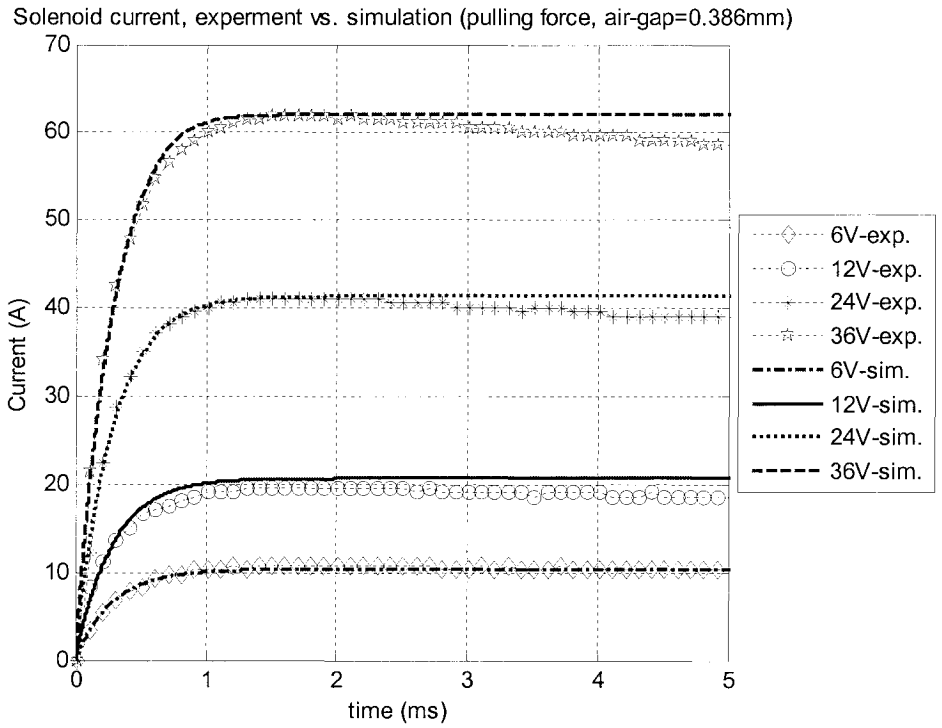


**Figure 2.22 Current experimental vs. simulation results (pulling force, air-gap=0. 386mm)**

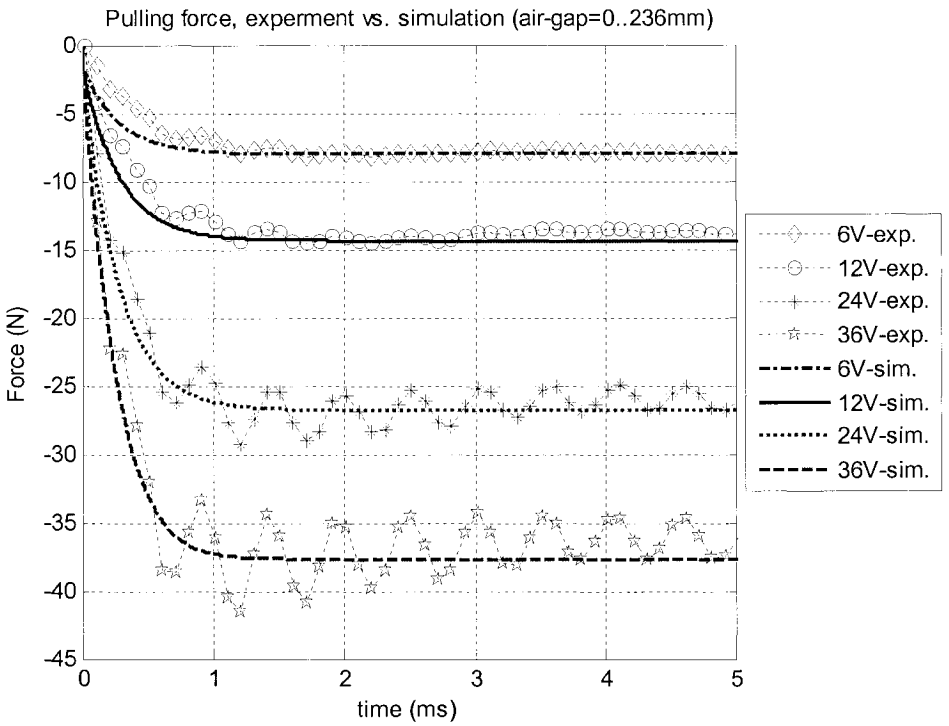


**Figure 2.23 Pushing force experimental vs. simulation results (air-gap=0.386mm)**

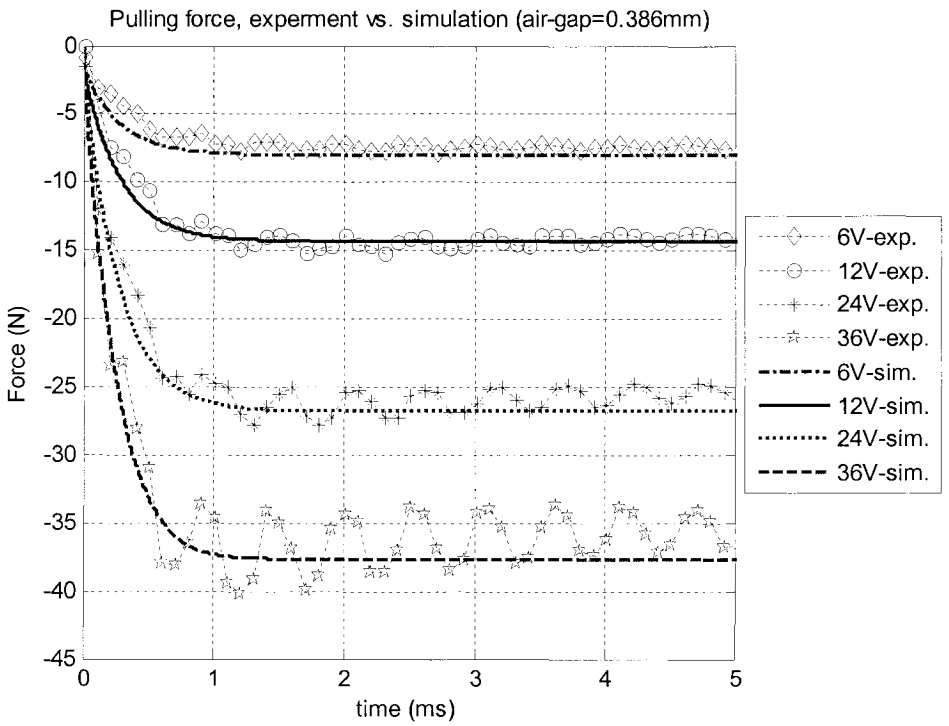


**Figure 2.24 Pulling force experimental vs. simulation results (air-gap=0.386mm)**

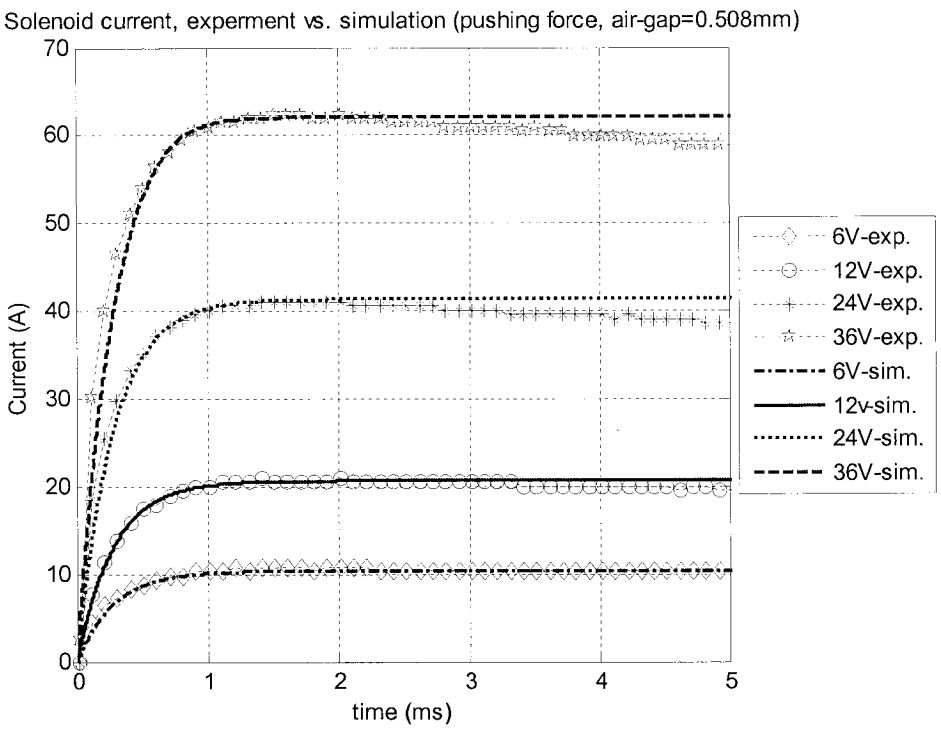


**Figure 2.25 Current experimental vs. simulation results (pushing force, air-gap=0.508mm)**

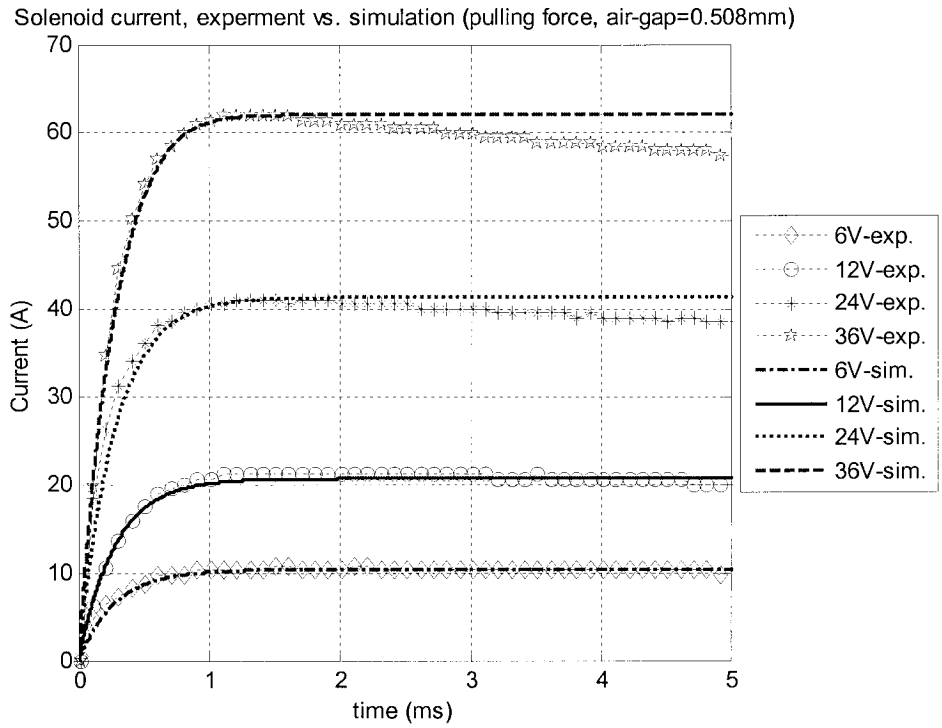


**Figure 2.26 Current experimental vs. simulation results (pulling force, air-gap=0.508mm)**

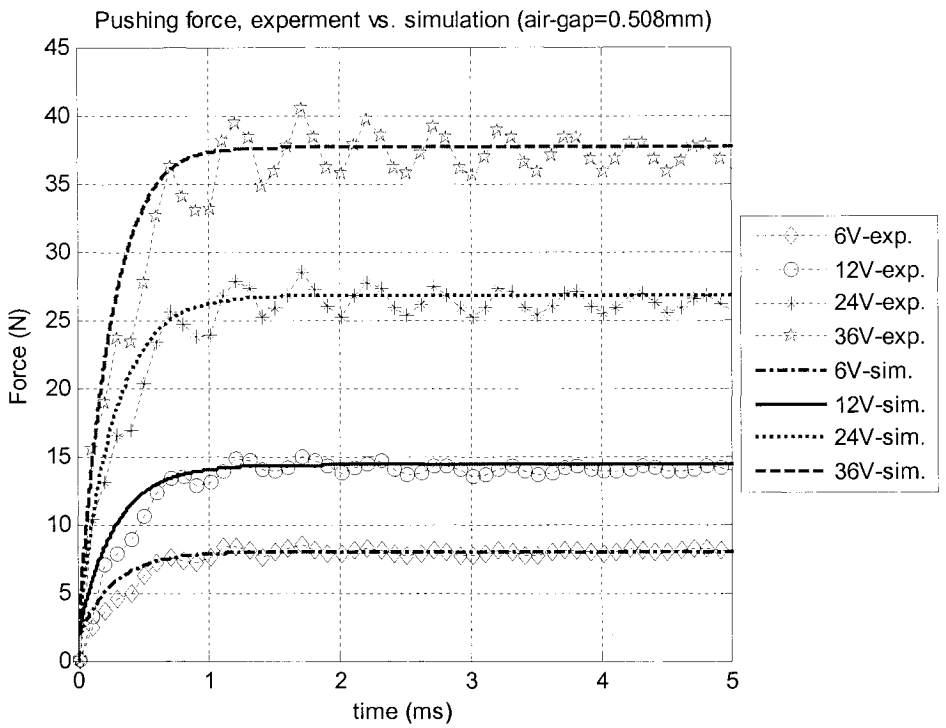


**Figure 2.27 Pushing force experimental vs. simulation results (air-gap=0.508mm)**

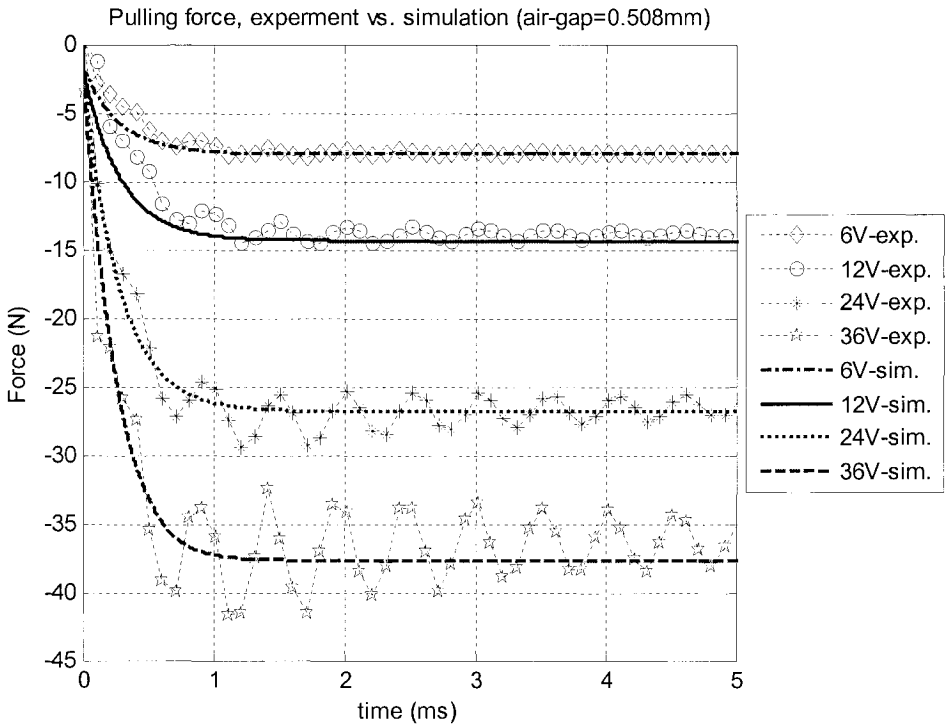


**Figure 2.28 Pulling force experimental vs. simulation results (air-gap=0.508mm)**

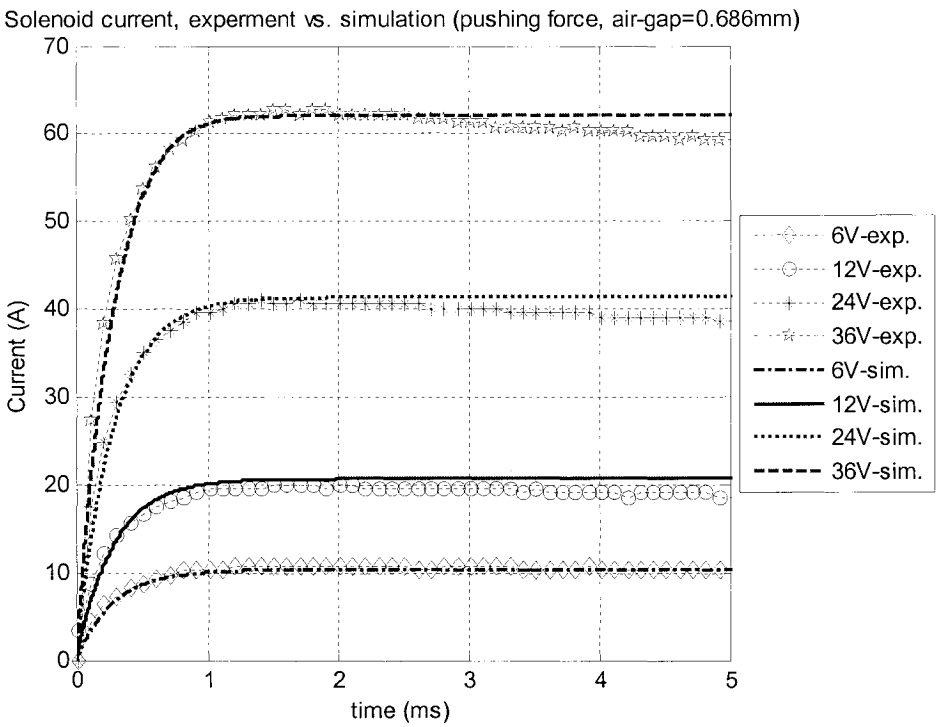


**Figure 2.29 Current experimental vs. simulation results (pushing force, air-gap=0.686mm)**

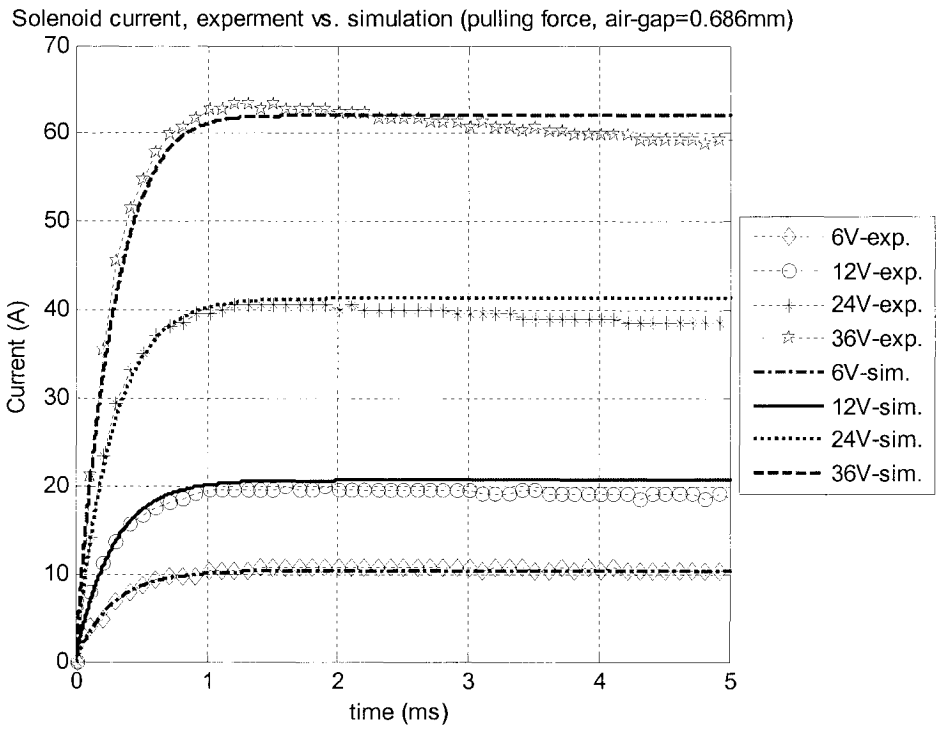


**Figure 2.30 Current experimental vs. simulation results (pulling force, air-gap=0.686mm)**

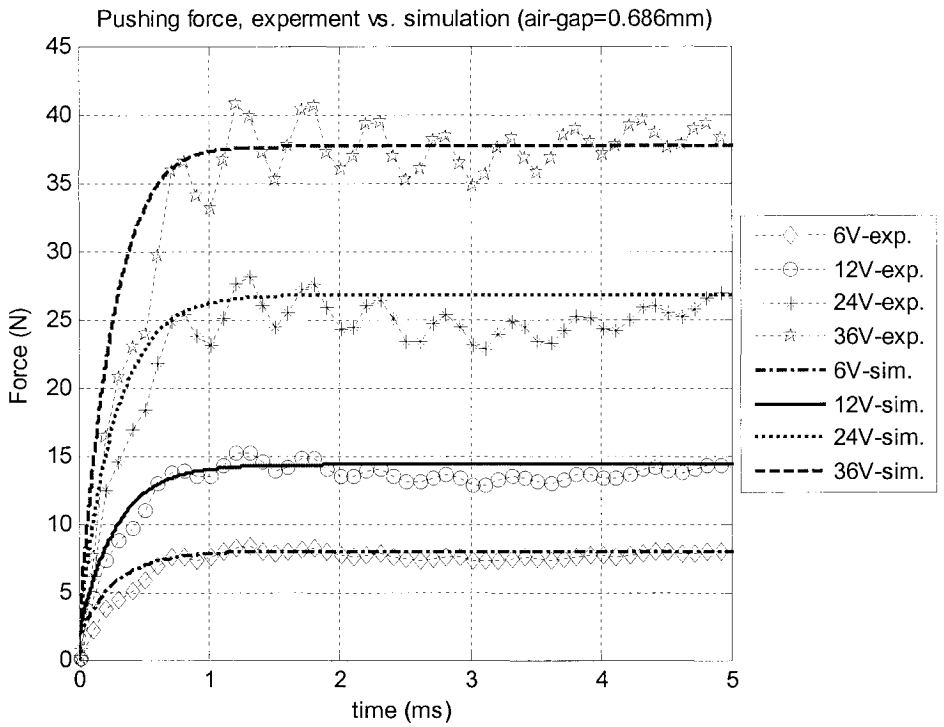


**Figure 2.31 Pushing force experimental vs. simulation results (air-gap=0.686mm)**

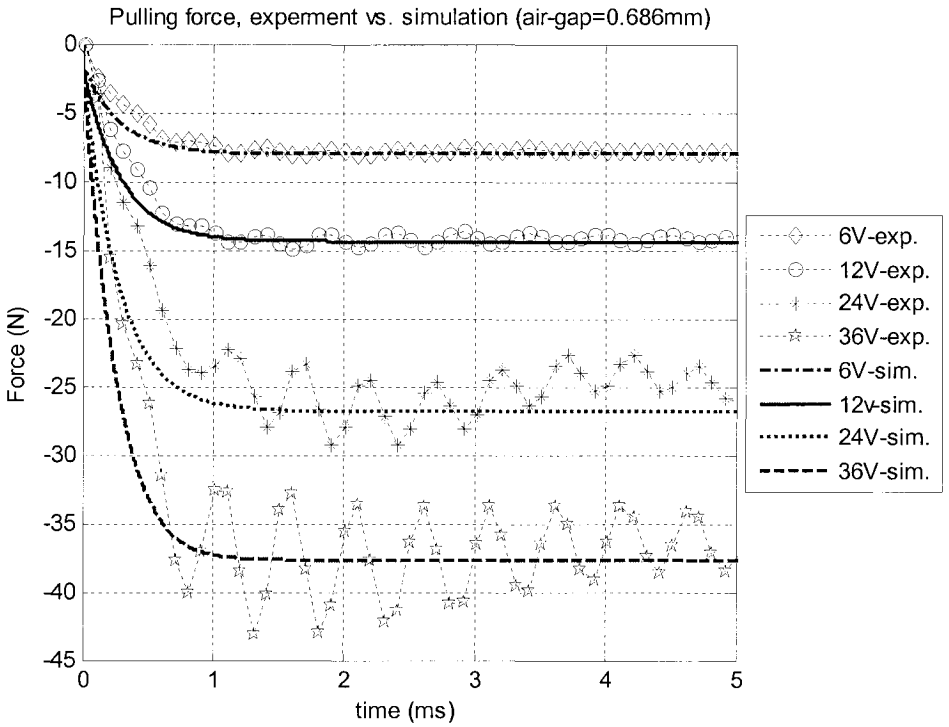


**Figure 2.32 Pulling force experimental vs. simulation results (air-gap=0.686mm)**

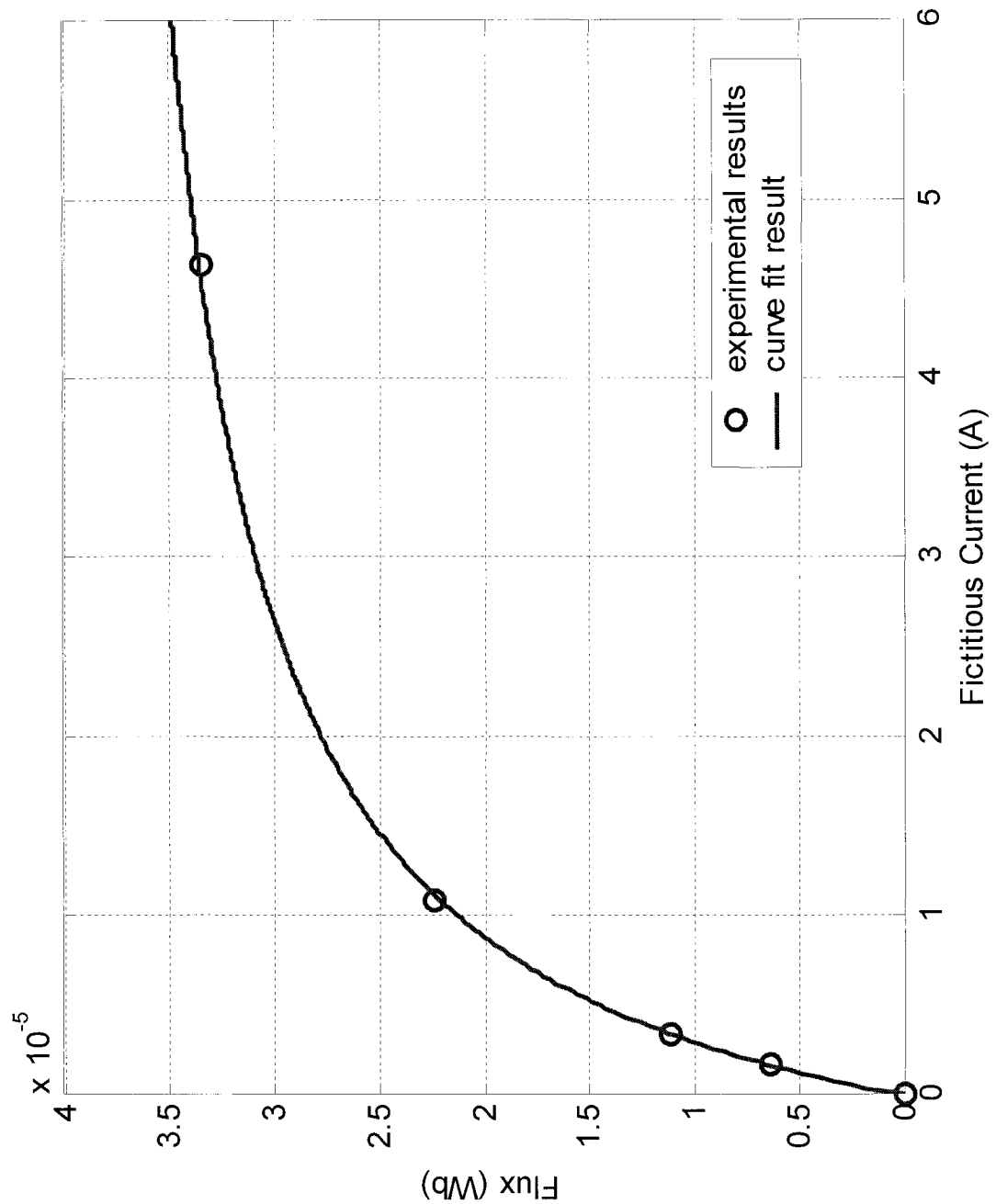


**Figure 2.33 Magnetization curve fitting $i_f$ vs. $\phi_{coil}$**

The plot of fictitious current $i_f$ vs. the flux through the coil $\phi_{coil}$ drawn by the Matlab curve fitting function is shown in Figure 2.33. Also, the parameters $a$ and $b$ which were obtained from the Matlab curve fit function are determined as:

$$a = 65.49(A/Wb) \tag{2.57}$$

$$b = 3.99 \times 10^{-5}(Wb) \tag{2.58}$$

Since the parameters $a$ and $b$ are now known, the magnetic characteristic $\phi(i)$ in equation (2.35) can be obtained; also, the solenoid inductance $L(i)$ can be evaluated by equation (2.39). The solenoid $\phi(i)$ and $L(i)$ curves are shown in Figure 2.34 and Figure 2.35, respectively.

Figure 2.34 shows the solenoid magnetic characteristic curves. The dash line curve is the solenoid ferromagnetic material body magnetic characteristic, where the reluctance effect as showed in equation (2.53), is due only to the material of the solenoid body and its structure; the solid line curve shows the solenoid total magnetic characteristic, where the reluctance effects as showed in equation (2.52), are due to the body material and its structure , as well as the reluctances due to the two air-gaps, namely the boss-end air-gap and the plunger displacement air-gap.

It can be seen in Figure 2.34 that when the solenoid current is lower than 70 Ampere, the solenoid magnetic characteristic $\phi(i)$ is regarded as linear and when the current is higher than 70A, the $\phi(i)$ trends to saturation. When $\phi(i)$ is saturated, it will be

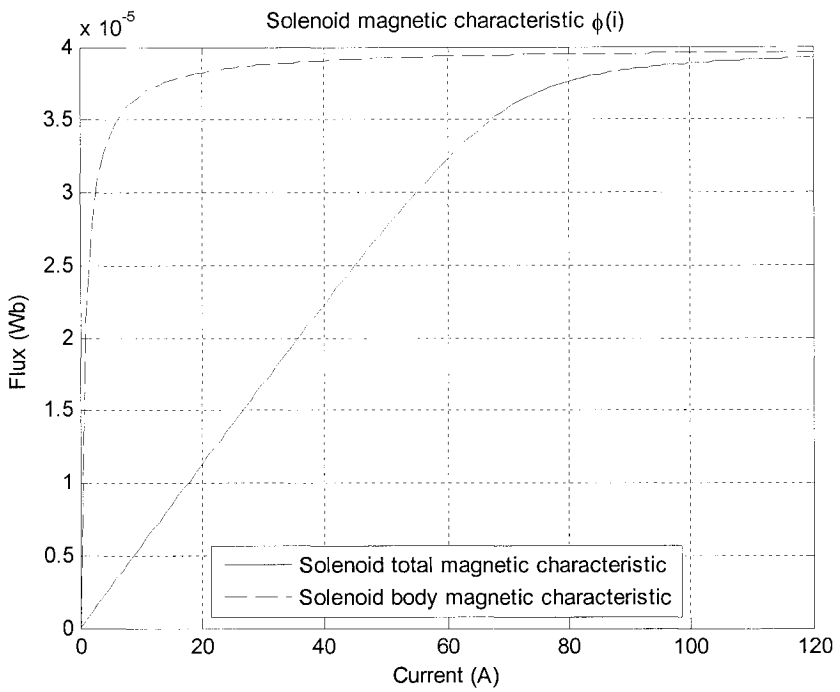


**Figure 2.34 Solenoid magnetic characteristic curves**

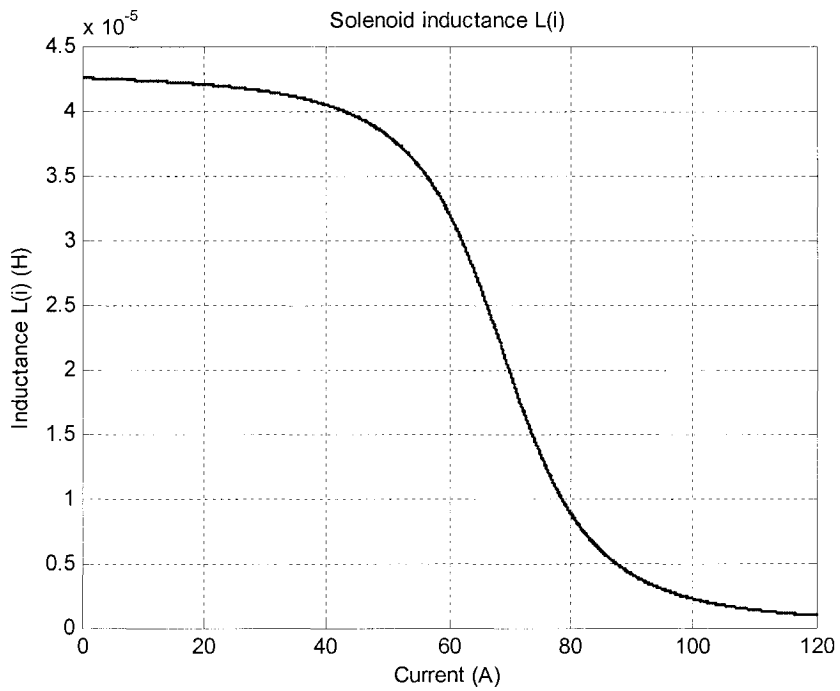


**Figure 2.35 Solenoid inductance curve**

invariable with respect to the current, and it remains at its saturation value. For the solenoid inductance $L(i)$ as shown in Figure 2.35, as the current increases the solenoid flux increases, hence, the inductance $L(i)$ decreases. When $\phi(i)$ approaches saturation, $L(i)$ trends to zero. While the flux $\phi(i)$ saturates, it can be known from equation (2.47) that the force due to the coil current will saturate.

## 2.8 Simulation of the PM Plunger Bi-direction Actuator and Experimental Verification

This section will present the state equations of the PM plunger bi-directional moving actuator. Solving the actuator state equations, the dynamic simulation results of the actuator will be obtained. To verify the mathematic model of the actuator, the simulation results will be compared with the experiment results.

### 2. 8.1 State Equations of the PM Solenoid Actuator

To obtain the solenoid actuator dynamic simulation results, the actuator dynamic equations must be solved.

Rearranging the dynamic equation (2.15), the current state equation is yielded as:

$$\frac{di}{dt} = \left( V - iR - N\frac{\partial \Phi(i,x)}{\partial x}\frac{dx}{dt} \right) \frac{1}{L_e + L_{coil}(i,x)} \tag{2.59}$$

As demonstrated previously, the total magnetic field of the solenoid and the coil inductance are expressed as:

$$\begin{aligned}\Phi(i,x) &= \phi_{coil}(i,x) + \phi_{PM}(i,x) \\ &= \phi_{coil}(i) + \phi_{PM}(x)\end{aligned} \tag{2.60}$$

and

$$L_{coil}(i,x) = L_{coil}(i) \tag{2.61}$$

Hence, equation (2.59) becomes:

$$\frac{di}{dt} = \left(V - iR - N\frac{\partial\phi_{PM}(x)}{\partial x}\frac{dx}{dt}\right)\frac{1}{L_e + L_{coil}(i)} \tag{2.62}$$

As discussed previously, the total force $F(i,x)$ acting on the PM plunger is the sum of the forces due to the coil current and the force due to the PM, and it is expressed as:

$$\begin{aligned}F(i,x) &= F_{coil}(i,x) + F_{PM}(i,x) \\ &= F_{coil}(i) + F_{PM}(x)\end{aligned} \tag{2.63}$$

Then, equation (2.16) can be rewritten as the state equation:

$$\frac{dv}{dt} = \frac{1}{m}\left(F_{coil}(i) + F_{PM}(x) - mg\right) \tag{2.64}$$

Consequently, the actuator dynamic equation (2.18) becomes the state equation:

$$\begin{cases} \dfrac{di}{dt} = \left(V - iR - N\dfrac{\partial \phi_{PM}(x)}{\partial x}\dfrac{dx}{dt}\right)\dfrac{1}{L_e + L_{coil}(i)} \\ \dfrac{dv}{dt} = \dfrac{1}{m}\left(F_{coil}(i) + F_{PM}(x) - mg\right) \\ \dfrac{dx}{dt} = v \end{cases} \tag{2.65}$$

Since the magnetic characteristics of the solenoid and the inductance property of the solenoid were determined, therefore all state parameters in the right hand side of equation (2.65) are known. Therefore, dynamic response given by equation (2.65) can be solved by numeric methods for the variables $x$ and $i$ with respect to time $t$. In this research, the 4$^{th}$ order Runge-Kutta method written in a C++ program is applied to solve the state equations.

### 2.8.2. Simulation Results and Experimental Validation

Application of the bi-directional actuated solenoid actuator for automobile alternative fuel injectors assumes that the travel stroke of the actuator is very short, from 0.5 to 0.7mm [3, 38]. To simplify the model of the actuator under investigation the assumptions shown below have been made:

1) The PM plunger has the maximum travel limit of $x = 0.7mm$;
2) To avoid the large attraction force between the PM plunger and the iron core at zero air-gap, the minimum air-gap between the PM plunger and the iron core is limited to 0.1mm;
3) It is assumed that there is no friction between the two moving parts, namely between the PM plunger and the solenoid sleeve.

The values of the actuator physical parameters used in the simulation are given in Table 2.2.

**Table 2.2 parameter values used in simulation**

| | | | | | |
|---|---|---|---|---|---|
| *Pole end area* | $A\ (m^2)$ | $9.677\times10^{-5}$ | *PM plunger mass* | *m(kg)* | $11\times10^{-3}$ |
| *boss-end area* | $A_g\ (m^2)$ | $1.745\times10^{-4}$ | *Solenoid resistance* | *R(Ohm)* | 0.55 |
| *Solenoid winding turns* | *N(turns)* | 75 | *Solenoid coil length* | $L_c\,(m)$ | $14\times10^{-3}$ |
| *PM plunger length* | $l_m\,(m)$ | $15.62\times10^{-3}$ | *PM plunger diameter* | *d (m)* | $11.1\times10^{-3}$ |

The leakage inductance $L_e$ is estimated from the experiment results. The method to estimate $L_e$ is by selecting different values of $L_e$ and then comparing the simulation results of the solenoid current with experimental results. When both results match well, $L_e$ is selected as:

$$L_e = 0.92L_{coil} \tag{2.66}$$

Since the parameters of the PM solenoid system are now known, the mathematical model for current given by equation (2.15) or (2.65), and current generated force by equation (2.47), can be computer simulated to compare to experimental data at fixed air-gaps. These simulation results are plotted on the same graphs of the experimental data in Figures 2.13 to 2.32, for direct comparison. The comparison shows excellent correlation, indicating that the mathematical model of the PM solenoid system is correct. The major deviations occur during the transient force rise time, which could be attributed to unaccounted eddy current losses that contributes a time delay to the magnetization of ferromagnetic materials [42]. This assumption requires further research for verification.

To see the effects of PWM applied voltages, Figure 2.36 to Figure 2.41 shows the simulation results and experimental results of the solenoid currents and the actuator pushing/pulling forces due to different source voltage $V_s$ values at the fixed air-gap of 0.254mm and 0.686mm. To implement bi-directional motion, a 250 Hz bi-directional source voltage (a square wave from $+Vs$ to $-Vs$) is supplied to the PM plunger solenoid actuator, with the source voltage control signal waveform shown in Figure 2.42. This square waveform is generated by a PWM drive. In the experimental tests, the source voltages $V_s$ applied to the solenoid are 16.5V, 24.5V and 36V. The force measurement method and the current measurement methods are as similar to that as previously described.

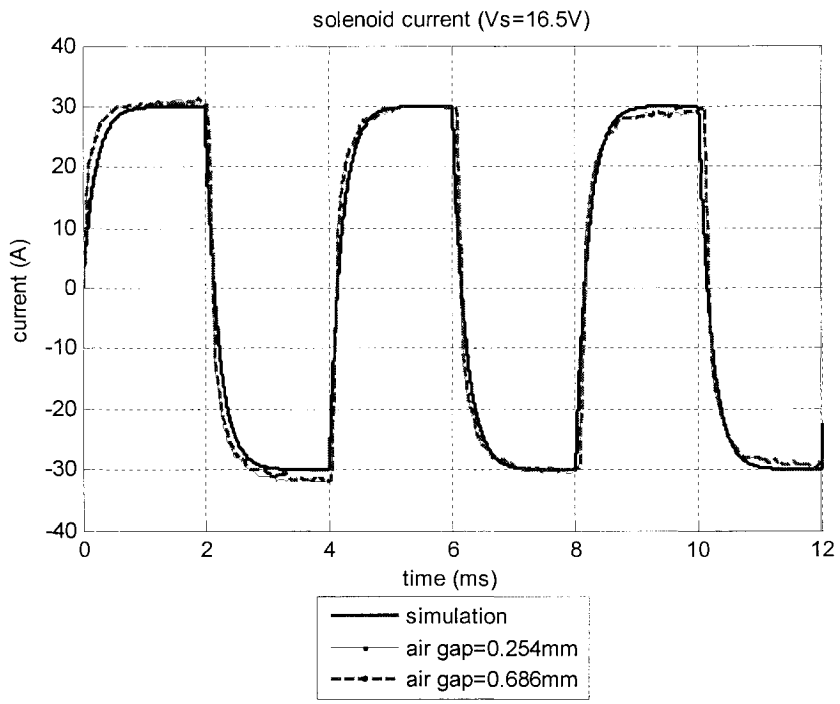


**Figure 2.36 Solenoid current simulation and experimental results (Vs=+/-16.5V)**

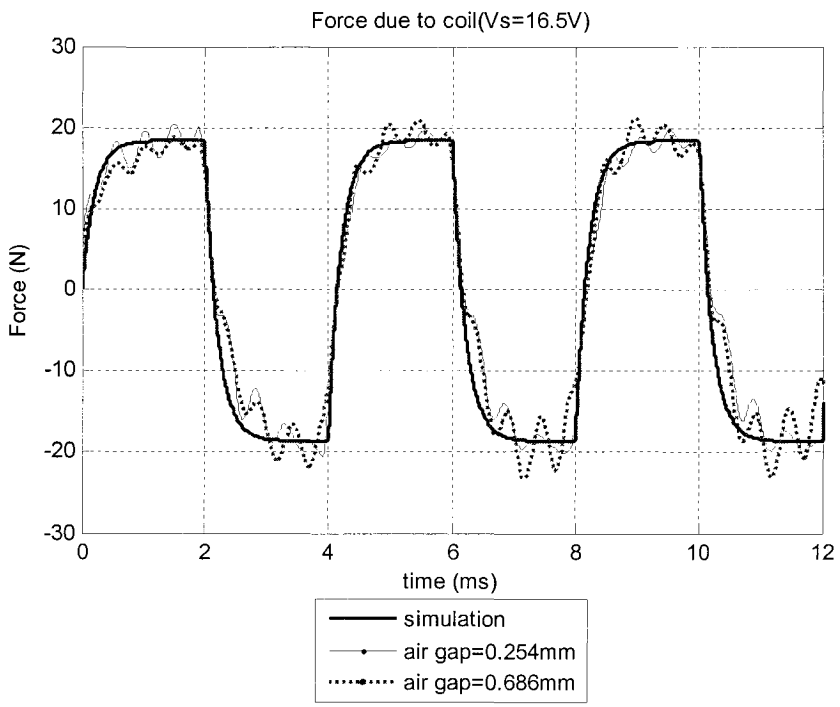


**Figure 2.37 Actuator force due to current simulation and experimental results (Vs=+/-16.5V)**

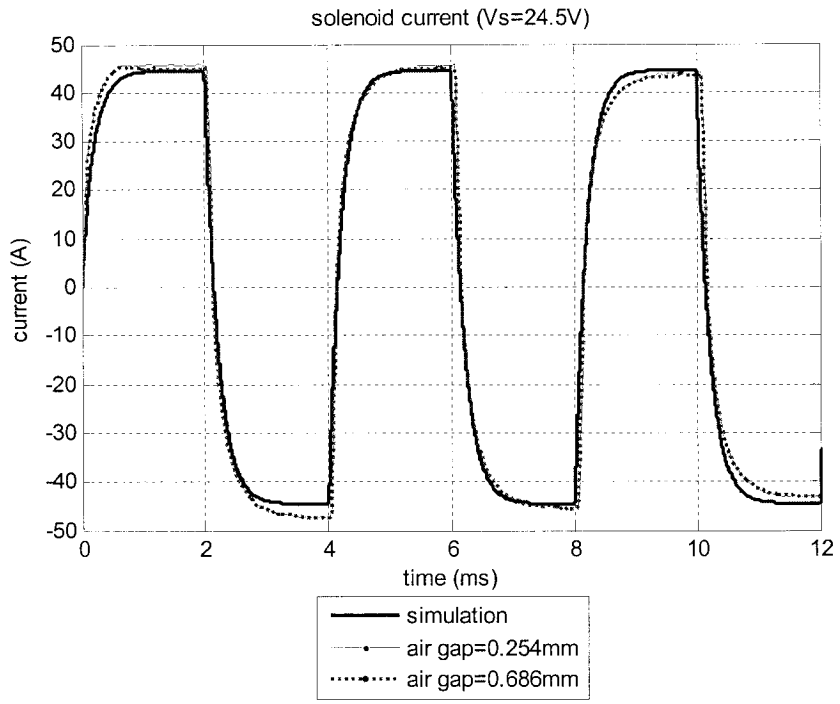


**Figure 2.38 Solenoid current simulation and experimental results (Vs=+/-24.5V)**

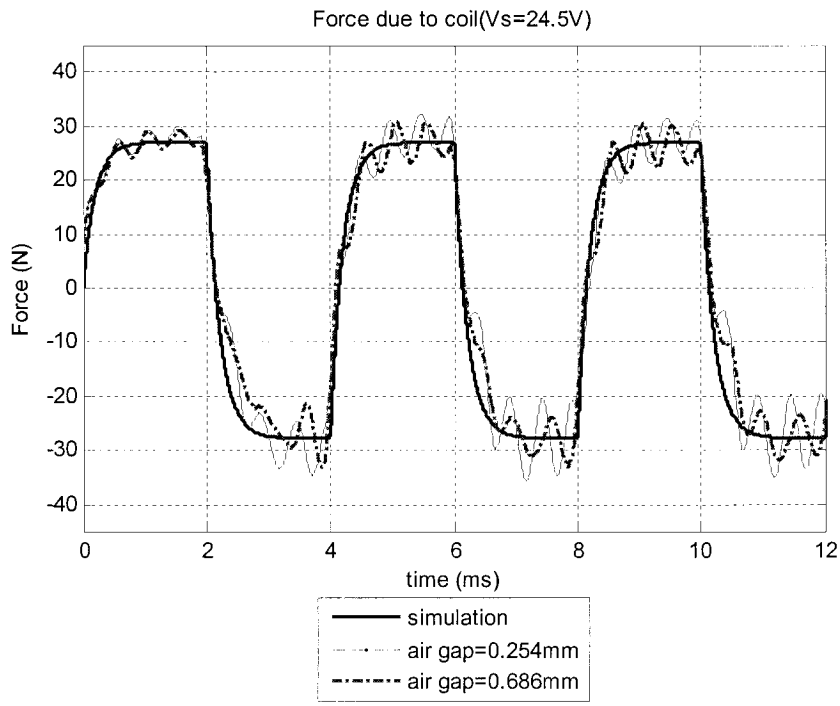


**Figure 2.39 Actuator force due to current simulation and experimental results (Vs=+/-24.5V)**

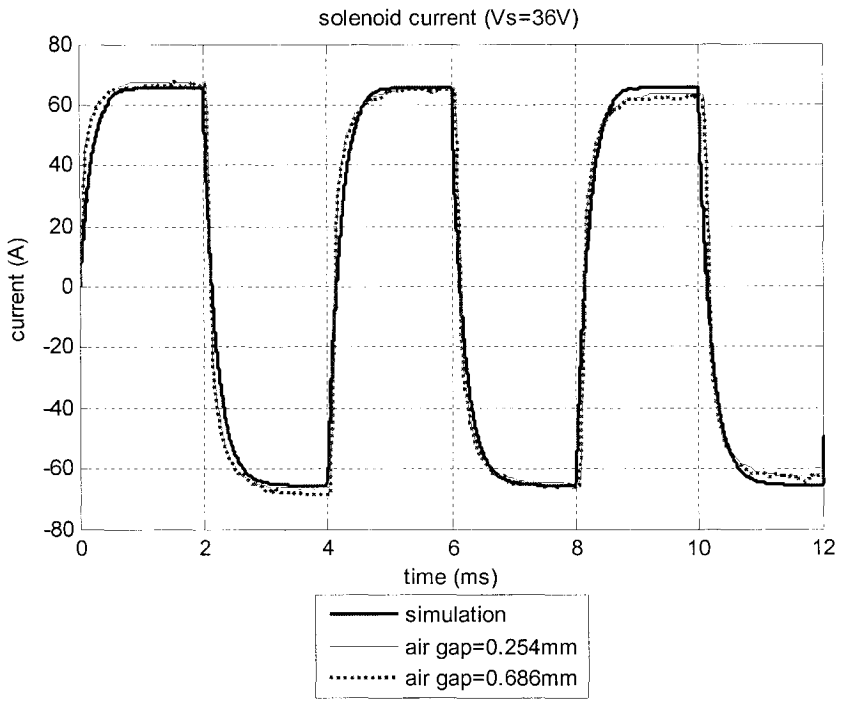


**Figure2.40 Solenoid current simulation and experimental results (Vs=+/-36V)**

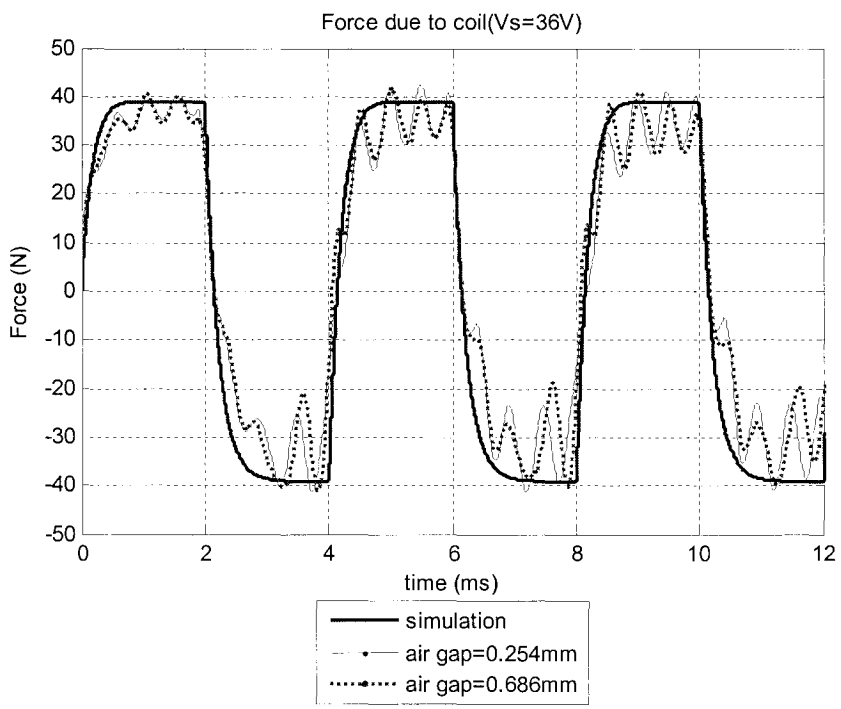


**Figure 2.41 Actuator force due to current simulation and experimental results (Vs=+/-36V)**

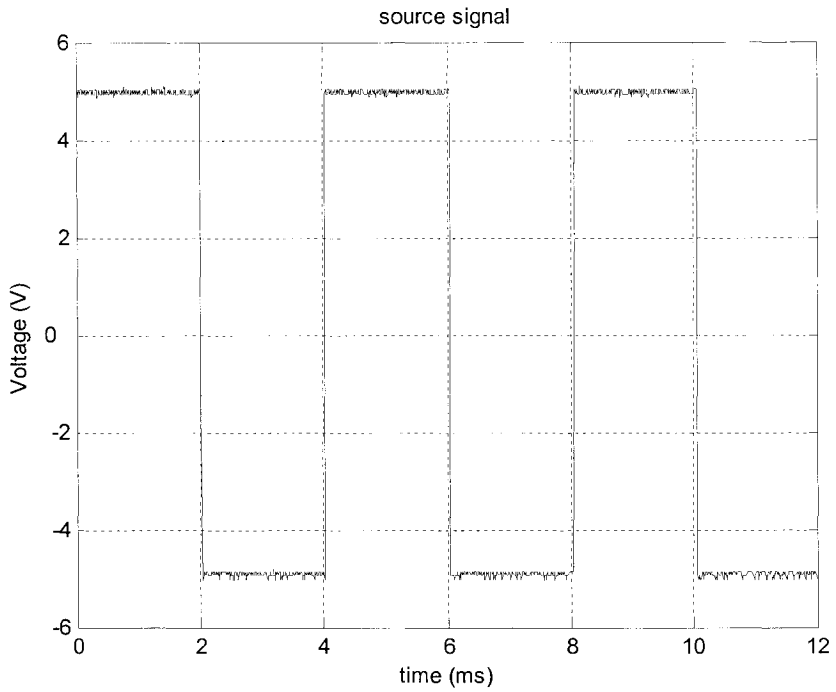


**Figure 2.42 Source signal waveform**

From Figure 2.36 to 2.41, it can be seen that, as the source voltage varies from $+Vs$ to $-Vs$, or from $-Vs$ to $+Vs$, the current direction through the solenoid will vary with the voltage, and consequently, the alternating current in the solenoid produces an alternating magnetic force to push or to pull the PM plunger. As a result, the actuator bi-directional motion can be achieved. Also, from the simulation and experiment results, as the supply voltage increases, the drive force due to the coil current also increases. In addition, it can be seen that the simulation results and the experimental results match very well. It indicates that the mathematical model and the parameters of the PM plunger solenoid actuator are valid.

Note that the fluctuation phenomena of the force due to current occur in experiment, as discussed previously, it is because of two reasons, the stiffness of the fixture and the contact surface between the load cell transducer and its contact parts. During the experiments it showed that as the stiffness of the experimental setup was improved, or if the contact surfaces are adjusted more finely, the force fluctuation phenomena in the experiments will diminish.

Figure 2.36 to 2.41 also show that for different PM plunger air-gaps, when the supply voltages are the same, the solenoid currents and the magnetic forces due to the current do not vary. It shows that, as previously explained in section 2.5.2, the solenoid current and the magnetic force due to the current are not functions of the PM plunger air-gap because $\mu_m \approx \mu_0$. The simulation results and experimental results match well, indicating that the mathematical model of the bi-directional moving PM plunger solenoid actuator is valid.

For the air-gap allowed to move, Figures 2.43 to 2.51 present the PM plunger solenoid actuator dynamic simulation results at supply voltages of the square waveform $\pm 16.5$V, $\pm 24.5$V and $\pm 36$V, and at the same frequency of 250 Hz as in the previous experiments.

It can be seen from Figure 2.44 that when the supply voltage is $\pm 16.5$V (Figure 2.43 shows the current profile), the PM plunger does not move. This is because the supply voltage is too low and as a result, the force due to the current is not enough to

overcome the PM force of attraction between the PM plunger and the stator iron core. In Figure 2.45, it can be seen that the PM force is around 20 N, and the maximum magnetic pushing force due to the current is about 18 N; therefore, the force due to the current is too small to overcome the PM force to move the PM plunger.

As shown in Figure 2.46 to Figure 2.48, when the supply voltage is raised to $\pm 24.5$V, the maximum pushing force due to the current reaches to 27 N. It is larger than the PM force of attraction between the plunger and the iron core; therefore, the PM plunger will move. Its motion locus is shown in Figure 2.47. From this figure, it is seen that when the supply voltage waveform is positive the force due to the current overcomes the PM force of attraction and pushes the plunger away from the stator iron core. On the other hand when the voltage waveform is negative, the force due to the current becomes the pulling force. This force will be in the same direction as the PM force of attraction; hence, both forces combine to pull the PM plunger to the iron core. Therefore, the PM plunger moves inside the solenoid faster than it moves outside of the solenoid. Also it should be noted that, in Figure 2.46, when the PM plunger is moving, the dynamic current in the top part of the solenoid is not as smooth as the current where the plunger does not move. It is because an induction voltage is produced while the plunger is in motion; and its direction is always opposing the source voltage. From equation (2.15), it is known that when the plunger moves it produces an induction voltage in the solenoid circuit system. This induction voltage due to the plunger motion can affect the system current, and always resists the source current. As the velocity of the plunger increases the induction voltage increases proportionately.

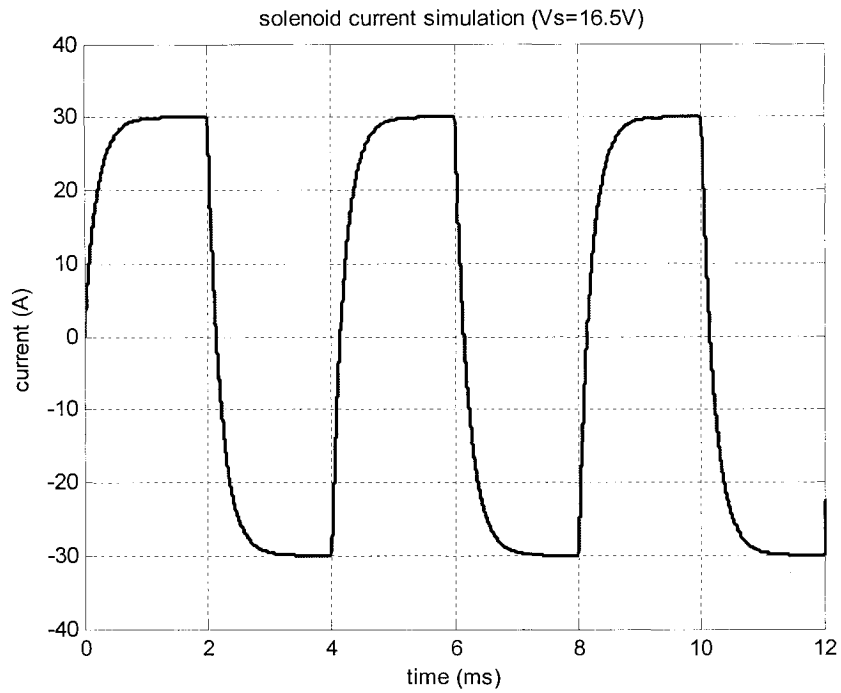


**Figure 2.43 Solenoid current dynamic simulation (Vs=+/-16.5V)**

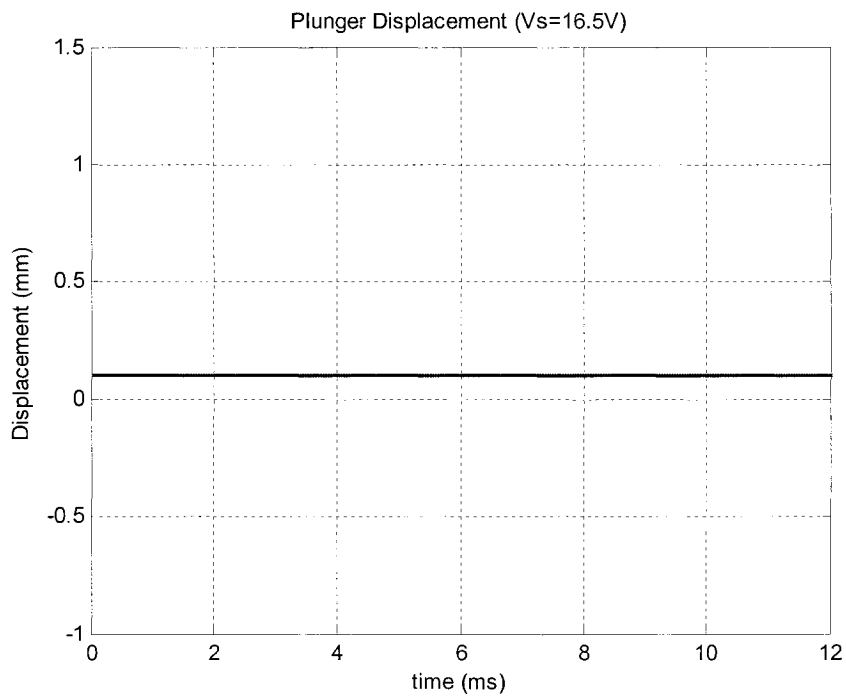


**Figure 2.44 PM plunger displacement dynamic simulation (Vs=+/-16.5V)**

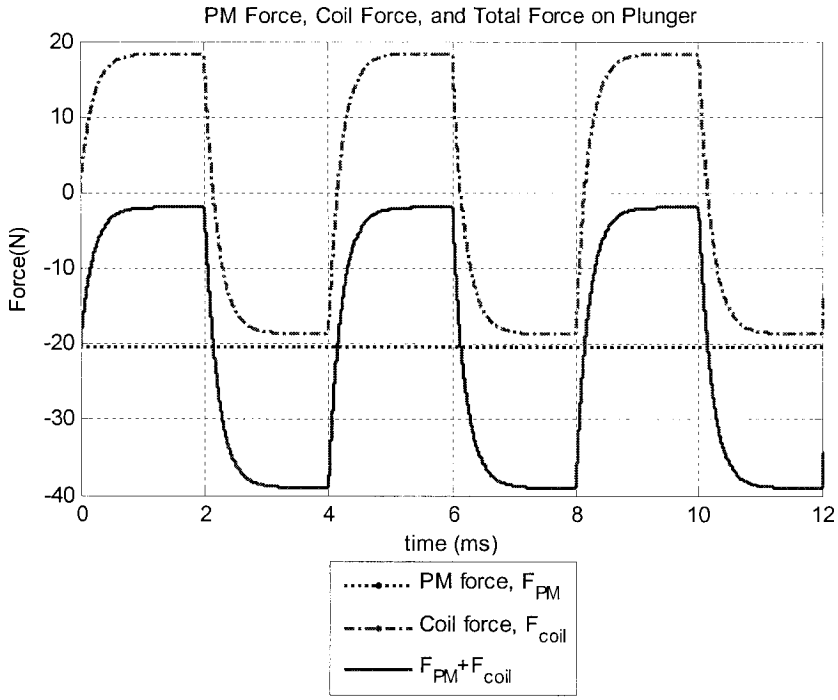


**Figure 2.45 PM force, coil force, and total force acting on PM plunger dynamic simulation (Vs=+/-16.5V)**

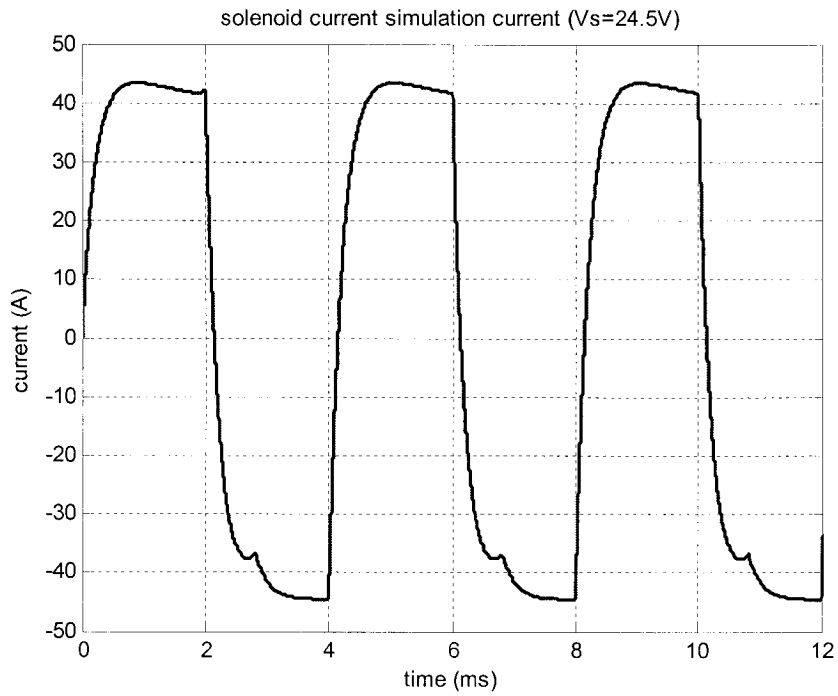


**Figure 2.46 Solenoid current dynamic simulation (Vs=+/-24.5V)**

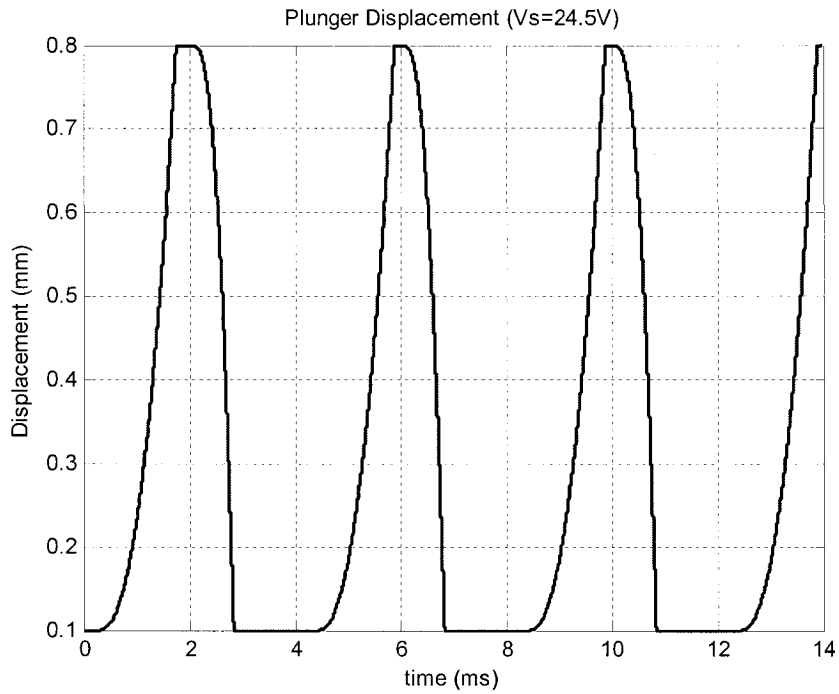


**Figure 2.47 PM plunger displacement dynamic simulation (Vs=+/-24.5V)**

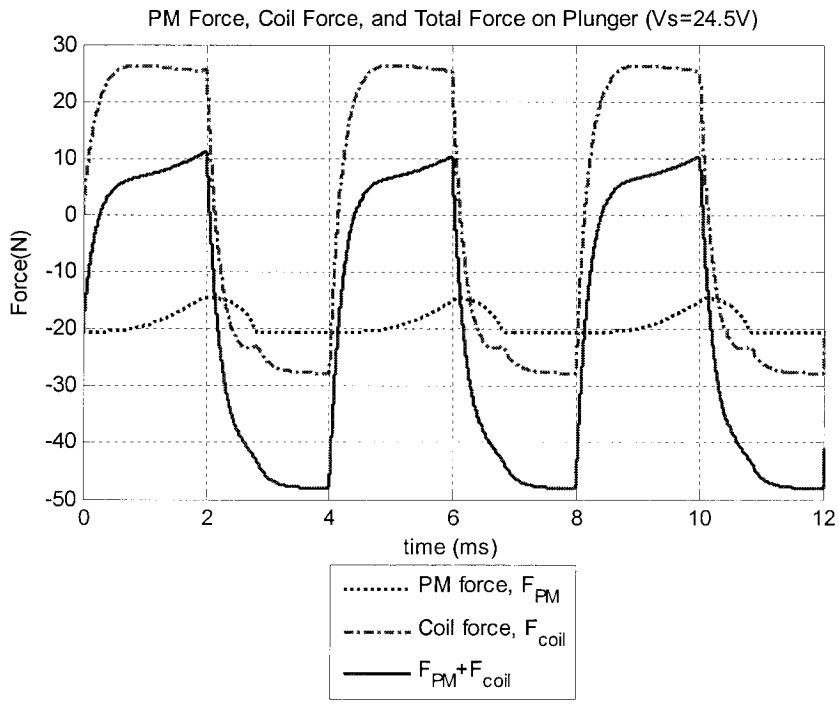


**Figure 2.48 PM force, coil force, and total force acting on PM plunger dynamic simulation (Vs=+/-24.5V)**

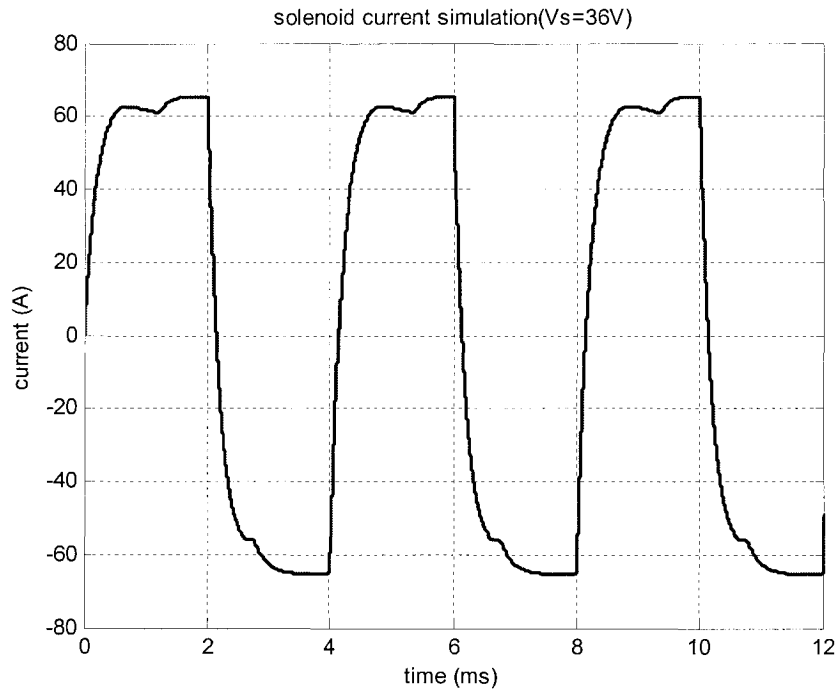


**Figure 2.49 Solenoid current dynamic simulation (Vs=+/-36V)**

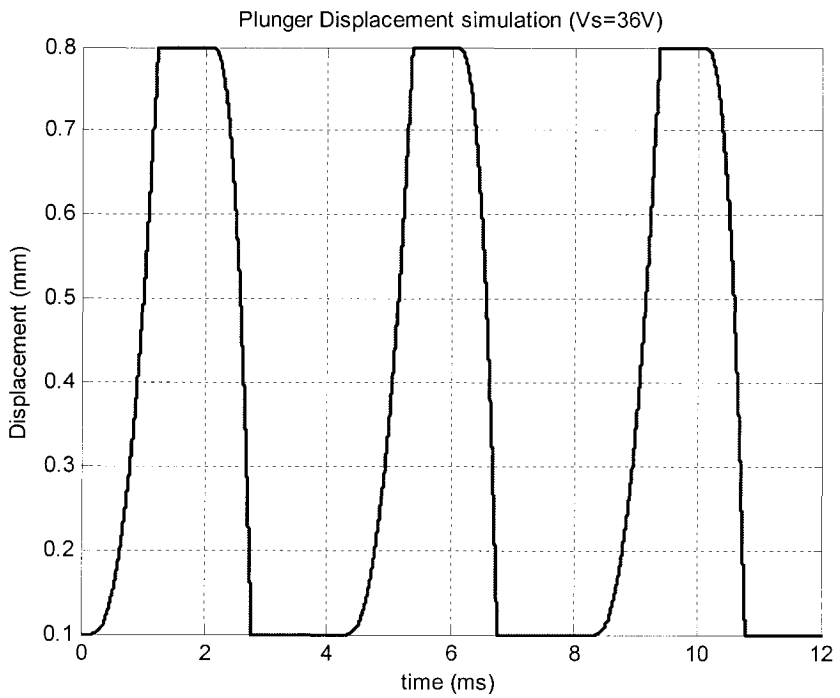


**Figure 2.50 PM plunger displacement dynamic simulation (Vs=+/-36V)**

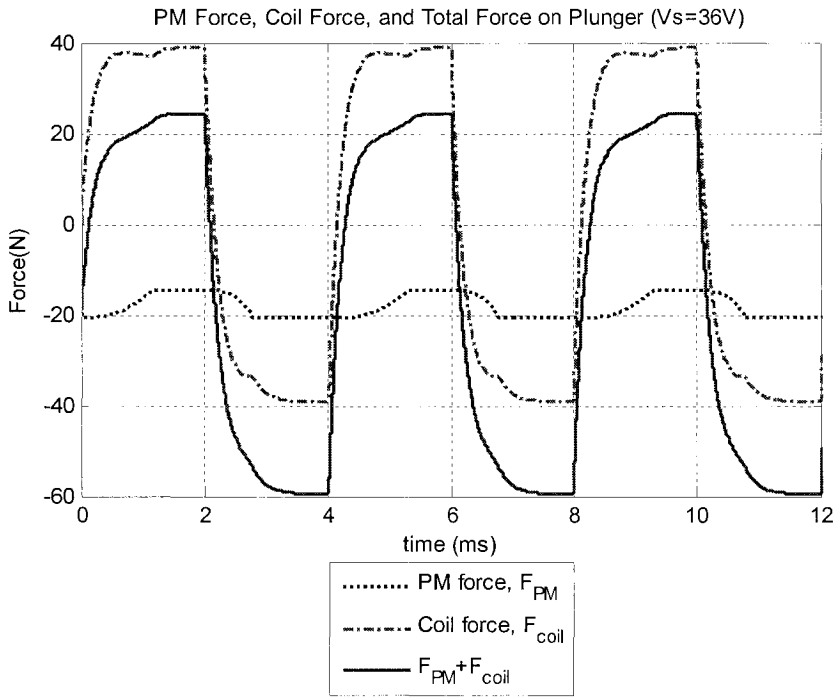


**Figure 2.51 PM force, coil force, and total force acting on PM plunger dynamic simulation (Vs=+/-36V)**

When a higher supply voltage ($\pm$ 36V) is applied to the solenoid, as shown in Figure 2.49 to Figure 2.51, the higher magnetic force due to the current is achieved. As the PM force is not a function of the solenoid current, therefore, a higher force acting on the PM plunger is produced. As a result, the PM plunger will move faster at a higher supply voltage. Comparing Figure 2.48 with Figure 2.51, it can be seen that as a higher voltage is applied to the solenoid, the total force acting on the PM plunger is larger. The maximum plunger push force increases from around 11 N to 23 N when the applied voltage increases from $\pm$ 24.5V to $\pm$ 36V; meanwhile, the maximum plunger pull force increases from around 48 Newton to 60 Newton. The larger pushing force and larger pulling force causes the PM plunger to increase its speed. As shown in Figure 2.47 and 2.50, when the +24.5V voltage is applied to the solenoid, the plunger takes 1.8 ms to

reach the maximum position of 0.8mm from the initial position of 0.1mm. With the applied voltage of +36V, it takes 1.17ms. When -24.5V is applied to the solenoid, the plunger takes 0.84ms to return to the initial position, compared with 0.77ms when the applied voltage is -36V.

It should be noted that a supply voltage that is too high, will burn the solenoid. From the experiments, it was found that at a supply voltage of $\pm 48$V, the solenoid got burnt.

## 2.9 Summary

In this chapter, a bi-directional linear solenoid actuator with a moveable PM plunger is described. This actuator is different from traditional linear solenoid actuators in which the moving plunger is a PM instead of being made of carbon steel (ferromagnetic) material. A bi-directional voltage applied to the solenoid, produces a pushing and pulling force acting on the PM plunger to produce the bi-directional motion.

Neodymium iron boron (NdFeB) is selected as the solenoid actuator plunger, because this type of PM material has very high magnetic energy, very high remanence and coercivity, and excellent magnetic characteristics.

The dynamic mathematical model of this solenoid actuator has also been derived. The solenoid model is set up by the equivalent circuit method (Figure 2.4). To simplify

calculations, the magnetic circuit of the solenoid is seen as an ideal magnetic circuit and a loss factor $k$ is introduced to correct the theoretical model to match the experimental results more closely. The total force acting on the PM plunger combines two parts, the force due to the PM and the force due to the current through the solenoid. When the force due to the current is larger than the force due to the PM, the force can drive the PM plunger in bi-directional motion.

To have an accurate mathematical model of the solenoid actuator, the nonlinear magnetization property of the ferromagnetic material, such as the solenoid steel housing, is included in the model. To determine the nonlinear magnetization curve, experiments were performed to measure the currents and corresponding forces of the solenoid actuator.

Theoretical calculations and experimental results show that for a small stroke PM plunger solenoid actuator, the magnetic field of the solenoid in the center part can be considered equal. As well, the PM was selected to have permeability close to that of air. Because of these two conditions, the magnetic force due to the solenoid current for the actuator is not a function of the PM plunger air-gap. In other words, the force due to the current acting on the plunger will not change with the air-gap. Therefore, the material parameters $a$ and $b$ in equation (2.52) can be determined using the steady-state magnetic forces due to the different supply voltages and the corresponding currents of the solenoid. When the parameters $a$ and $b$ are determined, the nonlinear magnetization characteristic curve of the solenoid actuator can be established, as well as the nonlinear inductance of the solenoid.

Since the simulation results and the experimental results of the bi-directional PM plunger solenoid actuator match well, it indicates that the mathematical model of the solenoid actuator is appropriate. It should be noted that if the PM plunger moves out from the solenoid, it must overcome the magnetic force of attraction between the PM plunger and the stator iron core. Therefore, a proper supply voltage is required to be applied to the solenoid while the plunger moves out; if the PM plunger moving direction is into the solenoid, the magnetic force of attraction between the PM plunger and iron core and the force due to the current act together in the same direction on the plunger. Obviously, for the PM plunger the pulling force is larger than the pushing force while it is driven; therefore, the plunger moves faster into the solenoid than it moves out of it. When higher supply voltages are applied to the actuator, larger drive forces can be obtained. However, too high a voltage will result in a corresponding large current which may burn the solenoid.

# CHAPTER 3

# DEVELOPMENT OF A PERMANENT MAGNET PLUNGER BI-DIRECTIONAL SOLENOID ACTUATOR FOR AN ALTERNATIVE FUEL INJECTOR

A new type of Permanent Magnet (PM) plunger bi-directional actuated solenoid actuator was developed in Chapter 2. In this chapter, a new type of injector actuated by a PM plunger bi-directional actuated solenoid actuator will be developed. The literature review showed that there is currently no fuel injector operated by a bi-directional motion actuator. The injector is developed for the direct injection of alternative fuels into the combustion chamber of compression ignition (CI) engines. The mathematical model of the injector will be developed and the performance and the parameters of the injector will be discussed.

## 3.1 Design of the Alternative Fuels Direct Injection Injector Actuated by a PM Plunger Bi-directional Motion Actuator

The fuel injector operated by the PM plunger bi-directional motion solenoid actuator is illustrated in Figure 3.1. It is based on a previous design of a conventional solenoid-operated diesel injector for low-viscosity liquid and gaseous fuels [3]. The previous injector design is shown in Figure 3.2. In this design, the assumption is that the injector has the same working conditions as the previous injector. Therefore, some construction elements and components of the previous injector are used in this current

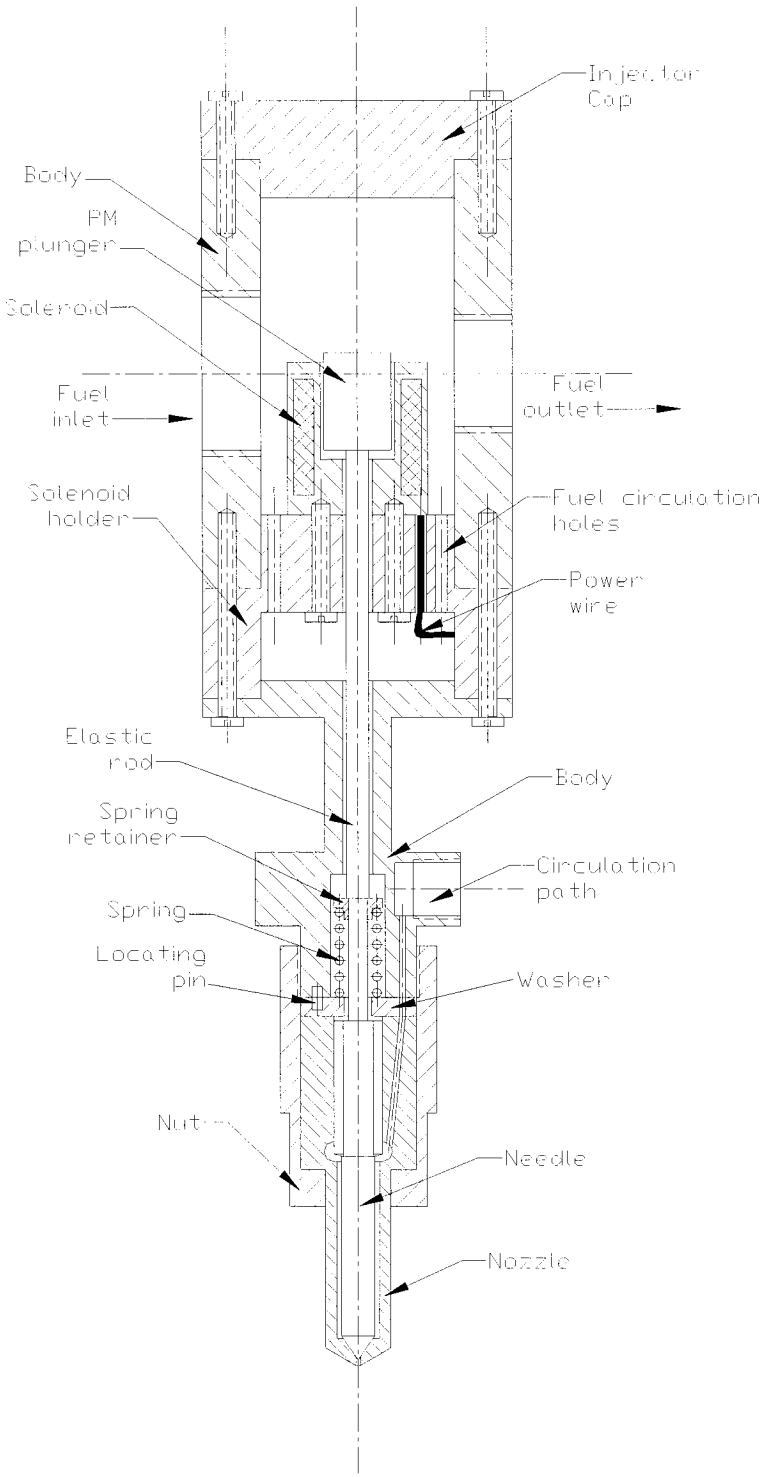


**Figure 3.1 PM plunger Bi-direction actuator operated alterative fuel injector**

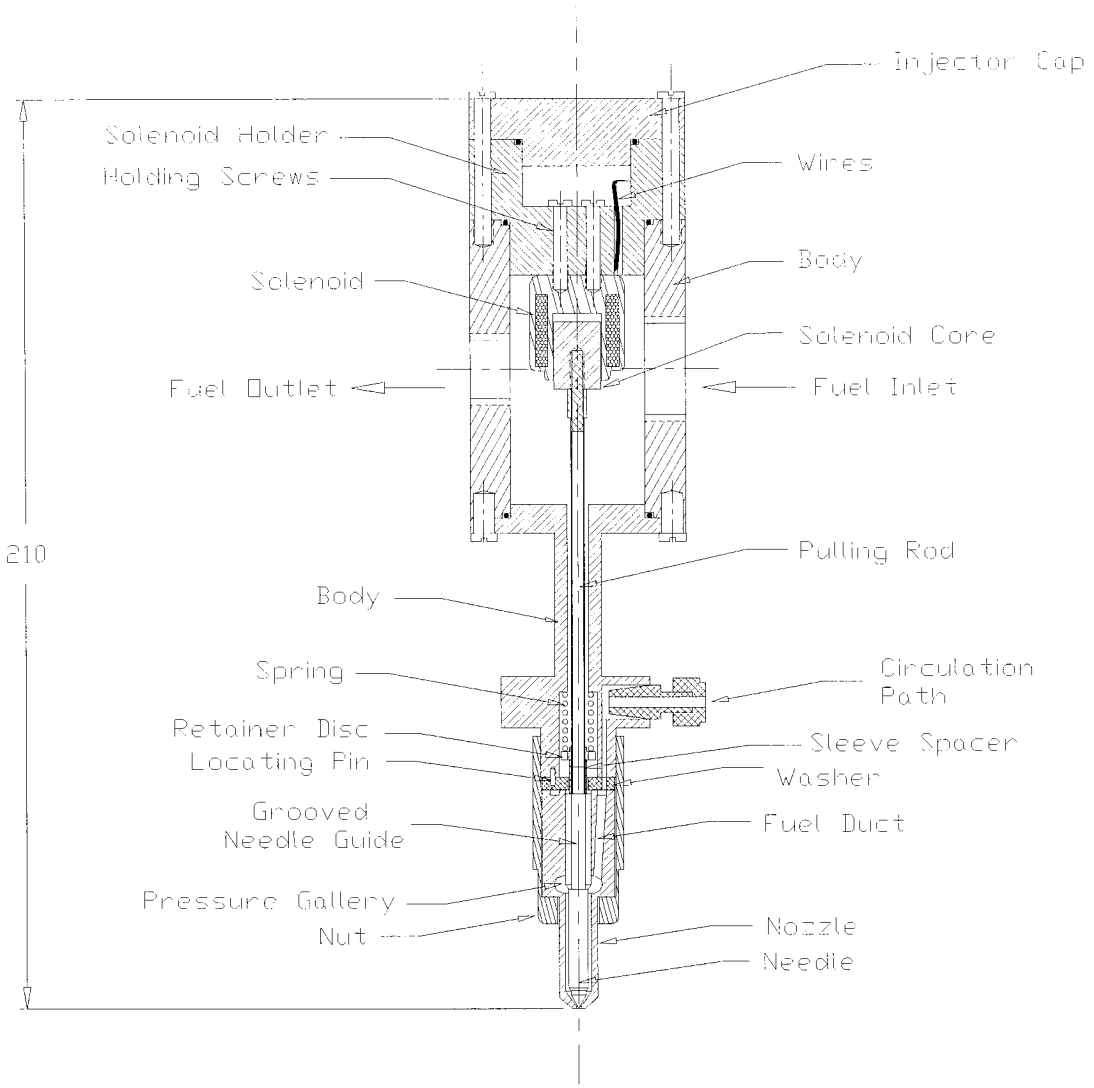


**Figure 3.2 Conventional solenoid operated alterative fuels injector [3]**

injector design.

As in the previous injector which is actuated by a conventional solenoid actuator, this design uses the nozzle and needle Bosch size 'S' with a body diameter of 9mm and a head diameter of 17mm. Furthermore, the needle assembly, the injector body, and the fuel volume chamber body used in the previous design are employed in this design. In

addition, the bi-directional actuated solenoid actuator is contained in the volume chamber so that the fuel flow can help to cool the solenoid and PM plunger.

The main differences from the previous design are:

1. The bottom of the solenoid actuator is in the downside position and fixed on the solenoid holder, since a magnetic force between the PM plunger and the static steel core will pull the PM plunger downwards. Therefore, this force can be used to keep the injector closed without power to actuate the injector and thus a return spring is not required as in the previous injector designs.

2. Six fuel circulation holes with 2.5mm diameter are drilled through the solenoid holder. The six holes allow fuel delivery into the nozzle.

3. A pre-loaded spring is added to assist injector opening since the force of attraction due to the PM pulls the plunger down, and a rod connects the plunger to the injector needle. Therefore, to open the injector the solenoid force created by the current must be able to overcome this PM force. Thus, the pre-loaded spring is added in this design to help overcome the PM magnetic attractive force to open the injector faster.

4. An initial air-gap of 0.1mm is established between the PM plunger and the stator steel core, such as by a brass shim, in the free power mode. This air-gap has two functions, first to avoid the large attractive force between the PM plunger and the steel core at zero air-gap; secondly to avoid the impact between the plunger and the steel core.

5. The material of the solenoid holder, injector cap, fuel volume chamber body, and the injector body is made of a nonmagnetic material, namely, brass and stainless steel. The nonmagnetic material will not affect the magnetic field path of the solenoid and PM plunger; therefore, the actuator functions and mathematical model as described in the last chapter can be employed in this injector analysis.

The basic principle of this injector design is: when there is no power supplied to the solenoid, an attractive force between the PM plunger and the solenoid stator steel core pulls the PM plunger down; the plunger is connected to the needle via a pulling rod. As a result, this attractive force pulls the needle down against the seat of the nozzle and the injector is closed. When a current is applied to the actuator, the induced magnetic field pushes on the PM plunger to overcome the attractive force due to the PM and moves the PM plunger up to open the injector. To make the injector open response faster, a pre-loaded spring pushes the pulling rod to overcome the force due to the PM. A washer acts as a stopper to block the needle when it is at its fully open position. While the current is reversed and applied to the actuator, the coil current produces a pulling force to pull the

PM plunger down to close the injector. This force pulls in the same direction as the PM, and the combined forces act to close the injector faster.

### 3.2 Mathematical Model of the Injector

The lump spring-mass-damper system of the injector in Figure 3.3 represents the model of the fuel injector in Figure 3.1.

$m_n$ and $m_c$ are respectively the mass of the injector needle and the mass of the PM plunger of the solenoid actuator. $x_n$ and $x_c$ are the displacements of the needle and the PM plunger, where the upward direction is taken as positive in their motion. The needle position at $x_n = 0$ is where the needle just touches the injector seat, and the needle is fully open at position $x_n = H_{\max}$. The injector needle and the PM plunger are connected together with a hollow stainless steel pulling rod. The spring stiffness of the elastic rod is $k_r$ and the material damping is $d_r$.

When the needle impacting with the injector seat at closing, the needle-to-seat interface is modeled as a spring with stiffens $k_t$ and a material damping $d_t$. When the injector is fully open the needle is limited by a stopper, and the needle-to-stopper interface is modeled as spring with stiffens $k_p$ and a material damping $d_p$. The pre-load

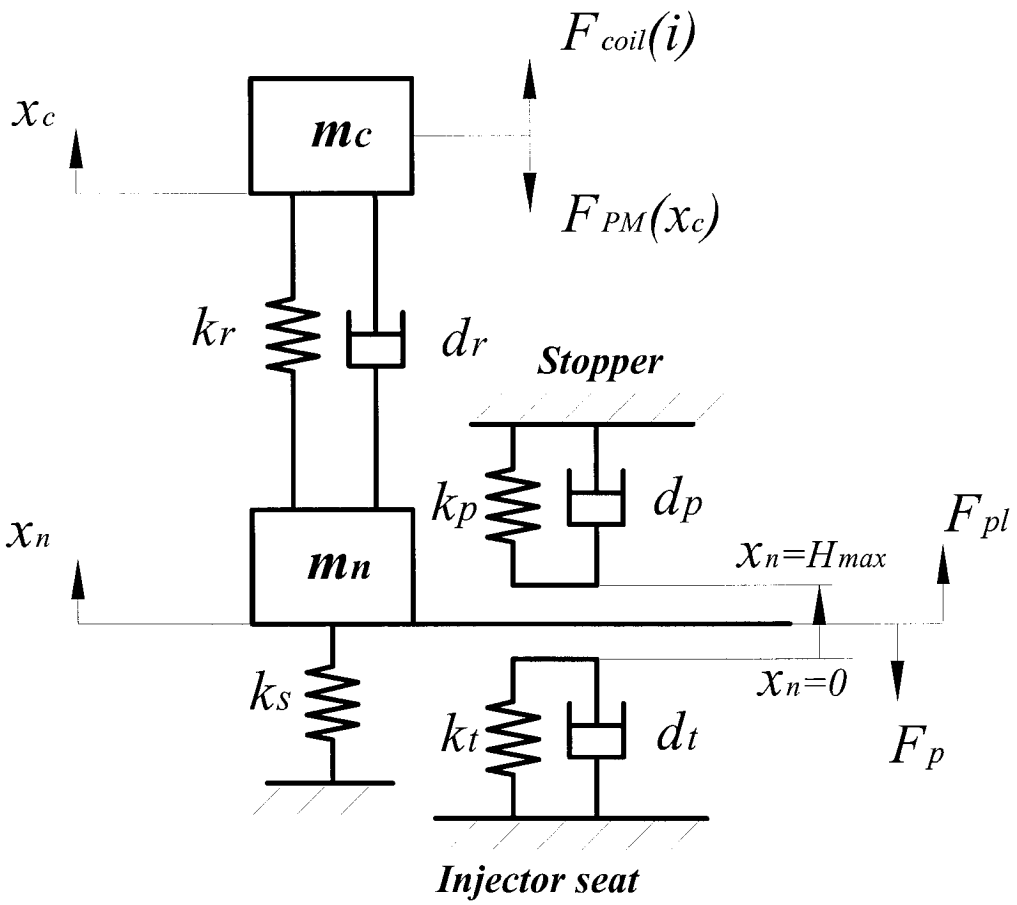


**Figure 3.3 Spring-mass-damper model of the injector**

spring which has a pre-load force $F_{pl}$ to assist faster injector opening is represented as stiffness $k_s$. The force due to the PM plunger is represented as $F_{PM}$ , and its direction is always downward. The force due to the current in the coil is represented as $F_{coil}$. When $F_{coil}$ direction is upward, it shows as a positive direction; contrarily, it shows as a negative direction while $F_{coil}$ is downward. Similarly, the current direction that makes the $F_{coil}$ upward is taken as positive; on the other hand, the current direction that makes the

$F_{coil}$ downward is taken as negative. The calculation of the forces $F_{PM}$ and $F_{coil}$ have been discussed in Chapter 2.

$F_P$ is the fuel pressure force acting on the injector needle and resulting from the pressure drop across the injector nozzle orifice, for the pressure balanced injector design, it always trends to close the injector, and it can be approximately expressed as [19, 38] :

$$F_P = A_m(P - P_e) \tag{3.1}$$

where the differential pressure $(P - P_e)$ is acting on the effective needle area $A_m$. $P$ is the pressure inside the injector above the effective area, and $P_e$ is the pressure below this area which may be taken as the pressure inside the combustion chamber.

For a seat diameter of the nozzle orifice $d_o$, the effective area $A_m$ is a function of the needle lift $x_n$, and is given by [19, 38]:

$$A_m = \pi(x_n \sin\theta)(d_o - x_n \sin\theta\cos\theta) \tag{3.2}$$

where $\theta$ is the haft angle of the needle conical tip.

The viscous damping forces due to the needle and PM plunger motion relative to the fluid viscosity inside the injector are neglected because large clearances are allowed.

The needle reaction force with the injector seat or stopper is defined as $F_R$. Therefore, from Newton's Second Law, the dynamic equations of the PM plunger and the needle are expressed as, respectively:

$$m_c \frac{d^2 x_c}{dt^2} = F_{coil} - F_{PM} - k_r(x_c - x_n) - d_r \left| \frac{dx_c}{dt} - \frac{dx_n}{dt} \right| sign\left(\frac{dx_c}{dt}\right) - m_c g \tag{3.3}$$

$$m_n \frac{d^2 x_n}{dt^2} = F_R - F_P + F_{pl} - k_s x_n - k_r(x_n - x_c) - d_r \left| \frac{dx_n}{dt} - \frac{dx_c}{dt} \right| sign\left(\frac{dx_n}{dt}\right) - m_n g \tag{3.4}$$

The *sign* in equations (3.3) and (3.4) express the direction of the damping force due to the long connecting rod between the PM mass and the needle mass, and they are always dissipative in the direction of mass motion. The reaction force $F_R$ in equation (3.4) depends on the following conditions:

$$F_R = -k_t x_n - d_t \frac{dx_n}{dt} \qquad \text{if} \quad x_n \le 0 \tag{3.5}$$

$$F_R = 0 \qquad \text{if} \quad 0 < x_n < H_{\max} \tag{3.6}$$

$$F_R = -k_p(x_n - H_{\max}) - d_p \frac{dx_n}{dt} \qquad \text{if} \quad x_n \ge H_{\max} \tag{3.7}$$

Same as in Chapter 2, when a source voltage is applied to the injector, the state system equations of the injector operated by a PM plunger solenoid actuator are expressed as:

$$\begin{cases} \dfrac{dx_c}{dt} = v_c \\ \dfrac{dv_c}{dt} = \dfrac{1}{m_c}\left[F_{coil} - F_{PM} - k_r(x_c - x_n) - d_r \left| \dfrac{dx_c}{dt} - \dfrac{dx_n}{dt} \right| sign(\dfrac{dx_c}{dt}) - m_c g\right] \\ \dfrac{dx_n}{dt} = v_n \\ \dfrac{dv_n}{dt} = \dfrac{1}{m_n}\left[F_R - F_P + F_{pl} - k_s x_n - k_r(x_n - x_c) - d_r \left| \dfrac{dx_n}{dt} - \dfrac{dx_c}{dt} \right| sign(\dfrac{dx_n}{dt}) - m_n g\right] \\ \dfrac{di}{dt} = \left(V - iR - N\dfrac{d\phi_{PM}(x_c)}{dx_c}\dfrac{dx_c}{dt}\right)\dfrac{1}{L_e + L_{coil}(i)} \end{cases} \tag{3.8}$$

where $v_c$ and $v_n$ is the velocity of the PM plunger and the needle, respectively. As discussed in Chapter 2, the dynamic force $F_{coil}$ and $F_{PM}$ can be evaluated by equation (2.40) and (2.43); the reaction force follows the conditions of equations (3.5) to (3.7). As in Chapter 2, using the 4$^{th}$ order Runge-Kutta method written in a C++ program, the system equation (3.8) can be solved.

### 3.3 Simulation and Discussion

This section will present the dynamic simulation results of the injector and compares them with the injector operated by the conventional solenoid actuator. The parameters which affect the injector operation will be discussed as will be the needle bouncing after injection and its reaction force.

### 3.3.1 Injector Simulation

As mentioned previously, the design in this research is based on previous work, and some components of the previous injector designs are employed in this novel injector, along with a hollow pulling rod that tends to bounce less by absorbing the relative kinetic energy between the PM plunger and injector needle [3]. The parametric values used for simulation are listed in Table 3.1.

**Table 3.1 Parameters used in injector simulation**

| Spring stiffness, material damping, plunger and needle mass | Hollow stainless steel rod |
|---|---|
| $k_t(kN/mm)$ | 17 |
| $d_t(kg/s)$ | 160 |
| $k_p(kN/mm)$ | 20 |
| $d_p(kg/s)$ | 170 |
| $k_r(kN/mm)$ | 5.3 |
| $d_r(kg/s)$ | 100 |
| $m_n(kg)$ | 0.0105 |
| $m_c(kg)$ | 0.011 |

The stiffness of the pre-load spring $k_s$ is chosen as 5N/mm and the pre-load is set at 15N; and the pressure inside the injector is constant at 20MPa, the injection time is 5ms, the needle fully open position is $H_{\max} = 0.6mm$ , and the voltage applied to the injector is a +/-36V square waveform. Under these conditions the simulation results of the injector are obtained and presented in Figures 3.3 to 3.6.

Figure 3.4 shows the displacements of the injector needle and actuator PM plunger when a +/-36V voltage square waveform is applied to the injector. With a +36V voltage applied to the injector, a force is produced to lift the needle up. At approximately 0.11ms, the needle leaves the injector seat and reaches the fully open position at 1.31ms.

At this position, the needle hits the stopper (washer), and an impact force causes the needle to bounce back down, and the force acting on the PM plunger pushes the plunger to go back up; consequently, the needle upper bouncing stop will occur and can last to 2.8ms. At 5ms, the injector fuel injection is complete, a -36V voltage is applied to the injector, and the injector starts to close. At 5.84ms, the needle hits the injector seat, and in the same way as with the upper bouncing, the impact makes the needle to bounce up. Meanwhile, the force which combines coil current force and PM attractive force acting on the PM plunger pulls the plunger to go downward at the same time; as a result, injector seat bouncing occurs. This bouncing will last to 7.2ms. Obviously, the bouncing at the needle seat is more harmful than the bouncing at the upper stop. It can lead, not only to post-injection, but also to nozzle seat and needle wear.

Also, Figure 3.4 shows the difference in displacement between the needle and the PM plunger. This difference is due to the extension and compression of the elastic pulling rod, which connects the PM plunger to the injector needle. The rod can absorb a portion of the energy transferred from the PM plunger to the needle and this reduces the needle bouncing.

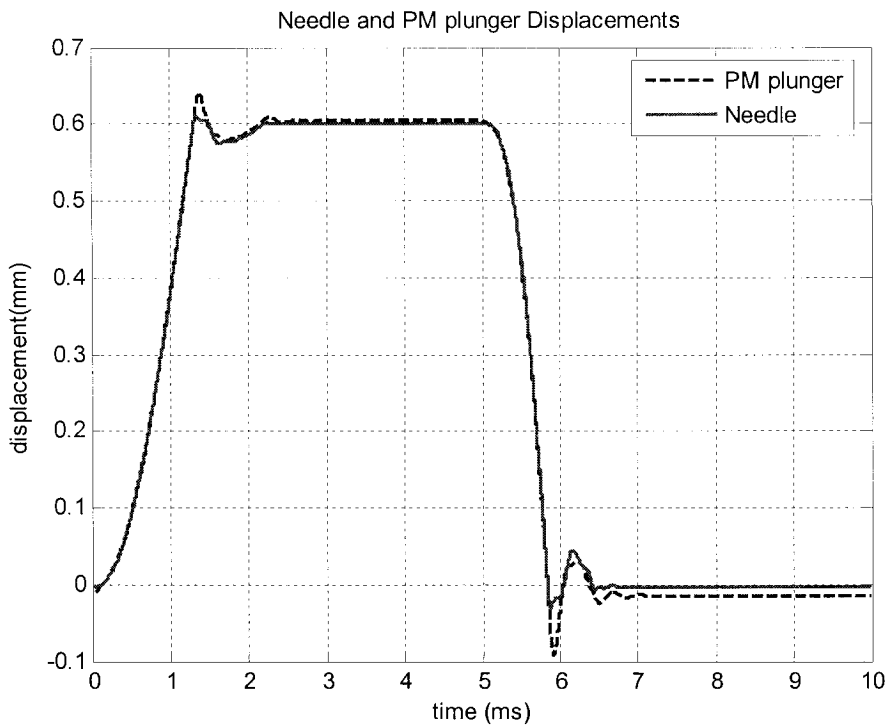


**Figure 3.4 Injector needle and PM plunger displacement simulation results**

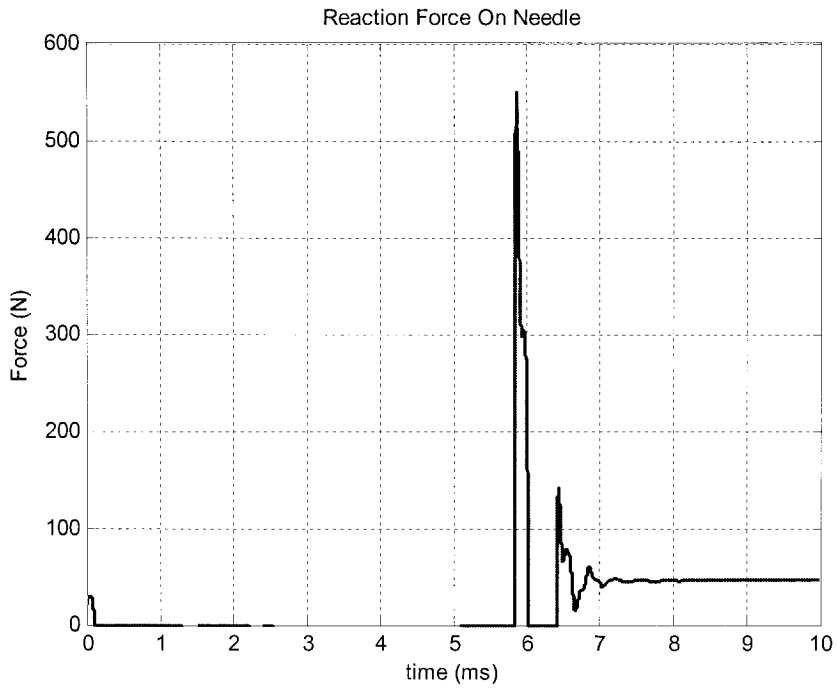


**Figure 3.5 Injector seat impact force acting on needle simulation result**

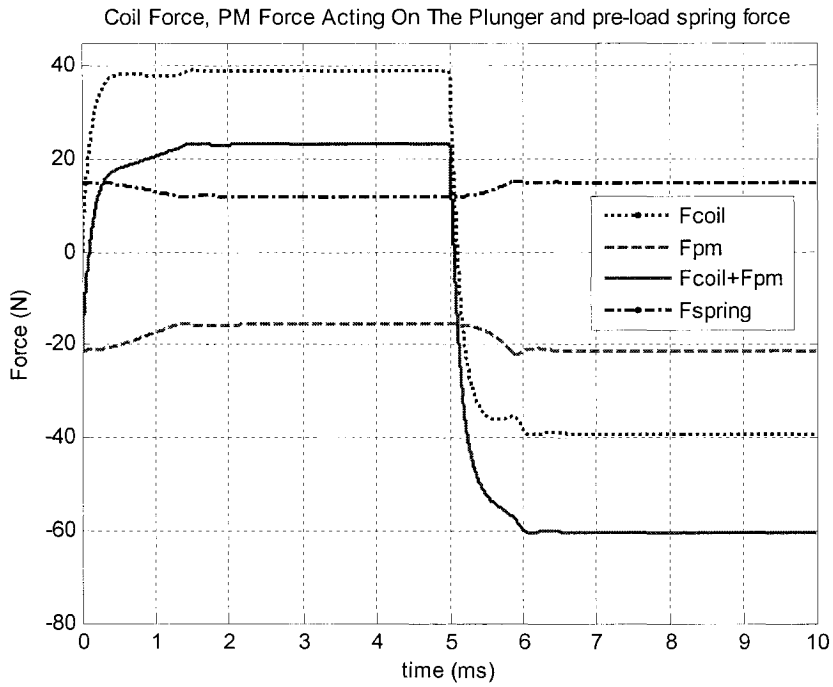


**Figure 3.6 PM force and coil Forces acting on the PM plunger and pre-load spring force simulation results**

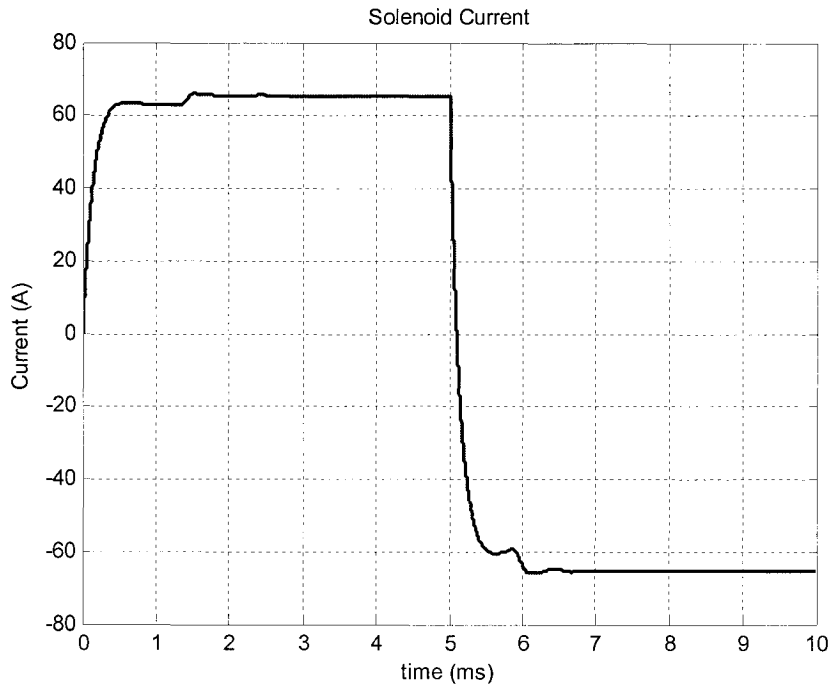


**Figure 3.7 Solenoid current simulation result**

Figure 3.5 presents the injector seat reaction impact force acting on the needle. When the injector is closing, the first impact force reaches to 546.5 N, produced from the combined forces due to the PM, the coil current that pulls the needle down from the fully open position, and the fuel pressure. This combined force causes the needle to attain a high velocity as it hits the seat. During bouncing the impact force gradually reduces, and it continues and dies out at about 7.2ms.

Figure 3.6 shows the forces due to the PM and the coil current as they act on the PM plunger, and the pre-load spring dynamic force. It can be seen from this figure that for the injector to open, the electromagnetic force due to the current must overcome the PM attractive force. When the injector is closing, both the force due to the current and the PM pull the plunger down. Therefore, the injector can close faster. To help the injector to open faster, a pre-loaded spring is added in this design. While the injector is opening, the pre-load spring help to overcome the PM attractive to open the injector. Note that if the pre-load is too large, it will slow down the injector closing time, and it will create injection timing problems; for these reasons the pre-load must be carefully chosen. The effect of the pre-load will be discussed section 3.3.3.

Figure 3.7 shows the current that passes through the solenoid. It can be seen that while the PM plunger is moving in the direction of the force due to the current, the solenoid current is actually going down, or is decreasing. It is because an induced voltage due to the plunger motion always resists the supply voltage. As the plunger motion

velocity increases, the induced voltage is higher, and this effect is more distinct. This phenomenon is expressed as in equation (3.8).

### 3.3.2 Comparison with the Previous Injector

Figure 3.8 presents the needle displacement of the previous injector as compared to the bi-directional actuator operated injector. In this comparison, it is assumed that both injectors are working at the same conditions. The pressure inside both injectors is 20MPa; the injection time of both injectors is 5ms; moreover, the needle material, nozzle material, pulling rod material, and the fully open stop washer material of both injectors are the same. The differences between the two injectors are that the supply voltage for the previous injector is 80VDC, and the bi-directional actuated injector is +/-36V square waveform; the return spring stiffness of the previous injector is 20N/mm with 20N pre-load, and the assisted opening spring stiffness of the bi-directional actuated injector is 5N/mm with 15N pre-load.

It can be seen from Figure 3.8 that both injectors start to open at almost the same time about 0.1ms, but the previous injector reaches to the fully open position faster taking 0.87ms while the bi-directional actuated injector reaches to the fully open position at 1.31ms. However, at the injector closing phase, the bi-directional injector is faster than the conventional injector. The bi-directional injector hits the seat at about 5.83ms while the previous injector hits the seat at 6.43 ms. Comparing the combined total closing

and opening times, the bi-directional injector is faster than the previous injector by about 0.16ms.

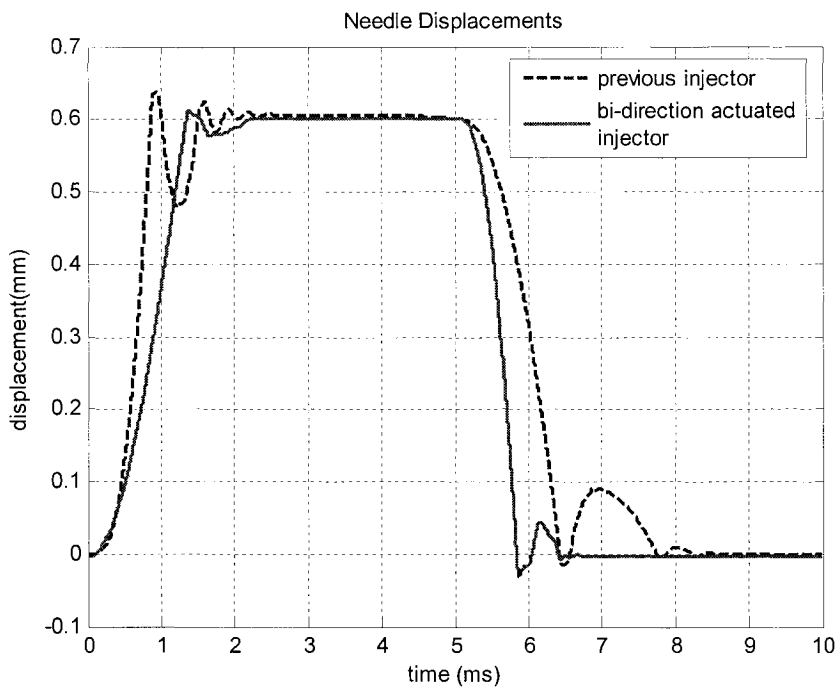


**Figure 3.8 Needle displacement comparison -- previous injector and bi-direction actuated injector**

In addition, with regards to needle bouncing, it can be seen that the conventional injector has much larger bouncing amplitude than the bi-directional injector along with a longer bounce time in the closing stage. The larger bounce amplitude and longer bounce time in the closing stage means that the injector has more post-injection. Post-injection is one of the main causes of tail pipe pollution.

Figure 3.9 shows the needle reaction impact forces of the previous injector and that of the bi-directional actuator operated injector in the conditions of Figure 3.8. The

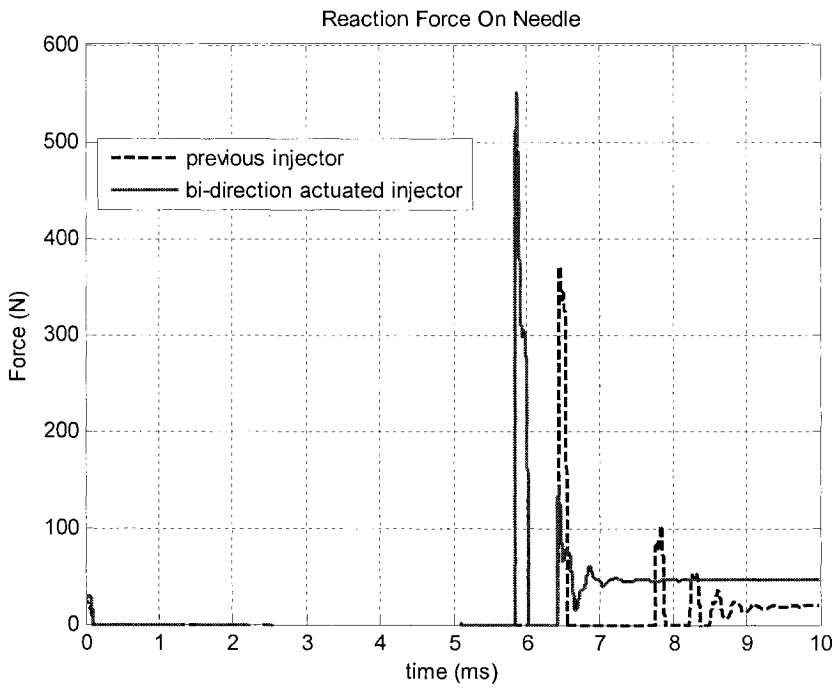


**Figure 3.9 Seat reaction impact force on needle comparison – Previous injector and bi-directional actuated injector**

figure shows that the bi-directional actuated injector has an initial higher impact force than the previous injector. While the first peak impact force of the bi-directional injector reaches 546.5N, the first peak impact force of the previous injector is 368.4N. Also, it can be seen that the needle of the previous injector has more and longer bouncing than that of the bi-directional actuator. This is because for the previous injector, only a return spring is used; however, for the bi-directional actuated injector, the PM attraction force and magnetic force due to current are employed to close the injector, and the sum of these two forces are larger than the return spring force as in the previous injector.

### 3.3.3 Effects of the Pre-load of the Open Assistance Spring

In this section, the effects of the pre-load of the open assistance spring will be discussed.

Figure 3.10 shows the needle simulation displacement paths at difference values of pre-load for the open assistance spring. The stiffness of the open assistance spring $k_s$ is set to 5 N/mm, the pre-loads $F_{pl}$ are set to 10, 15, 20, and 25N in each simulation. It can be seen from the figure that as $F_{pl}$ is increased, the injector will open faster to its fully open position. The fully open time is around1.47ms at $F_{pl}$=10N, and it is around 1.11ms at $F_{pl}$=25N. However, to the closing stage, as the pre-load $F_{pl}$ increases, the closing time will be longer. The simulation results show that the closing stage, when the pre-load is 10N, the needle first time to hit the injector seat is approximately at 5.8ms; when the pre-load is 25N, the needle first time to hit the injector seat increase to 5.93ms. For the needle total bouncing time, it takes around 6.61ms at the pre-load of 10N, while it takes around 6.77ms at the pre-load of 25N. It can be regarded that the variations of spring pre-load in this range does not affect appreciably the total bouncing time of the injector needle. But as the pre-load is increased, it requires more time to close the injector; also, it can be seen in the figure that the displacement of the bouncing will decrease a little bit as the pre-load is increased, but these variations are not significant.

Figure 3.11 shows the injector seat reaction force acting on the needle. The

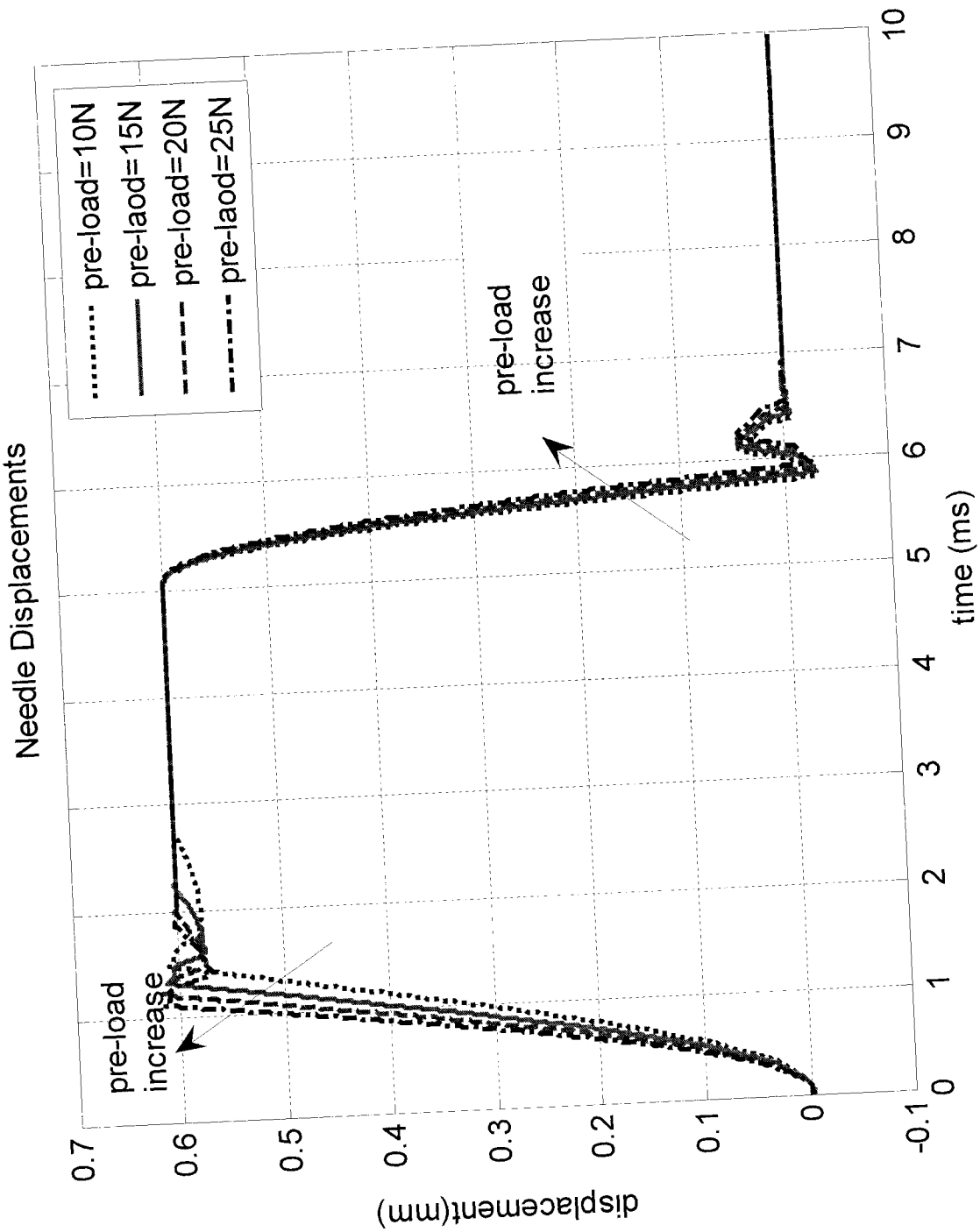


**Figure 3.10 Needle displacements with different pre-loads ($k_s = 5N/mm$)**

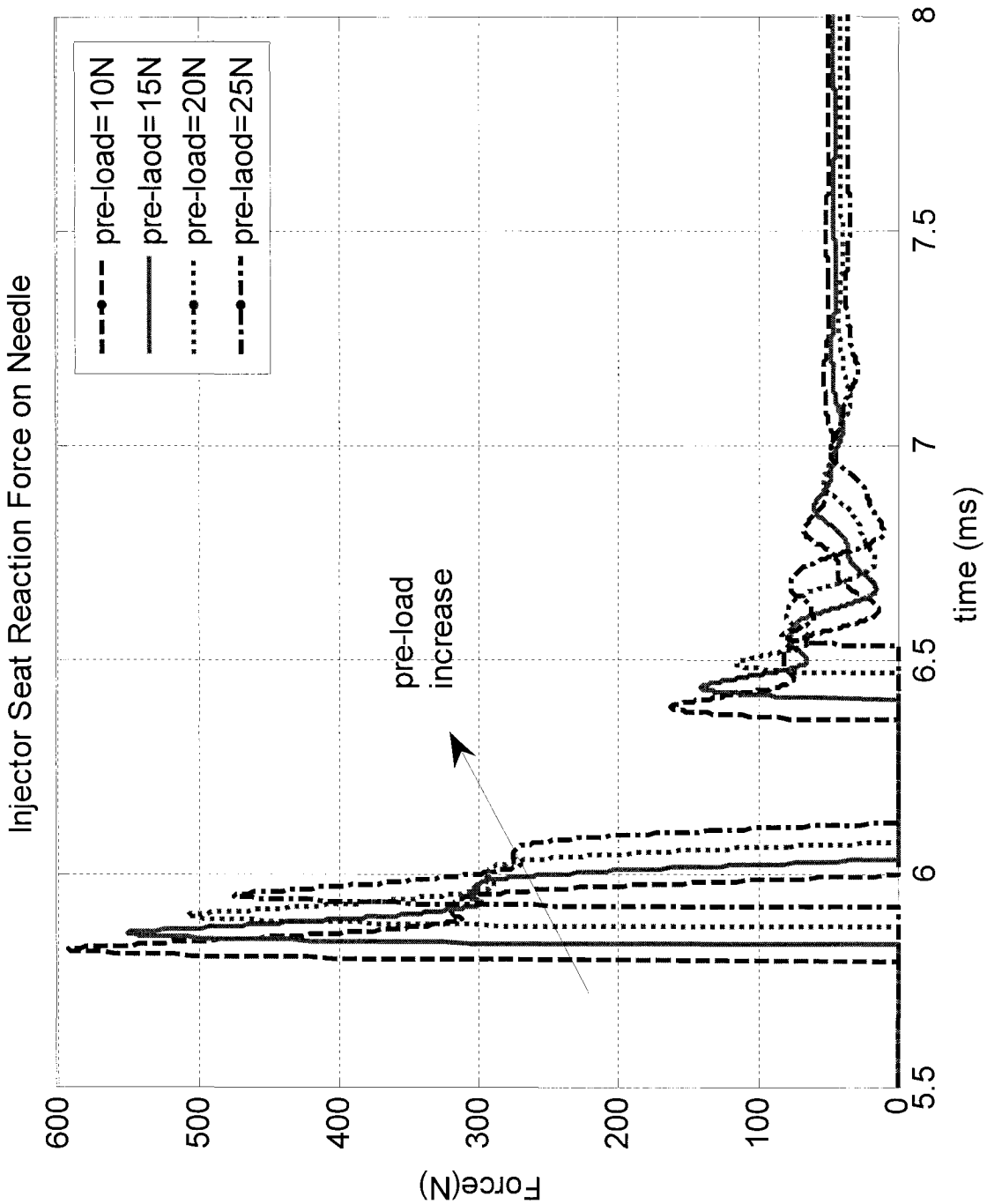


**Figure 3.11 Seat reaction force acting on the needle with different pre-loads ( $k_s = 5N/mm$ )**

simulation results show that as the pre-load increase, the needle reaction force is decrease. At first peak, when $F_{pl}$=10N, the seat reaction force is around 590N; but when $F_{pl}$=25N, the seat reaction force is around 475N. This is because as the pre-load increased, the spring force in needle open direction is increased. As this spring force is increased, the force which is used to close the needle is decreased; therefore, the impact force between the needle and the seat will be decreased.

The injector open assistant spring dynamic forces with the different pre-load are shown in Figure 3.12. Obviously, the force of the open assistant spring follows the displacement of the needle motion. As the needle lift displacement increases, the spring force is decreased. As the spring pre-load force is set higher, the spring force will assist the injector needle to open faster.

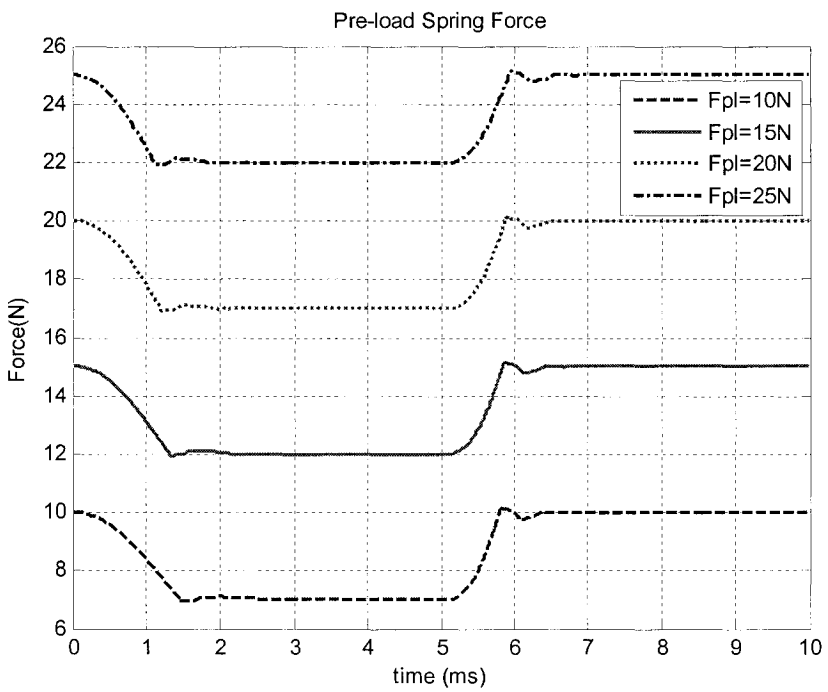


**Figure 3.12 Dynamic force of the open assistant spring with different pre-load($k_s = 5N/mm$)**

### 3.3.4 Effects of the Stiffness of the Open Assistance Spring

In this section, a discussion due to the effects of the stiffness of the opening assistance spring $k_s$ on the injector performance will be presented.

Figure 3.13 presents the needle displacement paths at different stiffness values of the opening assistance spring while the pre-load is set at 15N. The different stiffness values $k_s$ for simulation are 1, 5, 15, and 20N/mm. The simulation results show that as $k_s$ increases, the needle will take a longer time to achieve the fully open position. While $k_s$=1N/mm, the needle reaches the fully open position at 1.29ms; with $k_s$=20N/mm, the needle takes 1.41ms to reach the fully open position. This time difference is very small. At the injector closing stage, as $k_s$ is increased, the injector closing time is faster. The figure shows that when the spring stiffness is 1N/mm, the needle hits the seat at 5.85ms; while the spring stiffness is 20N/mm, the needle hits the seat at 5.78ms. Figure 3.13 shows the injector seat reaction force acting on the needle at differences values for the stiffness of the opening assistance spring. The simulation results show that as $k_s$ is increased, the needle reaction force increased. Thus as $k_s$ increase, the spring becomes "harder", and it will absorb less energy from the needle; therefore, the impact force between the seat and the needle increases. Hence, the seat and needle are more susceptible to wear. Note that while $k_s$ = 20N/mm, the needle cannot reach its fully open position within the allocated time span. This is because as $k_s$ is larger, more energy is

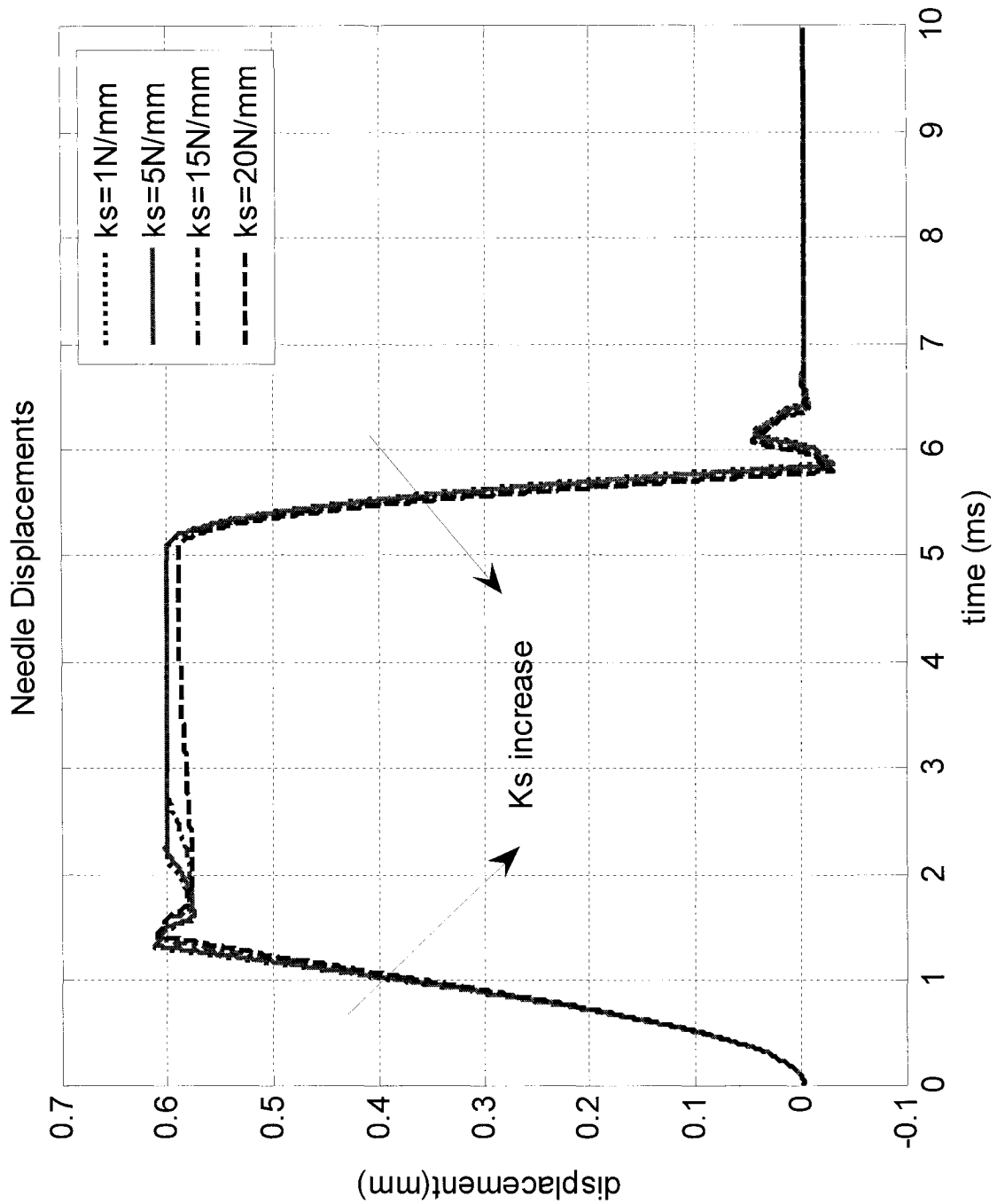


**Figure 3.13 Needle displacements with different stiffness (pre-load=15N)**

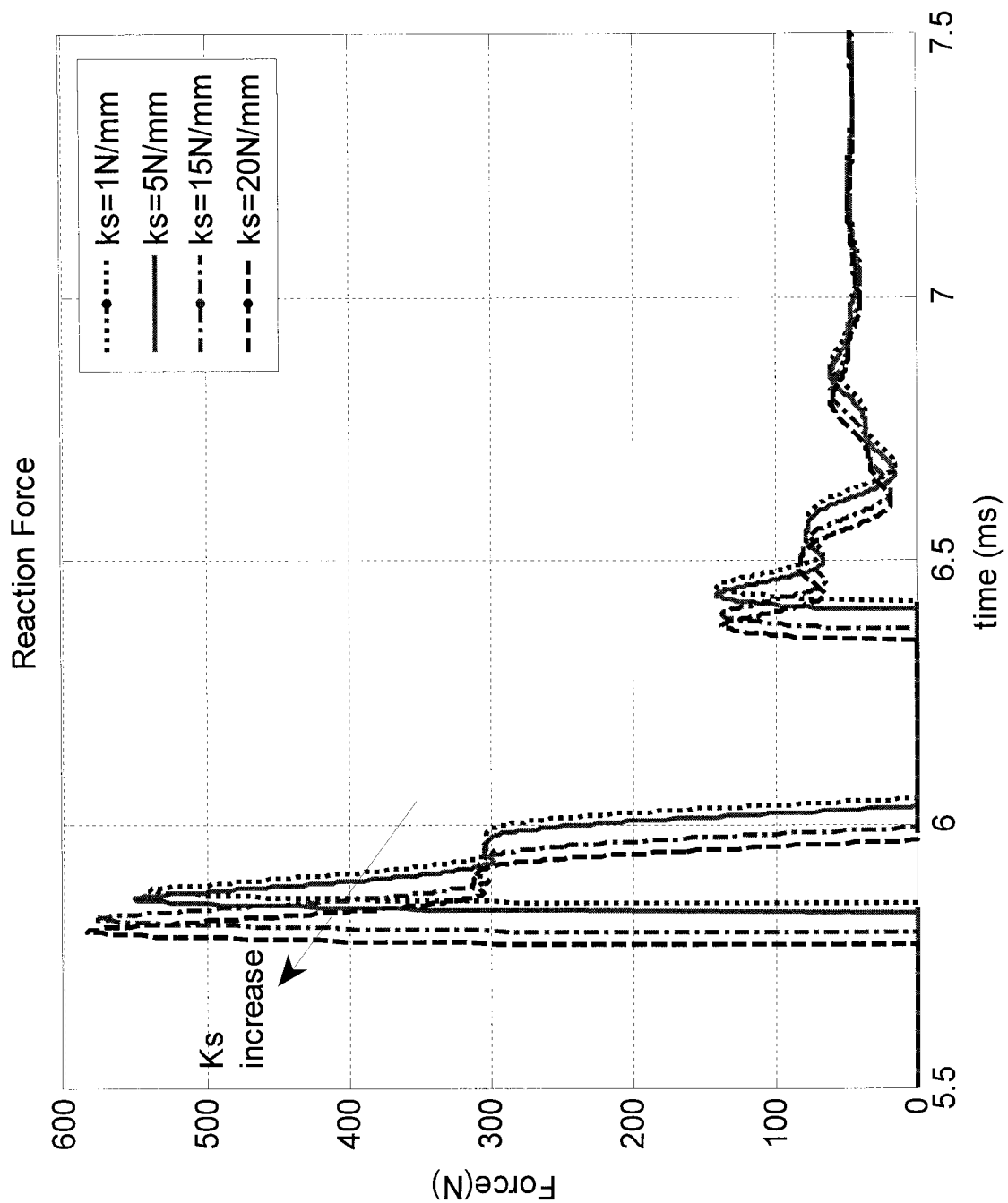


**Figure 3.14 Seat reaction forces acting on the needle with different stiffness (pre-load=15N)**

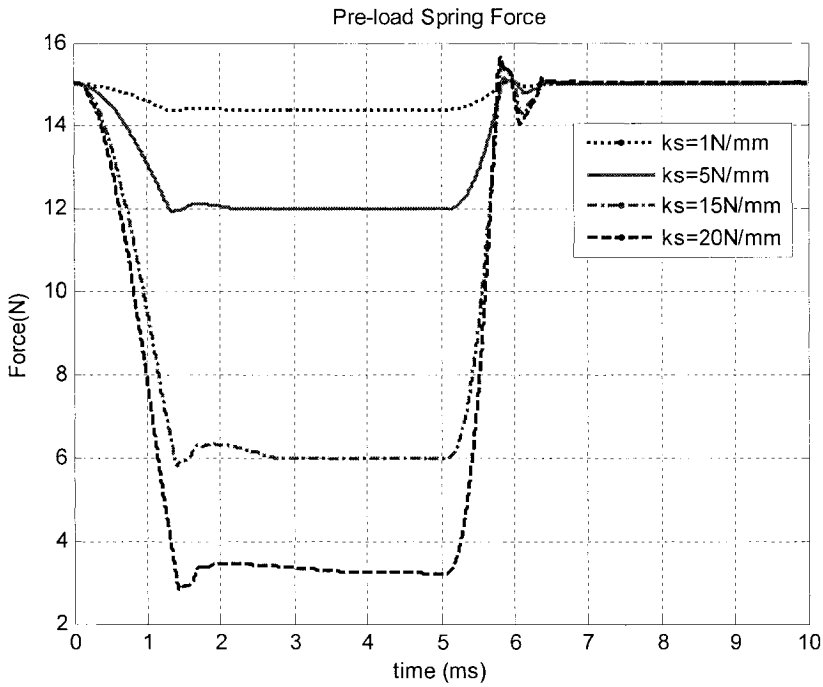


**Figure 3.15 Dynamic force of the open assistant spring with different stiffness (pre-load=15N)**

required to extend (or compress) the spring. Therefore, for the springs having the same pre-load, while $k_s$ is increased, more force is required for the needle system to reach the same displacement. The pre-load spring dynamic forces for different spring stiffness are showed in Figure 3.15.

## 3.4 Summary

A new type of alternative fuel direct injection injector operated by a PM plunger bi-directional motion solenoid actuator was developed. This injector was developed from a previous conventional solenoid-operated direct injection injector for alternative fuels. The differences, compared with the previous injector included the bottom of the solenoid actuator is now downward facing and fixed in a solenoid holder; the solenoid has six

holes for fuel circulation; a 0.1 air-gap was set between the PM plunger and the static iron core of the solenoid at its closed position; a needle open assistance spring was added to help the injector to open faster; some parts of the injector design employed nonmagnetic materials to avoid affecting the magnetic path of the actuator.

The mathematical model of the PM plunger bi-directional actuator for alternative fuel injectors for CI engines has been developed. The model of the injector was expressed as a lumped spring-mass-damping model. This model was used for the injector design and its dynamic performance was analyzed.

The injector performance was simulated by a program written in C++ using the fourth-order Runge-Kutta method for solving the differential system equations. Comparing the performance of the injector operated by the PM plunger bi-directional actuator with the previous injector operated by a traditional solenoid actuator, the simulation results showed that both injectors start to open at almost the same time, but the traditional solenoid-operated injector reaches to the fully open position faster; however, at the closing stage, the bi-directional actuator operated injector closes faster. Based on the total time of injector closing and opening, the bi-directional actuator operated injector is faster; moreover, this new type of injector exhibits less needle bouncing, which is beneficial to reduce post-injection.

The effects of the pre-load and stiffness of the open assistance spring were also discussed. The simulation results showed that as the spring stiffness was fixed, and as the

pre-load increased, the injector opened faster, but closed slower. Also, as the pre-load increased, the seat reaction force acting on the needle is decreased. If the pre-load is fixed, while the stiffness of the spring is increased, the injector opens slower, but closes faster. Also, as the stiffness of the spring is increased, the seat force acting on the needle increases.

# CHAPTER 4

# CONCLUSIONS AND RECOMMENDATIONS FOR FUTURE RESEARCH

## 4.1 Conclusion

In this research project a new type of bi-directional rapid response solenoid actuator has been developed. An alternative fuel injector for CI engines actuated by this new type of bi-direction actuator has been implemented. The faster response of this design of fuel injector means that a more precise dose of fuel can be injected into the combustion chamber, leading to improved fuel economy and reduced tailpipe emission pollutants. The bi-directional actuated solenoid linear actuator design that is developed in this project differs from the conventional linear bi-directional motion actuator design. While it has the same structure as the existing, commercial, solenoid actuator, a key difference is that the carbon steel plunger typical of the traditional solenoid is replaced by a permanent magnet (PM) plunger. Thus, when a bi-directional square waveform voltage is applied to the actuator, the magnetic poles of the solenoid stator will alternate in phase with the current direction and the resultant magnetic force will alternately pull or push the PM plunger to implement bi-directional motion. The literature reviews showed that there is no such bi-directional actuator with the design described in this research or technique that exploited a bi-directional motion actuator for vehicle fuel injectors.

Neodymium iron boron (NdFeB) was investigated, and was selected as the material for the solenoid plunger. It exhibits favorable behaviors of:

1. Highest available magnetic energies;
2. Very high remanence and coercivity, and
3. Excellent magnetic characteristics.

A mathematical model of the PM plunger bi-directional actuated solenoid actuator was also developed. The dynamic equations of the solenoid actuator were expressed as in equation (2.18). With electrical power flowing through the solenoid, two magnetic sources exist in the solenoid actuator system: the magnetic field produced by the PM and the magnetic field produced by the current actuated solenoid. The total magnetic field in the solenoid actuator system is the sum of these two fields. Consequently, the force acting on the movable PM plunger can be treated as two parts, the attractive force between the PM plunger and the solenoid static iron core, and the electromagnetic force from the solenoid current that acts on the PM plunger. The total force acting on the PM plunger is the sum of these two forces.

To analyze the magnetic fields in the solenoid actuator, the traditional magnetic circuit method was employed. Unlike the finite element analysis (FEA) method that is widely used for magnetic field studies, the magnetic circuit method provided a simple and faster way to analyze the magnetic field. The large amount of numerical calculations typically required by using the FEA method was avoided. The experimental results showed that this method was appropriate for the magnetic field analysis for the solenoid actuator under research.

To express the mathematical model that describes the PM plunger solenoid actuator, the ferromagnetic material effect due to the solenoid frame and the carbon steel stator iron core were considered as reluctance, and was expressed by Froelich's equation. The equivalent circuit of the bi-directional solenoid actuator was presented, including the nonlinear inductance due to the solenoid coil and an additional inductance caused by the flux leakage.

The experimental setup for the measurement of the dynamic current and the corresponding force of the PM plunger bi-directional motion solenoid actuator was developed. From the experimental data, the parameters $a$ and $b$ in equation (2.52) which relates to the solenoid material and magnetic characteristics were determined. As a result, the nonlinear magnetic characteristics and the nonlinear inductance could be estimated. The experimental results also showed that the magnetic fields inside the solenoid central part could be regarded as being of equal magnitude. The experimental results match the theoretical calculations. Therefore, for a small stroke PM plunger, with the PM permeability chosen to be close to that of air, the force due to the solenoid current can be considered as independent to the plunger stroke.

In addition, an experimental setup for the measurement of the magnetic attractive force between the PM plunger and the solenoid static stator steel core was assembled. These experimental results were used to compute the loss factor $k$ in equation (2.50), to correct for the differences between the theoretical calculations and real results. The

results showed that having selected a proper loss factor $k$, the PM attractive force can then be predicated by the magnetic circuit method.

The simulation results of the PM plunger bi-directional actuated solenoid actuator were presented. The fourth-order Runge-Kutta method with a C++ program was applied to solve the solenoid actuator dynamic systems equations. The simulation results of current and current generated force matched the experimental results well which indicates that the mathematical model developed in this research is appropriate.

A design using this PM plunger bi-directional actuated solenoid actuator for alternative fuel direct injection vehicle injectors was presented. The literature review showed that there was no such bi-directional motion actuator employed in vehicle fuel injector designs. This design was based on the previous work that studied the application of the injector with low-viscosity liquid and gaseous fuels. Some modifications were made in the new design, such as:

1. Locating the solenoid static iron core on the lower part of the injector body so that the needle was closed via the PM attractive force;
2. Inserting six holes in the solenoid holder for fuel delivery;
3. Using a pre-loaded compressed spring to assist the needle to overcome the attractive force due to the PM at opening;

4. Some components were made of non-ferromagnetic material to avoid the affecting the magnetic path of the actuator.

When compared with the conventional solenoid actuated injector, the PM plunger bi-directional actuator injector starts opening almost at the same time. The injector operated by the conventional solenoid actuator reached the fully open position faster; but the conventional solenoid required an applied voltage of 80 V as compared to 36 V for the new design.. However, the injector operated by the PM plunger bi-directional actuator closed faster. Based on the total opening and closing response times, it may be said that the bi-directional motion injector has a more rapid response. Moreover, this new injector exhibits reduced needle bouncing that improves post-injection performance compared to the previous injector. The effects of the spring that is used to assist opening permit the following conclusions:

1. With a fixed stiffness spring, when the pre-load increased, the injector opens faster but closes slower, and the seat reaction force acting on the needle decreases.
2. When the pre-load is fixed, and the stiffness of the spring is increased, the injector opens slower, closes faster, and the seat force acting on the needle increases.

## 4.2 Recommendations for Future Work

Based on this research and its findings, the following recommendations on future work are suggested, as the author believes they can add significant research value to this field of knowledge:

1. Eddy current and hysteresis in modeling.

   Because the effects of the eddy current and hysteresis are very small, and to simplify the model of the PM plunger bi-directional motion actuator, they were not considered in this research. If these effects are included in the mathematical model of this actuator, the model will be more precise.

2. Experimental setup to measure the PM plunger motion path.

   The plunger motion paths were simulated in a well defined environment. Investigating the performance of the actuator in a real environment will help to improve the actuator design and performance.

3. Power supply for the PM plunger bi-directional motion actuator actuated injector.

   Higher voltages, when applied to the actuator, will improve the performance of the injector. However, an excessive voltage

will generate more heat in the solenoid and reduce the actuator and PM performance or indeed it may burn the solenoid coil. PWM power supply should be one way to solve this problem.

4. Optimal solenoid coil and resistance.

   The limitations concerning the number of coil windings, coil resistance, and wire gauge size should be optimized so that high voltages can be applied while maintaining fast electrical and magnetic dynamic responses for large force generation.

5. Injector system optimization.

   The design of this PM plunger bi-directional actuated injector based on the previous experience and research, to optimize the injector system, based on design factors such as the spring stiffness, pre-load, pulling rod material and structure, etc. should enhance the injector performance.

6. Field testing of the injector.

   Injector performance in this research is based on theoretical analysis. Field testing in conditions of operation will enhance the design and analysis of the injector performance.

7. Combustion products of the chemical composition measurement.

   Measurements of the chemical composition of the combustion products using the new injector design would reveal if a significant contribution to pollution reduction programs could be achieved.

8. Enhanced PWM driving circuit.

   A new PWM driving circuit should be designed. Only a large voltage is required to start (boost current) the needle to accelerate towards its open position. Once the needle is near its fully opened position, only a smaller current generated force is required to keep the needle fully opened. Similarly, only a large negative voltage of short duration is required to help accelerate the needle to close. Only the force of attraction from the PM is necessary to keep the needle closed upon its seat. This new PWM driving strategy will reduce needle impact forces.

9. Implementation of feedback control strategies.

   A sensor for position feedback should be implemented. In this way as the needle approaches it seat, position feedback can be used to reverse the solenoid force to reduce the needle-to-seat impact forces to eliminate wear and post-injections. As well, position feedback can be used to infinitely control the needle

position for fuel dosage control. In addition, position feedback control can implement the current boost strategies as proposed in (8) above.

Research as suggested above could greatly improve the performances of the PM plunger bi-directional actuated solenoid actuator and the bi-direction injector for alterative fuels.

## REFERENCE


[1] McIntosh, B. and Awad, A. J: "Alternate fuel: Not only For Automobiles Propane Conversion of a Residential Lawnmower", SAE paper, 1999-01-0281, 1999.

[2] AB Volvo, "Future Fuels for Commercial Vehicles", AB Volvo folder, Ref No. 011-949- 007, 2004.

[3] Hong, H. and Torab, B., "Solenoid-Operated Diesel Injectors for Low-Viscosity Liquid and Gaseous Fuels", Proceedings of the IMechE, Part D, Journal of Automobile Engineering, Vol. 215, No. 12, pp. 1281-1296, December 2001.

[4] Clark, R.E., Smith, D.S., Mellor, P.H. and Howe, D., "Design Optimisation of Moving-magnet Actuators for Reciprocating Electro-mechanical Systems", IEEE Transactions on Magnetics, Vol. 31, Issue 6, Part 2, pp. 3746-3748, Nov. 1995.

[5] Lequesne, B., "Fast-acting Long-Stroke Bistable Solenoid with Moving Permanent Magnets", IEEE Transactions on Industry Applications, Vol. 26, No. 3, pp. 401-407, May/June 1990.

[6] Ebihara, D. and Watada, M., "Development of a Single-winding Linear Oscillatory Actuator", IEEE Transactions on Magnetic, Vol. 28, No. 5, pp. 3030-3032, September 1992.

[7] Groom, N.J., "Design Consideration for an Air Core Magnetic Actuator", NASA Technical Memorandum 10429, February, 1992.

[8] Jung, K.S. and Baek, Y.S., "Contract-Free Moving-Magnet Type of Micropositioner with Optimized Specification", IEEE Transactions on Magnetics, Vol. 38, No. 3, pp.1539-1548, May 2002.

[9] Boledea, I. and Nasar, S.A., "Linear Electric Actuator and Generators", IEEE Transactions on Energy Conversion, Vol. 14, No. 3, pp. 712 – 717, September 1999.

[10] Abe, Y., Nakagawa, A., Watada, M., Torii, S., Yamane, K. and Ebihara, D., "Basic Characteristics of Linear Oscillatory Actuator for Liquid Hydrogen Pump", IEEE Transactions on Magnetics, Vol. 32, No. 5, pp. 5025-5027, September 1996.

[11] Lin, C.E. and Lin, K.G., "Implementation and Control of the Magnetic Linear Actuation System", Instrumentation and Measurement Technology Conference 2000. Proceedings of the 17th IEEE, Vol. 3, pp.1384 – 1387, 1-4 May 2000.

[12] Krepec, T., Tebelis, T. and Kwok, C.K., "Fuel Control Systems for Hydrogen-Fuelled Automotive Combustion Engines – a Prognosis", Int. Journal of Hydrogen Energy, Vol. 9, No. 1/2, 1984.

[13] Krepec, T., Giannacopoulos T. and Miele, D., "New Electrically Controlled Hydrogen-Gas Injector, Development and Testing", Hydrogen Energy, Vol. 12, pp. 855-861, 1987.

[14] Krepec, T., Giannacopoulos T. and Miele, D., "Electronic Injection System for Natural Gas in a Diesel Engine – Development and Testing", SAE Paper 890852, 1989.

[15] Green, J. and Wallace, S., "Electrically Actuated Injectors for Gaseous Fuels", SAE Paper 892143, 1989.

[16] Hong, H., Krepec, T. and Georgantas, A.I., "Design Optimization of Solenoid Operated Diesel Injectors for Gaseous Fuels", Proceeding CSME Forum 1992, Vol. II, page 349-354, 1 June- 4 June1992.

[17] Hong, H., Krepec, T. and Cheng, R.M.H., "Transient Response of Fast Acting Solenoid in Automobile Applications", Journal of Circuits, Systems and Computers, Vol. 4 No. 4, pp. 415-428, 1994.

[18] Kekedjian, H. and Krepec, T., "Further Development of Solenoid Operated Gas Injectors with Fast Opening and Closing", SAE Paper 940450, 1994.

[19] Hong, H., Krepec, T. and Kekedjian, H., "Shaping of Fuel Delivery Characteristics for Solenoid Operated Diesel Engine Gaseous Injectors", SAE Paper 960869, 1996.

[20] Torab, B., "The Adaptation of Solenoid Actuated Injectors for Use with Dimethyl Ether Fuel in Diesel Engines", a thesis in the Department of Mechanical Engineering, Concordia University, Montreal, Quebec, Canada, 1999.

[21] Yuan, K.Y. and Chen, S.C., "A New Algorithm for Coupled Solutions of Electric, Magnetic, and Mechanical Systems in Dynamic Simulation of Solenoid Actuators", IEEE Transaction on Magnetics, Vol.26, No.3, pp.1189-1197, May 1990.

[22] Sturman, O.E., Pena, J.A. and Petersen, P.W., "A CNG Specific Fuel Injector Using Latching Solenoid Technology", SAE Paper 951914, 1995.

[23] Barkhimer, R.L. and Wong, H.C., "Application of Digital, Pulse-Width-Modulated, Sonic Flow Injectors for Gaseous Fuels", SAE Paper 951912, 1995.

[24] Bates, G.J., Favrat, D., Germano, S. and Nicollerat, M., "Ultra Rapid Natural Gas Port Injection", SAE Paper 951913, 1995.

[25] Ganser, M.A., "Common Rail Injector with Injection Rate Control", SAE Paper 981927, 1998.

[26] Ando, R., Koizumi, M. and Ishikawa, T., "Development of a Simulation Method for Dynamic Characteristics of Fuel Injector", IEEE Transaction on Magnetics, Vol. 37, No. 5, pp.3715-3718, September 2001.

[27] Coppo, M., Dongiovann, C. and Negri, C., "Numerical Analysis and Experiment Investigation of a Common Rail Type Diesel Injector" ASME2002, Design, Application, Performance and Emissions of Modern Internal Combustion Engine Systems and Components, ICEF2002-507, ICE-Vol. 39, pp. 271-280, 2002.

[28] Passarini, L.C. and Pinotti, M. Jr., "A New Model for Fast-Acting Electromagnetic Fuel Injector Analysis and Design", Journal of the Brazilian Society of Mechanical Sciences, Vol. 25, No.1/95-106, January-March 2003.

[29] Passarini, L.C. and Nakajima, P.R., "Development of a High-speed Solenoid Valve: an Investigation of the Importance of the Armature Mass on the Dynamic Response", Journal of the Brazilian Society of Mechanical Sciences, Vol. 25, No.4/329-335, January-March 2003.

[30] Lisk Solenoid Catalog, G.W. Lisk Company, Inc

[31] Dexter Magnetic Technologies, "Reference & Design Manual"

[32] Campbell, P., "Permanent Magnet Materials and Their Application", New York, Cambridge University Press, 1994.

[33] Fitzgerald, A.E., Kingsley, Jr. C. and Umans, S.D., "Electric Machinery", -6th ed, McGraw-Hill Higher Education, Page 42, 2003.

[34] Dexter Magnetic Technologies Catalog, "Nd-Fe-B Material Properties".

[35] Lee, J.K., "The Analysis of a Magnetizing Fixture for a Multipole Nd-Fe-B Magnet", IEEE Transactions on Maganetics, Vol. 24, No. 5, pp 2166-2171, September 1998.

[36] Kang, D.H., Jeong, Y.H. and Kim, M.H., "A Study on the Design of Transverse Flux Linear Motor with High Power Density", Industrial Electronics, 2001. Proceedings ISIE 2001. IEEE International Symposium, Vol. 2, pp. 707 – 711, 12-16 June 2001.

[37] Furilani, E.P., Lee, J.K. and Dowe, D., "Predicting the Dynamic Behavior of Moving Magnet Actuator", Journal Appl. Phys., pp 3555-3557, April 1993.

[38] Hong, H, "Optimum Performance of Solenoid Injectors for Direct Injection of Gaseous Fuels in IC Engines", a thesis in the Department of Mechanical Engineering, Concordia University, Montreal, Canada, May, 1995.

[39] Brown, Jr., W.F., "Electric and Magnetic Forces: A Direct Calculation, I", American Journal of Physics, Vol. 19, pp 290-304, 1951.

[40] Haus, H.A. and Melcher, J.R., "Electromagnetic Fields and Energy", Prentice Hall, 1989.

[41] Moon, F.C. "Magneto-Solid Mechanics", John Wiley & Sons, Inc., 1984.

[42] Morrish, A.H., "The Physical Principles of Magnetism", John Wiley & Sons, Inc., 1965.

# APPENDIX A

## DESCRIPTION AND CALIBRATION OF PIEZO-ELECTRIC FORCE TRANSDUCER

A piezo-electric load cell transducer was used in Chapter 2 to measure the electromagnetic pushing force and pulling force due to the current; also, it was used to measure the attraction force due to the permanent magnet alone. The force transducer is a product of Kistler, type 9001. The main specifications of this transducer are in Table A.1:

**Table A.1: Kistler Force Transducer, type 9001 Specifications**

| | |
|---|---|
| Force Range | 0 to 7.5kN |
| Sensitivity | ≈ -4.3pC/N |
| Linearity | ≤ ±1 %FSO |
| Operating Temperature Range | -196 to 200 °C |
| Threshold | ≤ 0.01N |

A dual model charger amplifier produced by Kistler, model 504E, is used as a converter to amplify and transform the force signal.

In the calibration of the force transducer without preload, dead weights were applied to the load the transducer under compression and the voltage output was recorded. Figure A.1 shows the calibration curve for the transducer. The static gain of the force transducer is: 20.238 N/V

In calibration of the force transducer for with preload, a preload = 111.714N was put on the cell, and then dead weights were applied to the cell under compression and the output voltage was recorded. Figure A.2 shows the calibration curve for the transducer. The static gain of the force transducer is: 20.247 N/V.

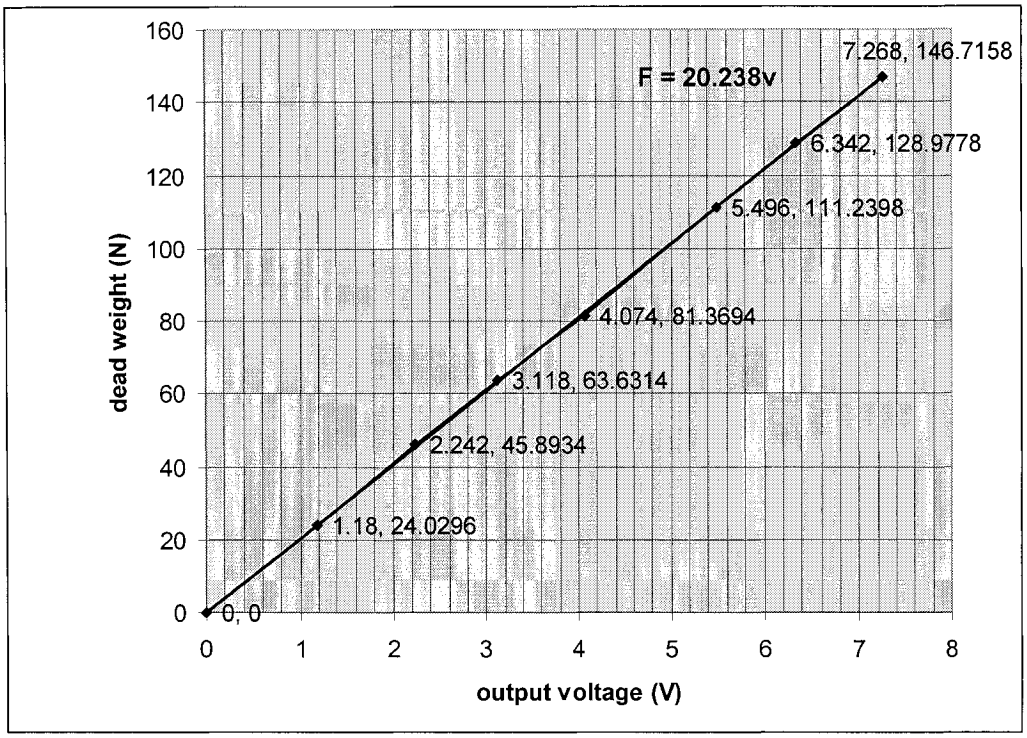


**Figure A.1 Piezo-cell force transducer calibration curve (without preload)**

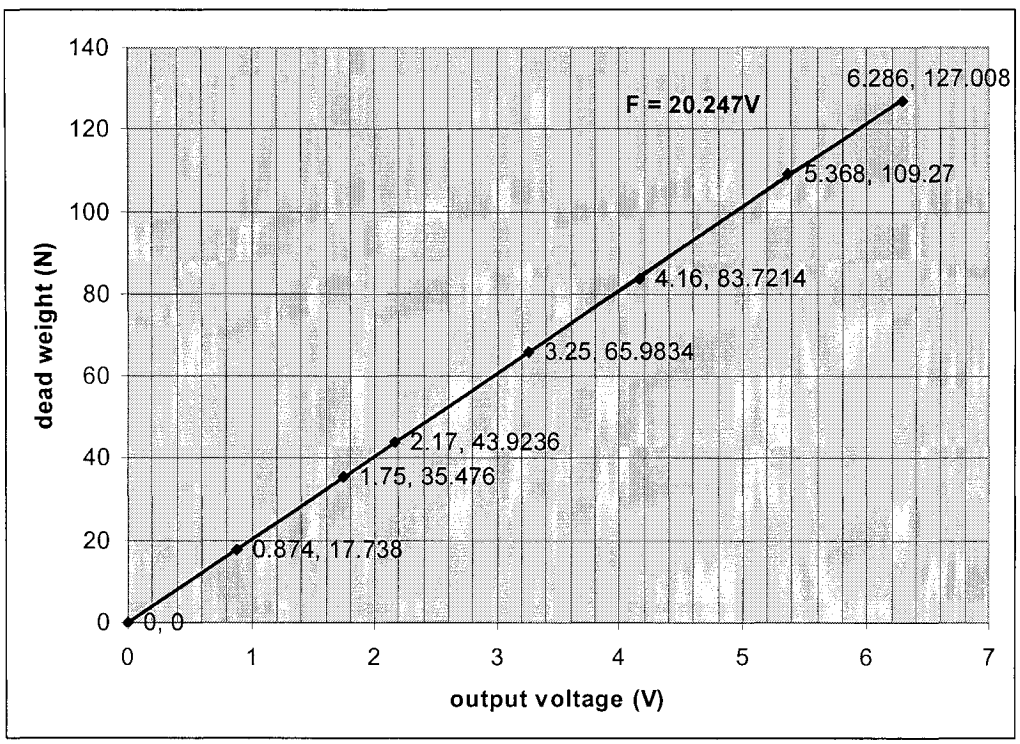


**Figure A.2 Piezo-cell force transducer calibration curve (with preload 111.714N)**